CLARIFICATION OF PHASE MORPHOLOGIES OF ALPHA AND BETA LEAD DIOXIDE FOR POSITIVE ELECTRODE APPLICATIONS

Cihan ARLI

Master's Dissertation

Department of Material Science and Engineering

Programme in Material Science and Engineering

Supervisor: Prof. Dr. Servet TURAN

(Co-Supervisor: Prof. Dr. Mehmet Ali GÜLGÜN)

Eskişehir

Eskişehir Technical University

Institute of Graduate Programs

August 2021

ABSTRACT

CLARIFICATION OF PHASE MORPHOLOGIES OF ALPHA AND BETA LEAD DIOXIDE FOR POSITIVE ELECTRODE APPLICATIONS

Cihan ARLI

Department of Material Science and Engineering

Programme in Material Science and Engineering

Eskişehir Technical University, Institute of Graduate Programs, August 2021

Supervisor: Prof. Dr. Servet TURAN

(Co-Supervisor: Prof. Dr. Mehmet Ali GÜLGÜN)

This study focused on to the morphology of positive active mass, PbO_2, polymorphs (orthorhombic α-PbO_2 and tetragonal β-PbO_2) used in the lead acid battery technology. In order to better understand the thermodynamics of the system, new E-pH diagrams are drawn as a function of temperature as well as pH and acid concentration. The macro/micro morphology and the phase composition of the positive electrode active mass structure were investigated by means of scanning electron microscope, transmission electron microscope and x-ray diffraction analysis. The results indicate that, both the formation acid concentration and the current-time profile effects the morphology and the phase composition, namely α-/β- ratio, of the active mass. In high acid concentration, production of α-PbO_2 greatly inhibited. In contrast, the PbO_2 formation rate is high, however, the total amount of PbO_2 formed is limited. In the light of this information, a model has been proposed here to explain the effect of acid concentrations on the positive active mass characteristics. Morphological investigations revealed that the needle like and spherical PbO_2 particles are dominant for the high and low formation acid concentrations, respectively. Transmission electron microscopy analysis showed that the β-PbO_2 can be in both needle like and spherical morphology. Most interestingly, phase transformation from β-PbO_2 to α-PbO_2 was observed during transmission electron microscopy analysis. Morphology of these particles that underwent a phase transformation changed as well.

Keywords: lead dioxide, α-PbO_2, β-PbO_2, positive active mass, morphology,

ÖZET

POZİTİF ELEKTROT UYGULAMALARI İÇİN ALFA VE BETA KURŞUN DİOKSİTİN FAZ MORFOLOJİLERİNİN AÇIKLANMASI

Cihan ARLI

Malzeme Bilimi ve Mühendisliği Anabilim Dalı

Malzeme Bilimi ve Mühendisliği Bilim Dalı

Eskişehir Teknik Üniversitesi, Lisansüstü Eğitim Enstitüsü, Ağustos 2021

Danışman: Prof. Dr. Servet TURAN

İkinci Danışman: Prof. Dr. Mehmet Ali GÜLGÜN

Bu çalışma, kurşun asit akü teknolojisinde kullanılan pozitif aktif kütle, PbO_2, polimorfların (ortorombik α-PbO_2 ve tetragonal β-PbO_2) morfolojisine odaklanmıştır. Sistemin termodinamiğini daha iyi anlamak için, yeni E-pH diyagramları, pH ve asit konsantrasyonunun yanı sıra sıcaklığın bir fonksiyonu olarak çizilmiştir. Pozitif aktif kütle yapısının makro/mikro morfolojisi ve faz bileşimi taramalı elektron mikroskobu, geçirimli elektron mikroskobu ve x-ışını kırınım analizi ile araştırılmıştır. Sonuçlar hem oluşum asit konsantrasyonunun hem de akım-zaman profilinin, aktif kütlenin morfolojisini ve faz bileşimini, yani α-/β- oranını, etkilediğini göstermektedir. Yüksek formasyon asit konsantrasyonunda, α-PbO_2 üretimi büyük ölçüde engellenirken, PbO_2 oluşum hızı artar, ancak anodik oksidasyonun miktarının düşük formasyon asit konsantrasyonuna kıyasla daha sınırlı olduğu görünmektedir. Bu bilgiler ışığında, pozitif aktif kütlenin oluşum aşaması sırasında kullanılan asit konsantrasyonlarının, PbO_2 polimorf oranının gelişimi üzerindeki etkisini açıklayan yeni bir model önerilmiştir. Morfoloji açısından bakacak olursak, yüksek ve düşük oluşum asit konsantrasyonları için sırasıyla iğne benzeri ve küresel PbO_2 partiküllerinin baskın olduğu görülmektedir. Geçirimli elektron mikroskobu analizi, β-PbO_2'nin hem iğne benzeri hem de küresel morfolojide olabileceğini göstermektedir. İlginç olarak, geçirimli elektron mikroskobu analizi sırasında, β-PbO_2'den α-PbO_2'ye faz dönüşümü gözlemlenmiştir. Faz dönüşümü geçiren bu parçacıkların morfolojileri de değişmektedir.

Anahtar Sözcükler: kurşun dioksit, α-PbO_2, β-PbO_2, pozitif aktif kütle, morfoloji

ACKNOWLEDGEMENTS

First and foremost, I would like to thank my advisors Prof. Dr. Servet Turan and Prof. Dr. Mehmet Ali Gülgün. It was a pleasure to work with them and this thesis could not be completed without their exceptional support.

I also want to thank to Prof. Dr. Selmiye Alkan Gürsel, Sinem Aydın and Sabancı University as a hole for the job opportunity.

Special thanks go to Dr. Pelin Sungur and Dr. Raghavendra Rao Juluri for their assistance on the transmission electron microscope analysis, and, Mine Ersöz and Tuğçe İşler Gül for their expertise on the lead acid battery system.

Also, I want to acknowledge the "TÜBİTAK 2211 Genel Yurt İçi Yüksek Lisans Burs Programı" program and thank TÜBİTAK for the financial support they provided throughout my thesis.

Cihan ARLI

20/08/2021

STATEMENT OF COMPLIANCE WITH ETHICAL PRINCIPLES AND RULES

I hereby truthfully declare that this thesis is an original work prepared by me; that I have behaved in accordance with the scientific ethical principles and rules throughout the stages of preparation, data collection, analysis and presentation of my work; that I have cited the sources of all the data and information that could be obtained within the scope of this study, and included these sources in the references section; and that this study has been scanned for plagiarism with "scientific plagiarism detection program" used by Eskişehir Technical University, and that "it does not have any plagiarism" whatsoever. I also declare that, if a case contrary to my declaration is detected in my work at any time, I hereby express my consent to all the ethical and legal consequences that are involved.

Cihan ARLI

CONTENTS

Page

LIST OF TABLES

Page

LIST OF FIGURES

Page

GLOSSARY OF SYMBOLS AND ABBREVIATIONS

α	:	Alpha
β	:	Beta
PAM	:	Positive Active Mass
SEM	:	Scanning Electron Microscope
TEM	:	Transmission Electron Microscope
Ah	:	Ampere·Hour
s.g.	:	Specific Gravity
1BS	:	$PbO \cdot PbSO_4$
3BS	:	$3PbO \cdot PbSO_4 \cdot H_2O$
4BS	:	$4PbO \cdot PbSO_4$
LO	:	Leady Oxide
F	:	Faraday Constant
E	:	Equilibrium Potential

1. INTRODUCTION

1.1. History

Batteries in the essence just a small reactor that converts chemical energy to electrical energy. For some, history of such device goes back to so called *Baghdad Battery* which dated around 200 BC[1]. This device made of ceramic pot that said to be contains an electrolyte solution and iron rod that enclosed in a copper cylinder. Even though their usage not fully explained by the archeological expeditions, modern replicas do work[2]. In 1749 Benjamin Franklin was the first to use the term *battery*[3], [4]. His battery consisted of glass capacitors that charged statically and linked together gave strong discharge[3], [4].

Obviously, battery technology came a long way since then. Increase of humanity demand for electricity facilitated an immense ingenuity. Yet, it can be said clearly, modern technologies are still falling short to satisfies our demand from the batteries. At this point it may necessary to make some distinctions related to batteries. There are two types of batteries namely primary and secondary. Primary battery is ready to create current as the components are assembled and when the active elements are consumed it cannot be recharge. While, secondary battery requires forming the electrochemically active materials and can be recharge. For this thesis, subject is related with the latter, more precisely the lead acid battery invented by the French physicist Gaston Planté as in 1859[5]. He investigated the polarization behaviors of metals in H_2SO_4 solution and summarized his findings in "Recherches sur la polarization voltaique,"[5]. This was the first type of the rechargeable battery to that point in time. Design consisted of two rolled sheets separated by a rubber immersed in H_2SO_4 solution. Most interestingly Planté never protected his invention with patents, his peers describe Planté as kind-hearted, modest, and unselfish man and a workaholic[6]. He even declined the invitation to run Member of the French Academy of Sciences by stating that he rather spend his time in the laboratory[6]. In 1989 Bulgarian Academy of Sciences established a medal in the great Gaston Planté with the approval of the French Academy of Sciences[6], [7]. After 10 years of the invention of lead acid battery, first direct current dynamo technology is developed by Zénobe Gramme. In 1873, Bréquet Company combine the both technology and produce the Planté lead acid batteries with easy and convenient way[6]. As the electricity usage become more mundane for public demand for the lead acid battery is increased and after the World

War II lead acid battery production immensely increased[6]. In this day it is used in variety of applications such as; SLI (starting, lighting, ignition) and traction batteries in automobiles and transport vehicles, respectively, stationary batteries for back-up power supply and more[6]. Performance criterion for lead acid battery obviously changes for each application, but very crudely can be reduced to capacity and cycle life. Lead acid battery technology used in the automotive industry for years however new technological trends like electrical cars along with the environmental concerns comes from the usage of lead, questions the adequacy of the lead acid battery and pushes the energy storage technology of the automotive industry to new horizons. It is known that the main drawback of the lead acid battery is the energy density, yet it is used due to its cost and the power to weight ratio[6], [8], [9]. **Table 1.1** summarizes how the lead acid battery fairs against other battery technologies.

Table 1.1. *Characteristics of various battery technologies.*[6], [10], [11]

Technology	Voltage (V)	Specific Energy (Wh/kg)	Energy Density (Wh/L)	Power Density (W/kg)	Energy Cost (€/kWh)	Advantages	Disadvantages
Sealed lead-acid (LA)	2.1	30-40	60-75	180	25-40 for OEM 100-180 for after-market	Cheap	Heavy
Nickel-cadmium (Ni-Cd)	1.2	40-60	50-150	150	200-500 for OEM	Reliable, inexpensive, high discharge rate, good low-temperature behavior	Heavy, toxic material, memory effect
Nickel-metal hydride (Ni-MH)	1.2	30-80	140-300	250-1000	275-550 for OEM 600 for HEVs	High-energy density, environment friendly	Higher internal resistance, gas formation, self-discharge
Lithium-ion $LiCoO_2$	3.6	160	270	1800	200-500 for OEM 400-800 for HEVs	High specific energy, low self-discharge	Expensive, Requires safety electronics
Lithium polymer	3.7	130-200	300	3000	200-500 for OEM 400-800 for HEVs	High specific energy, low self-discharge	Expensive, Requires safety electronics
Lithium-ion $LiFePO_4$	3.25	80-120	170	1400	200-500 for OEM 400-800 for HEVs	Safe	Technology in development

HEV, hybrid electric vehicle; *OEM*, original equipment manufacturer.

It can be seen from the table that the energy cost of the lead acid batteries is relatively low in the market which makes them still reliable technology. But it is obvious that the industry requires development. Lead acid batteries under serious scrutiny concerning their adequacy to satisfy the demand as the "go to power storage system". As an example, lithium-ion batteries can replace them in the automotive industry in some 10 years[9]. Even though lithium storage systems not fully matured, it is predicted that first the initially high-end sports car will use them. That being said the lead acid battery systems continue to be *benchmark* for up and coming storage system[9].

1.2. Lead Acid Battery

Focus of this section will be on the compounds of the workings of the lead acid battery and the parameters effecting its performance. As mentioned capacity and the cycle life are the main performance criterions for the lead acid battery. But what are the parameters effecting the capacity and life of the battery in the eyes of a material scientist? Lead acid battery comprise of positive active mass of PbO_2 and negative active mass of *spongy* Pb. It is said that the capacity and the cycle life more dependent on the positive electrode which is the focus of this thesis[8], [12]. It is now convenient to mentioned the compounds that formed in the $Pb/H_2SO_4/H_2O$ system.

1.2.1. Lead compounds of $Pb/H_2SO_4/H_2O$ system

Lead (Pb): Symbol Pb comes from the Latin word *plumbum*. It is a multivalent element in its ionic state, namely, plumbous (Pb^{2+}) and plumbic (Pb^{4+}). It is a dense, malleable metal with low melting point, it has face centered cubic crystal (FCC) structure[8], [13]. It is used in the negative electrode of the lead acid battery and reduced from the paste during the formation process[6], [8]. It is also present in the LO up to 30%[6].

Lead oxide (PbO): This phase has two polymorphs. tet-PbO (α-PbO) also named litharge, red in color and has a tetragonal structure. ort-PbO (β-PbO) also named massicot, yellow in color and has an orthorhombic structure. tet-PbO being slightly less dense (tet-PbO: 9.2-9.5 $g{\cdot}cm^{-3}$ and ort-PbO: 9.5-9.9 $g{\cdot}cm^{-3}$)[13] and ort-PbO being more soluble in water at 25 ℃ (tet-PbO: 0.05 $g{\cdot}l^{-1}$ and ort-PbO: 0.107 $g{\cdot}l^{-1}$)[13], [14]. It is obtained from the thermal oxidation of Pb in the lead acid battery industry and main component of the LO starting material for paste.

Basic lead sulfates: There are three main types of basic lead sulfates that appears in the $Pb/H_2SO_4/H_2O$ system. $PbO{\cdot}PbSO_4$(1BS), $3PbO{\cdot}PbSO_4{\cdot}H_2O$ (3BS) and $4PbO{\cdot}PbSO_4$(4BS). One can look at these materials as poor sulfates, means there is less SO_4^{2-} per Pb compare to the $PbSO_4$.

Thus, behaviors can be expected fall between the PbO and $PbSO_4$. 1BS forms in the very narrow pH range it is soluble in H_2SO_4 solutions[6]. 3BS is dominant in the temperatures below 60 ℃[6] and has a triclinic structure with space group $P\bar{1}$ [15].4BS forms when the temperature is above 80 ℃[6] and has a monoclinic structure with space group $P2_{1/c}$[16]. 3BS and 4BS pastes are commonly used in the lead acid battery technologies main difference being the morphology between these phases. 4BS crystals are larger in size[17]–[19] and it is believed that the this property improves the cycle life of the battery[6].

Lead sulfate ($PbSO_4$): This is the main discharge product of the lead acid battery during operation. PbO_2 at the positive electrode and Pb at the negative electrode reduced and oxidized to $PbSO_4$, respectively. One important property of this material is that its solubility in H_2SO_4 solution changes with the acid concentration. Danel and Plichon studied the solubility of the $PbSO_4$ in different H_2SO_4 molarities and calculate the diffusion coefficient of the Pb^{2+} in the solution[20]. Their results show that the solubility of $PbSO_4$, S_{PbSO_4}, reaches a peak at 1.16 M H_2SO_4 then continuously declines[20].

Red Lead (Pb_3O_4): This lead compound can exist in the alkaline environments according the E-pH diagram[21]. When it is added to the paste mixture in the H_2SO_4 environment it decomposed to the $PbSO_4$ and PbO_2[6]. Interestingly, Pb_3O_4 less reactive in the higher acid concentrations. Pavlov and Kapkov investigated the decomposition behavior of the Pb_3O_4 in H_2SO_4 solution with various concentrations and found that when the H_2SO_4 concentration is around 1.2 $g{\cdot}cm^{-3}$ (pH ~ -0.85) Pb_3O_4 yields the most amount of $PbSO_4$ and PbO_2[22]. It is generally used to improve the battery capacity performance of the batteries prepared by using the 4BS pastes.[22], [23].

Lead dioxide (PbO_2): Properties of this material will be explained in more detail in the following sections but brief introduction can be done as follows. It has two polymorphs with quite different properties. Crystal structures of α-PbO_2 and β-PbO_2 are orthorhombic and tetragonal, respectively and both being dark colored[13]. In reality both modifications are non-stoichiometric[24] and it is stated that the β-PbO_2 is more orderly structure meaning its chemical formula closer to PbO_2[25], [26]. Many researchers suggested different general chemical formula for the non-stoichiometric PbO_2.

$$Pb^{4+}_{1-x-y} \cdot Pb^{2+}_{y} \cdot O^{2-}_{2-4x-2y} \cdot (OH)^{-}_{4x-2y} \quad \textbf{(1)}$$

Eq.1 represents the most general case, here x and y represents cation vacancy fraction and fraction of Pb^{2+} present[27], similar equations can be found in the literature[28], [29]. Pavlov stated that the surface of the PbO_2 hydrates ($PbO(OH)_2$) and forms gel like structure that resembles a polymer chain and PbO_2 crystal and gel regions are responsible for the electron conductivity and proton conductivity, respectively[30]–[32]. According to author, this *gel-crystal* model explains the difference between the chemical and electrochemical PbO_2[31], [32]. Mindt investigated the conductivity of the α-PbO_2 and β-PbO_2 and found that even though α-PbO_2 has more charge carrier due to its less ordered structure mobility of these carrier are low compared to the β-PbO_2[33]. Electronic resistivities of α-PbO_2 and β-PbO_2 stated as 10^{-3} and 10^{-4} ohm-cm, respectively[33]. Discharge characteristics of these polymorphs also found to be different[34], [35]. It can be said that in the Pb/H_2SO_4/H_2O system formation of pure α-PbO_2 or β-PbO_2 is not possible, yet pure α-PbO_2 or β-PbO_2 can be produced in different solutions, where, α-PbO_2 prefers more alkaline solutions while the β-PbO_2 is stable in acidic mediums[29], [34], [36], [37]. As a rule of thumb, it is excepted that the α-PbO_2 and β-PbO_2 forms from the PbO and $PbSO_4$ precursors, respectively. This statement, even though simplified, holds a value since the E-pH diagram is investigated the $PbSO_4$ lies on the more acidic regions where the PbO resides in alkaline values[6], [38].

1.2.2. Production of lead acid battery

Production of the both positive and negative active mass is similar and can be classified under four main sections, namely, i) leady oxide (LO) preparation, ii) paste preparation and plate/gird pasting, iii) plate curing and iv) formation of the active masses.

Leady oxide (LO) production[6], [39]: Purpose being the oxidation of the pure lead during abrasion. To this day there is two main processes that dominates this step. Barton pot and ball-mill. Barton pot method uses a molten Pb which stirred and oxidized under humified atmosphere. Newly formed oxide particles then separated according to their size. Ball-mill process uses Pb balls that tumbles against each other, heat resulting from the friction is adequate enough to facilitate the oxidation process on the surface. PbO that formed in the surface of the balls continuously flakes of and this material is collected and separated according to size. Both processes yield a material that contains up to 85% PbO and remaining is free Pb called *leady oxide (LO)*[6],

[39]. Mayer and Rand investigated the desired leady oxide characteristics and also compared Barton pot and ball-mill processes[40]. According to these authors parameters that effects the leady oxide performance are; purity, free Pb content, polymorphism, reactivity, surface area, apparent density, occupational health/handleability, stability, active material/grid interface, cost, quantitative values of oxide characteristics[40]. Table that compare the compares the Barton pot and ball-mill processes are given below.

Table 1.2. *Comparison between Ball-mill and Barton pot methods*[40].

Characteristics	**Ball-mill**	**Barton pot**
Particle size	small particles	larger particles
Reactivity in air	generally high; can cause storage and long-distance transport problems	generally, more stable
Polymorphism	60-70 wt.% α-PbO 1-4 wt.% β-PbO	15 wt.% β-PbO
Acid absorption (mg H_2SO_4/g oxide)	240	140-160
Surface area ($m^2 g^{-1}$)	2.4-2.8	0.4-1.8
Free-lead content (wt.%)	~ 30	~ 25
Ease of making battery paste	makes a stiff paste which can require careful control	makes a softer paste which can result in easier pasting
Paste curing	capable of fast curing	average curing rate
Battery performance	batteries have good initial capacity, but possibly shorter life	enhances battery life, but can result in lower initial capacity
Deep-cyclability	usually good	sometimes good
Process control	easier; more consistent oxide	can be more difficult, but recent computer controls are helping
Typical production rate ($kg\ h^{-1}$)	up to 1000	300-800
Investment considerations	costs more: requires more space; noisy: costlier to maintain	lower initial cost; compact in size; relatively quiet; costs less to maintain: uses less energy to run
Energy use ($kWh\ t^{-1}$)	100-300+	up to 100
Environmental aspects	with well-engineered environmental systems (including baghouse and storage), existing emission standards can normally be met: typically, in the range of less than 0.1 mg oxide per Nm^3	

Paste preparation and plate/gird pasting: At this stage, LO mixed and stirred with predetermined amounts of water and H_2SO_4 solution. The important parameters in this stage are the mixing time, temperature and the pH. Purpose is to produce basic lead sulfates from the leady oxide, mainly the two types of basic lead sulfate used as the paste in the industry 3BS and 4BS[6]. After this step paste mainly consist of basic lead sulfates but some unreacted PbO and Pb can remain in the system. Temperature ranges up to 60 ℃ 3BS phase is the stable one however for the paste production temperatures above 80 ℃ 4BS is formed in the expanse of the 3BS (see Figure 6.2B in reference [6]). It can be said that the formation of the 4BS mainly depends on the paste preparation temperature. That being said the pH or acid concentration also effects the which basic lead sulfates will form. Pavlov and Papazov investigated the effects on the H_2SO_4/LO on the paste composition of the pastes that produced at 80 ℃ with 40 minutes of stirring[41]. They found that the 4BS production peaks around H_2SO_4/LO is around 4wt.% then declines and 3BS starts to form when the H_2SO_4/LO is equal to 6wt.%[41]. Above H_2SO_4/LO equal 8.5wt.% no 4BS forms at 80 ℃ and 40 minutes of stirring. Thus, it can be concluded that the 4BS forms in the environments that is more alkaline compared to the 3BS. This is a logical finding. According to E-pH diagram, will be explained later, of the $Pb/H_2O/H_2SO_4$ system $PbSO_4$ and PbO lies in the most acidic and basic environments, respectively. Note that one can see the basic lead sulfates as the *poor sulfates* hence 4BS is "less" sulfate then the 3BS since it has more PbO per $PbSO_4$ in its structure, thus, resembles the PbO. There are two modifications of the PbO in the LO, tetragonal and orthorhombic modifications assigned tet-PbO and ort-PbO, respectively. Iliev and Pavlov found that the modification of the PbO also influences the paste composition[42]. They used pure tet-PbO and ort-PbO along with the mixture of both at 80 ℃ and 6wt.%. From their study it can be seen that tet-PbO is more reactive in the paste making process[42]. Yet it is clear that independent of the PbO modification 4BS forms in the expanse of the 3BS. It is believed that the type of the basic lead sulfates has a major influence on the PbO_2 polymorph. It is initially stated that the 4BS act as a precursor for the α-PbO_2 (tetragonal polymorph of PbO_2). Culpin challenged this idea because of the inconclusive results[43]. Reasons for this belief will be explained later, Dodson actually lay the ground work for the understanding parameters that effects the PbO_2 polymorphism. Dodson stated that the α-PbO_2 content depends on the paste density, pH, formation current density and temperature[25], [44]. Thus, making the statement that the 4BS lead to α-PbO_2 formation not

entirely true. When pastes prepared with desired composition they pasted on the grid plates and send to curing.

Plate curing: In the curing stage, paste particles forms the interconnected hard porous mass (skeleton). Pavlov summarizes the processes as follow; i) bigger paste particles grows in the expanse of the smaller ones (according to Ostwald-Freundlich equation), water between the particles evaporates, ii) depending on the temperature 3BS transforms in 4BS by reacting with the residual PbO, iii) residual Pb oxidizes and corrosion layer (CL) between the grid and the paste material forms, iv) hydrated particles in the paste re-crystallize as a result, interconnected skeleton forms[6], [45]. Depending on the paste characteristics like; composition, density and moisture, the important parameters that effecting the curing process are; humidity, temperature, atmosphere and time of curing[6]. It is common to use different temperatures and relative humidity (RH) values during curing process of the lead acid battery industry to ensure the high performance of the product. Formation of the CL and the adhesion between the grid and the active material has paramount importance especially in the automotive industry due to the effects of the vibrational loads on the battery.

Plate forming: This stage is the main focus of this thesis. Morphological differences between the α-PbO_2 and β-PbO_2 modifications as well as their electrochemical formation mechanism will be discussed in depth in the following sections. Purpose of this stage can is the form the active material from the cured paste. There are two main processes involved in formation of the positive active material (PAM), PbO_2. One is the electrochemical oxidation and second is the chemical sulfation. **Table 1.3** represents the reactions that occur in tandem during the formation of the PAM from 3BS paste. It is important to note that, in order to these reactions to occur the diffusion of the ionic species has paramount importance. Notice that if H^+ ion is not removed from the reaction environment it can decrease the pH value which in return can change the phase composition. Or, if H_2SO_4, HSO_4^- or SO_4^{2-} species cannot transferred to the interior of the paste sulfation reaction can stop which also effects the composition of the final composition of the PAM.

Table 1.3. *Chemical and electrochemical reactions during formation.*

Sulfation Reactions (Chemical)	Dissolution of $\boldsymbol{PbSO_4}$	Oxidation Reactions (Electrochemical)
$PbO + \boldsymbol{H_2SO_4} \leftrightarrow \boldsymbol{PbSO_4} + H_2O$		$Pb^{2+} \leftrightarrow Pb^{4+} + 2e^-$
$3BS + \boldsymbol{H_2SO_4} \leftrightarrow 2(PbO \cdot PbSO_4) + 2H_2O$ $1\text{BS} + \boldsymbol{H_2SO_4} \leftrightarrow \boldsymbol{2PbSO_4} + H_2O$	$\boldsymbol{PbSO_4} \leftrightarrow Pb^{2+} + SO_4^{2-}$	$PbSO_4 + 2H_2O \leftrightarrow PbO_2 + \boldsymbol{H_2SO_4} + \boldsymbol{2H^+} + 2e^-$
$3BS + \boldsymbol{3H_2SO_4} \leftrightarrow \boldsymbol{4PbSO_4} + 4H_2O$		$PbO + H_2O \leftrightarrow PbO_2 + \boldsymbol{2H^+} + 2e^-$

One can see that, the oxidation of the $PbSO_4$ and 3BS or 1BS (not given here for simplicity) produces acid which can be further used in the sulfation of the basic lead sulfates. **Figure 1.1** is the schematic representation of this self-feeding mechanism. This chaotic nature of the formation process depends on both the thermodynamics and the kinetics of the formation. One can even say that the oxidation and sulfation reactions are in some sort of race and the winner dominantly determines the PAM composition. Pavlov et. al. investigated the nature of this race and concluded that the formation process is a zonal process that is sulfation starts from the acid concentrated surface and the oxidation starts from region that close to conductive metal grid[46].

Figure 1.1. *Self-feeding mechanism*

Thermodynamic investigation of the formation of the PbO_2 modifications (α-PbO_2 and β-PbO_2) rather easy by using the E-pH diagram however the stability regions of the α-PbO_2 and β-PbO_2 is not clear in the literature. One problematic thermodynamic aspect is the pH gradient that occur during the formation. Kinetic aspect of the α-PbO_2 or β-PbO_2 formation depends mainly on the formation current of the process, this dependence also stated by the Dodson[25], [44]. But parameters like temperature, paste density, pore characteristics of the paste acid concentration and diffusion of the ionic species also effects the kinetics of the process. Thus, one can see the thermodynamic aspects as a road map and the kinetic aspects as selection of the driver, **Figure 1.2** represents the schematic of the analogy that start from a paste that mainly contains a 3BS, note that the E-pH diagram is just a representation. Oxidation path depends on parameters like; current,

ionic diffusion, electrical contact between the grid and PAM, ohmic resistance of the system and paste density. Parameters that governs the sulfation are; ionic diffusion, transformation rate, acid concentration, paste density.

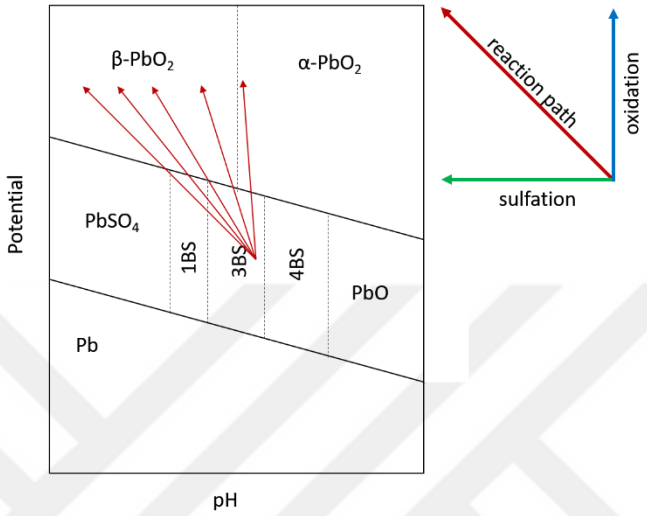

Figure 1.2. *Schematic of the road map and driver analogy*

Electrochemistry of the lead acid battery will be explained in the following sections and the formation of the α-PbO_2 and β-PbO_2 mainly disused in terms of the E-pH diagram. There are many parameters that effects the regions of the E-pH diagram, the road map, mainly the heterogeneities that formed during the formation.

Purpose of this research is to determine the morphological differences between the α-PbO_2 and β-PbO_2, to do so, one should understand the Pb/H_2SO_4/H_2O system and how these 2 polymorphs forms during the formation step. Formation process of the PbO_2 polymorphs investigated by samples provided by commercial battery manufacturer. In order to effectively investigate the oxidation mechanism novel E-pH diagrams are constructed with different ionic activities and temperatures. Phase boundary between the α-PbO_2 and β-PbO_2 tried to enlighten. and morphologies are clarified.

2. ELECTROHEMISTRY OF THE LEAD ACID BATTERY

This section will describe the thermodynamics and responsible mechanisms of the formation of the PbO_2. Equilibrium potential and the free energy of the system can be correlated by the following fundamental relationship[47];

$$\Delta G^0 = -nFE^0 \quad \textbf{(2)}$$

$$\Delta G = -nFE \quad \textbf{(3)}$$

Here ΔG^0 and E^0 represents standard Gibbs free energy and standard equilibrium potential respectively. Faraday's constant, F generally taken as 96500 C·mole^{-1} and n is the number of electrons involved in the electrochemical reaction. By using the **Eq. 2** and **3** we drive an expression for the equilibrium potential, E, as follows;

$$\Delta G = \Delta G^0 + RT\, ln\, Q \quad \textbf{(4)}$$

$$-nFE = -nFE^0 + RT\, ln\, Q \quad \textbf{(5)}$$

$$E = E^0 - \frac{RT}{nF} ln\, Q \quad \textbf{(6)}$$

$$E = E^0 - \frac{2.3RT}{nF} log\, Q \quad \textbf{(7)}$$

Here R and T gas constant and temperature, respectively. Q is the reaction quotient. **Eq. 7** is called Nersnt equation and correlates the equilibrium potential, E, with the thermodynamic activity of the products.

2.1. Pb/$PbSO_4$ Electrode Potential

Negative electrode of the lead acid battery is the Pb/$PbSO_4$ electrode. Electrochemical reaction 8 proceeds at the negative electrode during charging of the battery:

$$PbSO_4 + 2e^- \rightarrow Pb + SO_4^{2-} \quad \textbf{(8)}$$

Equilibrium potential, $E_{Pb/PbSO_4}$ can be calculated by the **Eq. 7** as follows:

$$E_{Pb/PbSO_4} = E^0_{Pb/PbSO_4} - \frac{2.3RT}{nF} log\, Q_1 \quad \textbf{(9)}$$

Where Q_1 is:

$$Q_1 = \frac{a_{Pb} \cdot a_{SO_4^{2-}}}{a_{PbSO_4}} \quad \textbf{(10)}$$

Standard equilibrium potential of the Pb/$PbSO_4$ electrode can be calculated from the **Eq. 2** and values from **Table 2.1**, where n is 2 for **Eq. 9** and F is 96.500 kC·mole^{-1}:

$$E^0_{Pb/PbSO_4} = -\left(\Delta G^0_{Pb} + \Delta G^0_{SO_4^{2-}} - \Delta G^0_{PbSO_4}\right) / nF \quad \textbf{(11)}$$

$$E^0_{Pb/PbSO_4} = -(0 + (-742.17) - (-811.43)) / 2 \cdot 96.500 = -0.359\ V \quad \textbf{(12)}$$

Then the equation potential of the Pb/$PbSO_4$ electrode at any state can be expressed as:

$$E_{Pb/PbSO_4} = -0.359 - 10^{-4} \cdot T \cdot log \frac{a_{Pb} \cdot a_{SO_4^{2-}}}{a_{PbSO_4}} \quad \textbf{(13)}$$

It is now evident that the Pb/$PbSO_4$ electrode potential depends on the activity of the SO_4^{2-} ions since the Pb and $PbSO_4$ are solid and their activities can be taken as 1.

2.2. PbO_2/$PbSO_4$ Electrode Potential

Similar procedure can be used for the PbO_2/$PbSO_4$ electrode as well. Again, during charging following electrochemical reaction takes place at the positive electrode:

$$PbSO_4 + 2H_2O \rightarrow PbO_2 + SO_4^{2-} + 4H^+ + 2e^- \quad \textbf{(14)}$$

Equilibrium potential for the **Eq. 14** can written as:

$$E_{PbO_2/PbSO_4} = E^0_{PbO_2/PbSO_4} + \frac{2.3RT}{nF} log\ Q_2 \quad \textbf{(15)}$$

where Q_2 is:

$$Q_2 = \frac{a_{PbO_2} \cdot a_{SO_4^{2-}} \cdot a^4_{H^+}}{a_{PbSO_4} \cdot a^2_{H_2O}} \quad \textbf{(16)}$$

Notice sing before the logarithmic term is reversed since the **Eq. 14** is anodic oxidation. Now, one can use the standard Gibbs free energies to calculate the standard electrode potential for this reaction, $E^0_{PbO_2/PbSO_4}$, by using the values at **Table 2.1.**

Again the n and F are equal to 2 and 96.500 kC·mole^{-1}, respectively, which leads to:

$$E^0_{PbO_2/PbSO_4} = \left(\Delta G^0_{PbO_2} + \Delta G^0_{SO_4^{2-}} + 4\Delta G^0_{H^+} - \Delta G^0_{PbSO_4} - 2\Delta G^0_{H_2O}\right) / nF = 1.683\,V \quad \textbf{(17)}$$

Equilibrium potential for the $PbO_2/PbSO_4$ at any state then can be written as:

$$E_{PbO_2/PbSO_4} = 1.683 + 10^{-4} \cdot T \cdot log \frac{a_{PbO_2} \cdot a_{SO_4^{2-}} \cdot a^4_{H^+}}{a_{PbSO_4} \cdot a^2_{H_2O}} \quad \textbf{(18)}$$

By doing some algebra and taking the $a_{H_2O} = 1$, **Eq. 18** reduces to:

$$E_{PbO_2/PbSO_4} = 1.683 + 10^{-4} \cdot T \cdot log a_{SO_4^{2-}} - 4 \cdot 10^{-4} \cdot T \cdot pH \quad \textbf{(19)}$$

It is stated by Pavlov that the differences between the electrode potential values in the literature mainly comes from the ΔG^0 and values excepted by authors and the weather more accurate 96.487 kC·mole^{-1} used as the Faraday constant[6]. By analyzing the **Eq. 19** it can be said that the $PbO_2/PbSO_4$ electrode potential effected by the both SO_4^{2-} concentration and pH, latter being the dominant parameter.

2.3. Potential of the Lead-Acid Cell

Potential developed between the $Pb/PbSO_4$ and the $PbO_2/PbSO_4$ electrodes can be calculated by the summation of the anodic and cathodic reaction potentials[47]:

$$E_{cell} = E_{anodic} - E_{cathodic} \quad \textbf{(20)}$$

For this system, during charging the anodic and cathodic reactions takes place at the $PbO_2/PbSO_4$ and $Pb/PbSO_4$ electrodes, respectively.

$$E_{cell} = E_{PbO_2/PbSO_4} - E_{Pb/PbSO_4} \quad \textbf{(21)}$$

Similar to **Eq. 20** and **21** standard cell potential, E^0_{cell}, can be expressed in terms of standard anodic and cathodic potential as follows:

$$E^0_{cell} = E^0_{PbO_2/PbSO_4} - E^0_{Pb/PbSO_4} = 1.683 - (-0.358) = 2.041\,V \quad \textbf{(22)}$$

Equilibrium potential of the cell then becomes;

$$E_{cell} = E^0_{PbO_2/PbSO_4} + \frac{2.3RT}{nF} log\, Q_2 - E^0_{Pb/PbSO_4} + \frac{2.3RT}{nF} log\, Q_1 \quad \textbf{(23)}$$

$$E_{cell} = E^0_{PbO_2/PbSO_4} - E^0_{Pb/PbSO_4} + \frac{2.3RT}{nF} log\, Q_2 Q_1 \quad \textbf{(24)}$$

note that for both reaction n is 2 and $Q_2 Q_1$is equal to;

$$Q_2 Q_1 = \left(\frac{a_{PbO_2} \cdot a_{SO_4^{2-}} \cdot a^4_{H^+}}{a_{PbSO_4} \cdot a^2_{H_2O}}\right)\left(\frac{a_{Pb} \cdot a_{SO_4^{2-}}}{a_{PbSO_4}}\right) \quad \textbf{(25)}$$

one can take the $a_{H_2O} = a_{Pb} = a_{PbSO_4} = a_{PbO_2} = 1$ then

$$Q_2 Q_1 = \left(a_{SO_4^{2-}} \cdot a^4_{H^+}\right)\left(a_{SO_4^{2-}}\right) = a^2_{SO_4^{2-}} \cdot a^4_{H^+} \quad \textbf{(26)}$$

substituting **Eq. 22** and **26** in to **Eq. 24** will give;

$$E_{cell} = 2.041 + \frac{2.3RT}{nF} log\, a^2_{SO_4^{2-}} \cdot a^4_{H^+} \quad \textbf{(27)}$$

finally, above equation can be re-written as;

$$E_{cell} = 2.041 + \frac{2.3RT}{nF}\left[2log a_{SO_4^{2-}} - 4pH\right] \quad \textbf{(28)}$$

It is now evident that the cell potential depends on the pH and the sulfate ion activity as well as the temperature. Thus, these parameters should be optimized in order to create the best operation conditions form the lead acid battery.

Table 2.1. Standard Gibbs free energies of the compounds in the $Pb/H_2SO_4/H_2O$ system[6].

Compounds	ΔG^0 (kj·mol^{-1})	Compounds	ΔG^0 (kj·mol^{-1})
Pb (crystal)	0	$PbSO_4$	-811.43
Pb^{2+} (aq.)	-23.98	1BS	-1017.79
Pb^{4+} (aq.)	-302.57	3BS	-1662.7
tet-PbO	-188.53	4BS	-1426.32
ort-PbO	-189.37	Pb_2O_3	-411.89
$HPbO_2^-$	-338.98	SO_4^{2-} (aq.)	-742.17
$Pb(OH)_2$	-421.01	HSO_4^- (aq.)	-753.05
α-PbO_2	-217.37	H_2SO_4	-742.17
β-PbO_2	-219.04	H_2O	-237.25
$5PbO{\cdot}2H_2O$	-1407.62	H^+ (aq.)	0.0
Pb_3O_4	-617.71	H_2 (gas)	0.0
PbO_3^{2-}	227.57		

2.4. Chemical and Electrochemical Reactions of $Pb/H_2SO_4/H_2O$ System

Potential versus pH diagram (E-pH diagram) of the $Pb/H_2SO_4/H_2O$ is the backbone of the lead acid battery thermodynamics. Similar E-pH diagrams, sometimes called Pourbaix diagrams, can be found for various electrochemical systems in the wonderful book by Marcel Pourbaix named Atlas of Electrochemical Equilibria in Aqueous Solutions[48]. E-pH diagram for the lead acid battery system first developed by the Delahay et. al. yet this diagram did not contained the stability regions for the basic lead sulfates that is commonly encountered in the lead acid battery[21]. Ruetschi and Angstadt re-drew the diagram just for the solid phases and utilized two different total sulfate activity ($a_{SO_4^{2-}}+a_{HSO_4^-}$), 1 and 10^{-7}, to highlighted the effects of the ion activity on the stability of the solid compound presents in the system[49]. Here it is clear that the by decreasing the total sulfate activity stability region of the $PbSO_4$ decreases and PbO (authors used $5PbO{\cdot}2H_2O$ instead of PbO but mentioned that these phases interchangeable) increases. Later, Barnes and Mathieson included these basic lead sulfates in to the diagram by Delahay et. al. (taking total sulfate activity as unity)and temperature as 25 °C) and presented a complete picture for both solid and ionic phases that present in the $Pb/H_2SO_4/H_2O$ system[38]. Following that Bullock developed a three-dimensional E-pH diagram for the $Pb/H_2SO_4/H_2O$ system by taking sulfate ion activity in to account and gave step by step explanation how to draw such diagrams.

One should note that there can be slight dissimilarities between the diagrams due small differences between the thermodynamic data used by the authors.

According to **Eq. 7** both sulfate and pH as well as the temperature effects the equilibrium potential between two compounds.

In that context similar E-pH diagram developed which also takes the temperature as an independent variable rather than constant at 25 °C[38]. Some comments about this also done back in 1965 but best to our knowledge no follow-up came. Even though some paid software's available, simple python program developed for the purpose of developing the E-pH diagram for the $Pb/H_2SO_4/H_2O$ system with varying pH, sulfate activity and temperature.

Reactions used for the graph given below. Reactions classified according to the oxidation state of the Pb in the compounds and similar to Ruetschi and Angstadt just the solid phases considered.

2.4.1. Reduction of Pb^{2+}

$$PbSO_4 + H^+ + 2e^- \rightarrow Pb + HSO_4^-$$

$$PbSO_4 + 2e^- \rightarrow Pb + SO_4^{2-}$$

$$1BS + 2H^+ + 4e^- \rightarrow 2Pb + SO_4^{2-} + H_2O$$

$$3BS + 6H^+ + 8e^- \rightarrow 4Pb + SO_4^{2-} + 4H_2O$$

$$4BS + 8H^+ + 10e^- \rightarrow 5Pb + SO_4^{2-} + 4H_2O$$

$$PbO + 2H^+ + 2e^- \rightarrow Pb + H_20$$

2.4.2. Reduction of $Pb^{2.67+}$

$$Pb_3O_4 + 3HSO_4^- + 5H^+ + 2e^- \rightarrow 3PbSO_4 + 4H_2O$$

$$Pb_3O_4 + 3SO_4^{2^-} + 8H^+ + 2e^- \rightarrow 3PbSO_4 + 4H_2O$$

$$2Pb_3O_4 + 3SO_4^{2^-} + 10H^+ + 4e^- \rightarrow 3 \cdot 1BS + 5H_2O$$

$$4Pb_3O_4 + 3SO_4^{2^-} + 14H^+ + 8e^- \rightarrow 3 \cdot 3BS + 4H_2O$$

$$Pb_3O_4 + 2H^+ + 2e^- \rightarrow PbO + H_2O$$

2.4.3. Reduction of Pb^{3+}

$$Pb_2O_3 + 2HSO_4^- + 4H^+ + 2e^- \rightarrow 2PbSO_4 + 3H_2O$$

$$Pb_2O_3 + 2SO_4^{2-} + 6H^+ + 2e^- \rightarrow 2PbSO_4 + 3H_2O$$

$$Pb_2O_3 + SO_4^{2-} + 4H^+ + 2e^- \rightarrow 1BS + 2H_2O$$

$$2Pb_2O_3 + SO_4^{2-} + 6H^+ + 4e^- \rightarrow 3BS + 2H_2O$$

$$3Pb_2O_3 + SO_4^{2-} + 6H^+ + 4e^- \rightarrow 3BS + 2H_2O$$

$$Pb_2O_3 + 2H^+ + 2e^- \rightarrow 2PbO + H_2O$$

$$3Pb_2O_3 + 2H^+ + 2e^- \rightarrow 2Pb_3O_4 + H_2O$$

Even though many authors found that the Pb_2O_3 do not appear in the diagram due to the fact Pb to PbO oxidation and PbO_2 to PbO reduction energetically more favorable to Pb to Pb_2O_3 and PbO_2 to Pb_2O_3 reactions governing equations still presented[21], [38], [49], [50].

2.4.4. Reduction of Pb^{4+}

$$PbO_2 + HSO_4^- + 3H^+ + 2e^- \rightarrow PbSO_4 + 2H_2O$$

$$PbO_2 + SO_4^{2-} + 4H^+ + 2e^- \rightarrow PbSO_4 + 2H_2O$$

$$2PbO_2 + 6H^+ + SO_4^{2-} + 4e^- \rightarrow 1BS + 3H_2O$$

$$4PbO_2 + 10H^+ + SO_4^{2-} + 8e^- \rightarrow 3BS + 4H_2O$$

$$PbO_2 + 2H^+ + 2e^- \rightarrow PbO + H_2O$$

$$3PbO_2 + 4H^+ + 4e^- \rightarrow Pb_3O_4 + 2H_2O$$

$$2PbO_2 + 2H^+ + 4e^- \rightarrow Pb_2O_3 + H_2O$$

2.4.5. Chemical reactions

$$SO_4^{2-} + H^+ \rightarrow HSO_4^-$$

$$1BS + SO_4^{2-} + 2H^+ \rightarrow 2PbSO_4 + H_2O$$

$$3BS + SO_4^{2-} + 2H^+ \rightarrow 2 \cdot 1BS + 2H_2O$$

$$4PbO + SO_4^{2-} + 2H^+ \rightarrow 3BS$$

Note that since none of the independent variables taken as constant, equilibrium potential equation for each reaction are not given, but if one interested to find the equations several references are available derived for room temperature[21], [38], [49], [50].

2.5. E-pH Diagrams of the $Pb/H_2SO_4/H_2O$ System

Independent variables temperature and pH are easy to integrate in to the diagram however, for the total sulfate activity certain assumptions must be made. Here, figure presented by Pavlov

et. al. in which concentration of HSO_4^- and SO_4^{2-} are given in terms of the H_2SO_4 concentration is used to determine the activities, see figure 18 in the article[51]. Following suit, since SO_4^{2-} concentration is practically not affected by an increase in H_2SO_4 concentration after 1 M H_2SO_4, activity of the HSO_4^- asymptotically approaches unity after 1 M H_2SO_4. Below 1 M H_2SO_4 total sulfate activity and the H_2SO_4 molarity are used interchangeably. As an example, one can assume, when H_2SO_4 molarity is 0.1 M, then the total sulfate activity is also taken as 0.1, etc., assuming the that the activity coefficient is 1 (one).

$$a \cdot H_2SO_4 \leftrightarrow x \cdot HSO_4^- + y \cdot SO_4^{2-} + z \cdot H^+ \quad \textbf{(29)}$$

Here, "x" and "y" in the **Eq. 29** are used as the activities of the HSO_4^- and SO_4^{2-} ions, respectively and they depend on "a", the concentration of H2SO4, based on the figure 18 in the article by Pavlov et. al.[51]. It is obvious that these assumptions are not ideal yet it is believed that they are adequate to understand the changes that occur at the E-pH diagram of $Pb/H_2SO_4/H_2O$ system.

Figure 2.1 shows several E-pH diagrams for $Pb/H_2SO_4/H_2O$ system. It can be said that the main stability regions affected are the fields for $PbSO_4$ and PbO. Especially, when the H_2SO_4 concentration is increased the $PbSO_4$ stability region shifts to much more acidic regions. Simultaneously equilibrium potential of the $PbO_2/PbSO_4$ decreases slightly. Temperature on the other hand, seem to affect the chemical reactions more strongly. The influence can be observed in the shifts in vertical lines. As the temperature increased from 298 K (25 ℃) to 323 (50 ℃), all the vertical lines shift to more acidic values. Hence, one can say that the temperature is a critical factor that especially influences the paste preparation step of the lead acid battery manufacturing process.

As a disclaimer, here, diagrams are not meant to be 100% accurate but they should provide a general guideline for the evolution of the thermodynamics of the $Pb/H_2SO_4/H_2O$ system in the lead acid battery production.

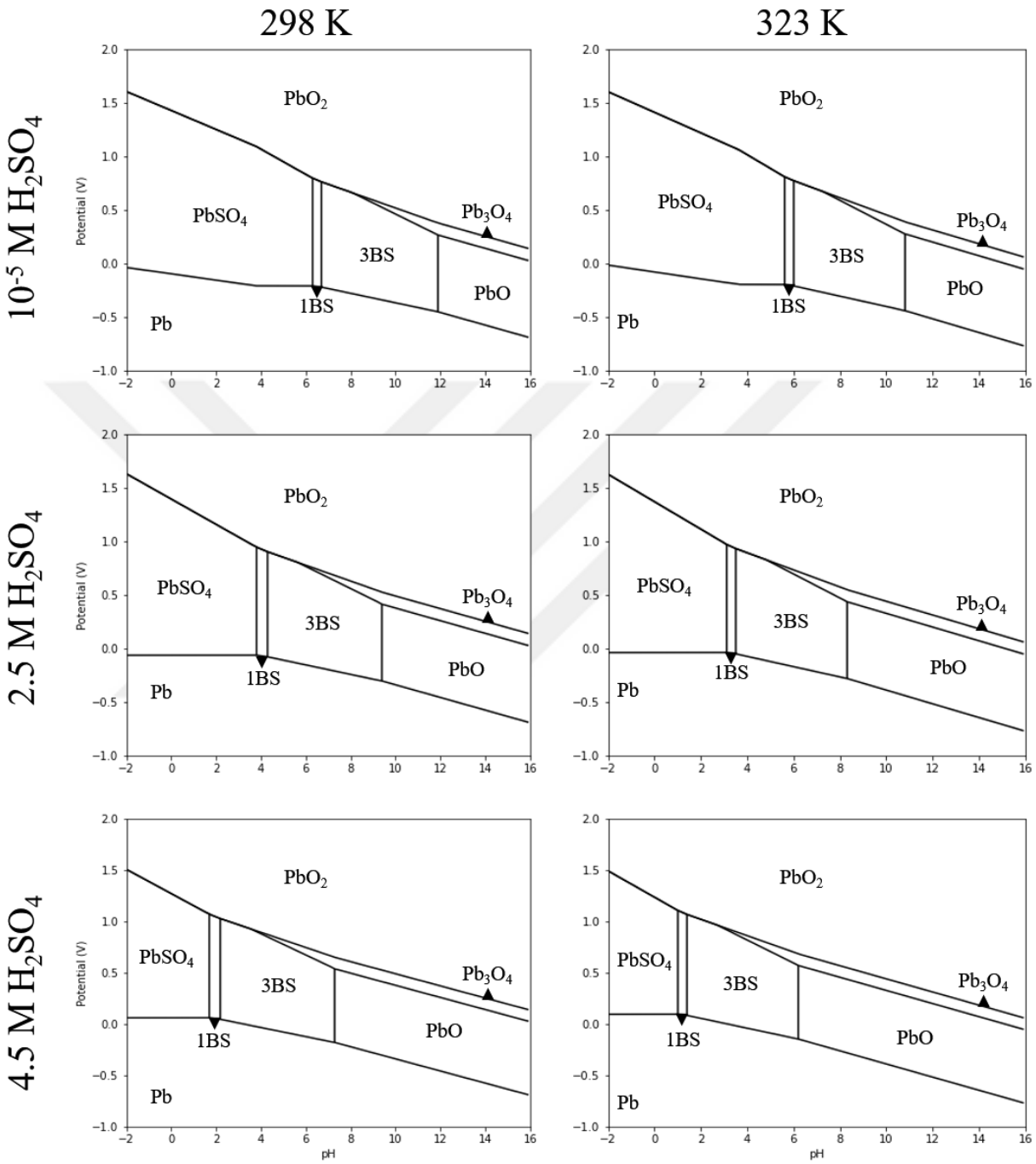

Figure 2.1. *E-pH diagrams with different temperature and H_2SO_4 concentrations.*

3. LEAD DIOXIDE

As mentioned, there are two crystal polymorphs of the PbO_2 structure, α-PbO_2 and β-PbO_2 also called as scrutinyite and plattnerite, respectively. β-PbO_2 first identified in 1845[52]. Existence of the α-PbO_2 discovered in 1946 by Kameyama and Fukumoto[6], [53], presence of the α-PbO_2 modification of the PbO_2 in the PAM first detected by Bode and Voss in 1956[54] and natural occurrence of this mineral latter proved in 1988[55]. These two modifications quite differ between each other in terms of crystal structures, chemical properties, electrochemical characteristics and stabilities, are considered. Following sections will investigate the characteristics of each polymorph.

3.1. Crystal Structure and Physical Properties of PbO_2 Polymorphs

α-PbO_2 polymorph has an orthorhombic structure similar to that of columbite. Lattice constants of this phase are[6];

$$a=4.938\text{Å};\ b=5.939\text{Å};\ c=5.486\text{Å}$$

Space group given as Pbcn, and each Pb atom has six-coordinate place in the center of an O octahedra. This octahedras chained in a zigzag manner which is different form the β-PbO_2. β-PbO_2 has a tetragonal symmetry and rutile like crystal structure. Lattice parameters can be given as[6], [33];

$$a=4.945\text{Å};\ c=3.378\text{Å}$$

Again, the Pb atom place in the middle of octahedra comprise of 6 neighboring O atoms. But the packing of the octahedras in β-PbO_2 occurs as a linear chain in the *c* direction. β-PbO_2 phase $P4_2/mnm$ as a space group. **Figure 3.1** gives the structure and the octahedral arrangement of the PbO_2 polymorphs.

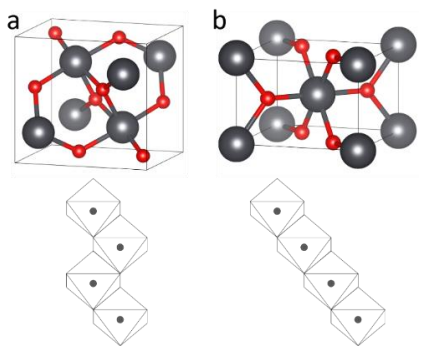

Figure 3.1. *Crystal structure and octahedral packing of (a) α-PbO_2 and (b) β-PbO_2.*

Pb-O distance for both modifications is similar around 2.16 Å[33]. Pavlov stated that the octahedral arrangement is the main difference between the PbO_2 modifications and β polymorph has well defined O layers[6]. Mindt measured the resistivities of the electrodeposited α-PbO_2 and β-PbO_2 modifications as 10^{-3} ohm·cm and 10^{-4} ohm·cm, respectively[33]. Actually, the α-PbO_2 has higher carrier concentration between the two polymorphs yet the mobilities of these carriers about 10 times lower compared to the β-PbO_2 modification. Mindt stated that difference in mobility can depend on several reasons but essential difference that reduces the α-PbO_2 carrier mobility is the octahedral packing[33]. Thomas also measured the conductivity of the dense PbO_2 samples and found the resistivity as $2 \cdot 10^{-4}$ ohm·cm and stated that the PbO_2 has tetragonal rutile like structure with lattice parameters of a=4.95Å; c=3.36Å, but no mention of the α-PbO_2 is found, probably samples contained some α-PbO_2 which makes the value $2 \cdot 10^{-4}$ ohm·cm very reasonable[56]. Measured densities of the PbO_2 modifications taken from the PAM as well as a deposited crystals reveals that the α-PbO_2 slightly denser while the samples taken from the PAM have lower densities compared to the electrodeposited samples[6]. Micka *et. al*. stated that the density measurements of the PbO_2 present in the PAM support the fact that some of the PbO_2 is amorphous which lowers the density[57]. This property of the PAM makes the quantitative XRD analysis problematic along with the fact the tet-PbO and α-PbO_2 has overlapping characteristic peaks[6], [58]. **Table 3.1** gives the XRD patterns for several lead compounds that is common in the lead acid battery. The d = 3.12 Å peak, highlighted with dark red, is a characteristic for some of the lead compounds and causes some problem for quantitative XRD characterization, causing overlap and broadening. Especially, the overlap between the tet-PbO and α-PbO_2 must carefully investigated for XRD analysis[6]. Pavlov et. al. investigated the phase composition evolution during formation with different acid concentration, according to their results, d = 3.12 Å initially represents the both tet-PbO and α-PbO_2 but after about 8 hours of formation, simultaneous chemical and XRD analysis shows that the d = 3.12 Å peak represents the α-PbO_2[46]. Note that XRD technique can quantitively identify the β-PbO_2[58], [59].

Table 3.1. *Calculated X-ray diffraction data for some lead compounds*[58], [59]. *Relative Intensity, RI > 10 listed.*

Pb

2θ	RI	h k l	d_{hkl} (Å)
31.27	100	111	2.86
36.26	50.3	002	2.48
52.22	34.6	022	1.75

tet-PbO

2θ	RI	h k l	d_{hkl} (Å)
28.62	**100**	**011**	**3.12**
31.83	31.6	110	2.81
35.72	11.3	002	2.51
45.63	15.7	020	1.99
48.59	25.2	112	1.87
54.76	30.4	121	1.67
59.26	10	022	1.56
59.9	10.8	013	1.54

ort-PbO

2θ	RI	h k l	d_{hkl} (Å)
29.08	100	111	3.07
30.32	24.9	200	2.95
32.6	21.6	020	2.74
37.81	16.7	002	2.38
45.12	15	220	2.01
49.21	12.3	202	1.85
50.77	11.7	022	1.80
53.1	18.9	311	1.72
56.03	14.5	131	1.64

3BS

2θ	RI	h k l	d_{hkl} (Å)
9.03	45	100	9.788
14.14	11	010	6.259
15.34	26	110	5.772
18.15	17	-110	4.884
20.88	19	210	4.25
25.04	12	-210	3.553
27.31	100	300	3.263
28.50	51	020	3.129
28.96	27	212	3.081
30.96	24	220	2.886
31.54	11	-120	2.834
32.01	12	302	2.794
32.87	17	-112	2.723
33.18	15	-310	2.698
35.92	18	320	2.498
43.54	14	-320	2.077

$PbSO_4$

2θ	RI	h k l	d_{hkl} (Å)
20.81	72.3	101	4.27
20.93	28.4	020	4.24
23.33	51.1	111	3.81
24.56	19.9	120	3.62
25.58	28	200	3.48
26.71	82.5	021	3.33
27.69	66.8	210	3.22
29.68	100	121	3.01
32.35	37.9	211	2.77
33.17	44.1	002	2.70
37.32	17.5	221	2.41
39.55	18.5	022	2.28
41.7	27.3	122	2.16
43.73	45.3	212	2.07
43.76	50.1	311	2.07
44.54	35.1	231	2.03
44.64	33.6	140	2.03
45.95	22.3	041	1.97
50.88	18.7	330	1.79

Pb_3O_4

2θ	RI	h k l	d_{hkl} (Å)
14.2	11.3	110	6.23
26.35	100	121	3.38
28.63	13.1	220	3.12
30.76	37.8	112	2.90
32.09	48.7	130	2.79
34.03	26.2	022	2.63
44.54	10.1	141	2.03
46.02	11.1	240	1.97
47.48	19	123	1.91
49.81	23.7	042	1.83
52.06	25.5	332	1.76
58.04	12.2	251	1.59

α-PbO_2

2θ	RI	h k l	d_{hkl} (Å)
23.25	21.6	110	3.82
28.47	**100**	**111**	**3.12**
32.74	17.4	002	2.73
34.3	19.3	021	2.61
35.97	11.6	200	2.49
49.43	15.4	202	1.84
49.43	12.6	130	1.84
50.55	17.5	221	1.80
55.86	14.6	113	1.64

β-PbO_2

2θ	RI	h k l	d_{hkl} (Å)
25.4	100	110	3.50
31.98	95.2	011	2.80
36.23	28.4	020	2.48
49.09	68.1	121	1.85
52.16	14.7	220	1.75
58.88	15.8	130	1.57

Reason for the similarities between the characteristics peak of the tet-PbO and the α-PbO_2 can be explained by analyzing their crystal structures. **Figure 3.2** represents the crystal structures of tet-PbO and α-PbO_2 as well as the Pb metal. This similarity first discovered by Bode and Voss[54]. Considering the positions of the Pb, tet-PbO and α-PbO_2 in the E-pH diagram, it can be said that the when the thermodynamic conditions are satisfied (which is the case for lead acid battery system) Pb first oxidizes to tet-PbO then the α-PbO_2. Pavlov and Rogachev investigated the such transformation and stated that when the tet-PbO to PbO_2 transformation occurs in solid state, α-

PbO_2 modification is formation and further reaction depends on the O species concentration on the tet-PbO[60].

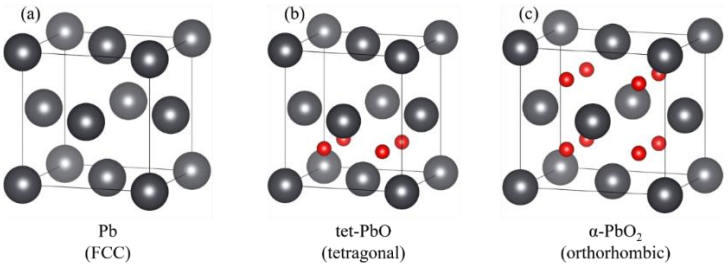

Figure 3.2. *Crystal structures of (a) Pb, (b) tet-PbO and (c) α-PbO_2.*

White *et. al*. investigated the polymorphism of the oxides of lead. Uniaxial pressures and temperatures up to 60,000 atm and 600 ℃ are used, respectively, to investigate the phase stability of the possible phases[61]. It is stated that the high-pressure form is the α-PbO_2 modification, authors also measured the lattice parameters of the α-PbO_2 as 4.988, 5.962 and 5.466 Å for a, b and c, respectively, which is quite accurate[61]. Phase transition between the α-PbO_2 and β-PbO_2 said to be reversible. It is said that the α-PbO_2 shows no sign of transformation to β-PbO_2 at room temperature but, when TEM increased to 100 ℃ trace amount of β-PbO_2 phase observed in 2 weeks. Regardless it is evident that the phase transition is sluggish. Heat of transition is calculated as 46 kJ·mole^{-1} at 1 atm and 32 ℃ by using Clapeyron equation[61]. Resulting *PT* phase diagram presented below[61].

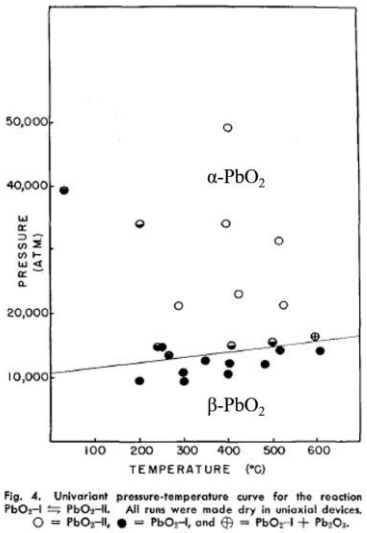

Figure 3.3. *PbO_2 phase diagram drawn by White et. al.*[61]
Empty, filled and crossed spheres represents α-PbO_2, β-PbO_2 and β-PbO_2 + Pb_2O_3, respectively.

3.2. Chemical Properties of PbO_2 Polymorphs

Stoichiometric ratio for the lead dioxide that found in the PAM structure is not 1:2 even though material normally represented by chemical formula of PbO_2. As stated earlier that electrochemically prepared α-PbO_2 being less ordered structure between the crystal modifications[33]. Later Moseley *et. al*. investigated defect structure of two polymorph with TEM imaging and also found that the α-PbO_2 has higher degree of disorder compared to the β modification[62]. Bagshaw *et. al*. produced several α-PbO_2 and β-PbO_2 samples with different routes and from their results α and β stoichiometry can be written as $PbO_{1.80\text{-}1.83}$ and $PbO_{1.81\text{-}1.98}$, respectively[26]. Addition to the its non-stoichiometric nature it is stated that the PbO_2 also has an amorphous modification[30]–[32], [63]. Caulder and Simon investigated the thermal behavior of the positive electrode and stated that the PAM also contains some amorphous PbO_2 as well as the other two modifications and this structure goes reordering as the battery is cycled facilitated by the loss of the hydrogen species[63]. This amorphous PbO_2 later investigated by the Pavlov and his coworkers and they found that the PbO_2 material comprise of different regions and has a heterogenous structure[30]–[32], [64].

4. OXIDATION TO LEAD DIOXIDE

There are many ways to investigate the PbO_2 oxidation in H_2SO_4 solution. Two main ones described here. First, electrodeposition on the positive (mostly Pb or Pt) electrode with or without addition of Pb ions in the H_2SO_4 solution, if the Pb electrode cycled this process also called Planté Process. Second, is the formation of the PbO_2 from the basic lead sulfate pastes like in the lead acid battery formation also called Faure process. For simplicity, first one will be mentioned as electrodeposition and latter is formation. Both methods are useful to identify the oxidation behavior of the PbO_2 in the acidic environment.

In the following chapters these two main mechanisms will be discussed in the context of thermodynamics and morphology of the PbO_2.

4.1. Electrodeposition of Lead Dioxide

Burbank found that the Pb electro surface consist of both α-PbO_2 and β-PbO_2 while the electrolyte oxide interface mainly consists of the "common tetragonal" lead dioxide (β-PbO_2). She also stated that the discharge efficiency of the β-PbO_2 is higher than the α-PbO_2 in 1.21 s.g. H_2SO_4 solution[65]. Morphological study showed that the α-PbO_2 that separated from the anodic surface

(substrate) is 0.1 μm in diameter and no apparent crystal form[65]. Formation of the α-PbO_2 at the places that closer to metal surface and mostly isolated from the acid medium is facilitated by the migration of the H^+ ions to the bulk of the solution hence increases the pH such that according to E-pH diagram α-PbO_2 is stable in those conditions and rate of α-PbO_2 transformation depends on the oxygen diffusion through the electrolyte/material interface[65]. Finally Burbank suggested that the sulfate deficient compounds can be used to improve the fraction of the α-PbO_2 in the oxidation product[65]. This statement later found to beneficial with usage of paste materials.

Ikari *et. al*. investigated the discharge behaviors of the PbO_2 polymorphs in 1.28 s.g. H_2SO_4 solution and it can be seen that β-PbO_2 output found to be larger than the α-PbO_2[34]. He also stated that the discharge progresses from surface to interior of the oxidation product. Importantly he stated that dischargeable thickness for α-PbO_2 and β-PbO_2 are 0.3-0.4 μm and 1 μ, respectively, when the material considered pore free[34]. While he did not supplied any image he stated that α-PbO_2 has fiber crystal structure when deposited in alkaline environment[34].

Mark more focused on the α-PbO_2 characteristics in 0.1 M H_2SO_4 solution and stated that the theoretical and actual capacity of the α-PbO_2 electrode is significantly different latter being lower[66]. He also found that α-PbO_2 discharge efficiency is limited and when the α-PbO_2 discharge appears to reached a steady state he removed the electro and stated that surface is covered with very adherent $PbSO_4$ layer[66]. Then this $PbSO_4$ layer is removed from the surface of the α-PbO_2 by washing with $NH_4C_2H_3O_2$, it was found that surface is no longer smooth, this means that $PbSO_4$ forms in the active sites in the α-PbO_2 crystals[66]. When, this now $PbSO_4$ free, electrode placed back in the electrolyte the discharge continued. Repeating this process 80-90% of the theoretical discharge was possible. $HClO_4$ as an electrolyte also used for discharge of the α-PbO_2 up to 94% theoretical discharge was possible without the washing process[66]. For the β-PbO_2 electrodes, Mark stated that β-PbO_2 surfaces had rougher appearance and $PbSO_4$ on the electrode surface was scattered on the electro and washing did not facilitated further discharge. Noticeably, formation of the $PbSO_4$ as a discharge product on the α-PbO_2 and β-PbO_2 also different according to this study. When $PbSO_4$ forms on the α-PbO_2 it covers the surface with adhesive film which leads the reduction on the discharge efficiency[66].

Ruetschi and Angstadt showed that, there are different reactions takes place above and below the oxidation product and stated that the reason is the local differences between the pH

values[49]. They constructed E-pH diagrams that contains the basic lead sulfates as well. They found that depending on the potential several anodic peaks, Pb to $PbSO_4$ and $PbSO_4$ to β-PbO_2, are observed when the Pb-Ca electrode immersed in 4.2 M H_2SO_4 solution[49]. They stated if the applied potential is increased above a certain value $PbSO_4$ to β-PbO_2 oxidation occurs at a such rate, which is facilitated by nucleation, of β-PbO_2, that alkalization of the interior might impeded. They constructed two E-pH diagrams with different SO_4^{2-} and HSO_4^- activities, from the diagrams it can be seen that the stability regions of compounds with poor sulfates characteristics e.g. PbO, 3BS and 1BS, increases with decreasing sulfate ion activities[49]. Such low activities can be produced at the interior of the oxidation product due to shielding form the acid attack and dense $PbSO_4$ layer causes a high electric field which repels the H^+ ions and stabilize the alkaline environment in the interior. Increasing the stability regions of poor sulfates and medium becomes more alkaline α-PbO_2 oxidation takes place more readily and with lower potentials then the $PbSO_4$ to β-PbO_2 oxidation. They highlighted the effect of the pH gradient and gave a schematic description for the electrodeposition product that forms on the Pb alloy electrode[49]. **Figure 4.1** shows a schematic of the corrosion products as function of reference electrode potential and distance from the surface[49]. Note that the formation of a species like PbO, 3BS, 1BS and α-PbO_2 is explained logically by pH gradients that facilitated by the ionic diffusion[49].

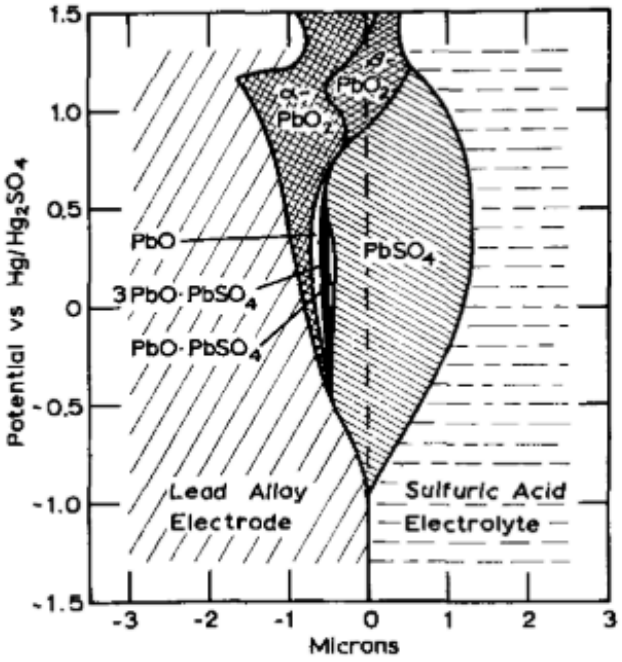

Figure 4.1. *Schematic of the theoretical model of the corrosion product composition*[49].

Pavlov studied the anodic oxidation of the Pb in 1 N H_2SO_4 solution and also stated that there is a pH gradient that results of the formation of poor sulfates[67], [68]. It stated SO_4^{2-} (and HSO_4^-) concentrations determined by the bulk H_2SO_4 concentration and Pb^{2+} concentration determines by the anodic reaction. When the rate Pb^{2+} formation exceeds the SO_4^{2-} diffusion electroneutrality achieved by H^+ migration towards the bulk of the solution since H^+ has 5 times the mobility Pb^{2+}. Here Pb^{2+} can be supplied from the $PbSO_4$ or Pb electrode. Microscopic investigation showed that the $PbSO_4$ forms at the surface of the Pb electrode rather uniform when the applied potential is raised the darker PbO_2 particle deposition is clearly on these $PbSO_4$ particles[67]. Also needle like $PbSO_4$ crystals observed on the Pb electrode as well, when the oxidation proceeded galvanostatically[65].

Pavlov et. al. investigated the potentiostatic oxidation of the Pb electrode in 1 N H_2SO_4 solution (pH about 0.3). Their results tabulated at **Table 4.1**, note that these results are in line with the E-pH diagram constructed by the Ruetschi and Angstadt[49]. It should be noted however when the Pb electrode first immersed in H_2SO_4 solution only interface is the Pb/H_2SO_4 interface and when the potential is increased to value where the $PbSO_4$ is stable this will be the only phase present. When the $PbSO_4$ layer forms, alkalization process can take place which explains the other divalent lead compounds that formed in the anodic layer when potential increased to -300 to 900 region[69].

Table 4.1. *Phase composition of the anodic layer as a function of potential*[69].

Potential (mV vs. Hg/Hg_2SO_4)	**Phase Composition**
-956 to -300	$PbSO_4$
-300 to 900	Large amount $PbSO_4$ tet-PbO Small amounts of; 1BS, 3BS, $5PbO{\cdot}2H_2O$ or ort-PbO and α-PbO_2
Above 900	Increase in α-PbO_2 content
Above 1200	β-PbO_2 formation

Also note that according to Pavlov *et. al*. first tetravalent lead compound that forms in the acidic environment is the α-PbO_2 which is known to form in the basic environments[29], [34], [36], [37]. Additionally, some of their oxidation runs α-PbO_2 formed in the -100 to 200 range which they stated;

"*This shows that between -200 and + 900 mV the formation of α-PbO_2 is determined by fortuitous factors*."[69].

Note that, this is also possible according to E-pH diagram of the Pb/H_2SO_4/H_2O system[49]. Following that, Pavlov and Rogachev stated that the PbO to α-PbO_2 transformation occurs in solid state while if the PbO first dissolves in the solution β-PbO_2 forms as a oxidation product[60].

Pavlov also studied the solid-state anodic oxidation of the Pb electrode in H_2SO_4 solution[70]. Here author suggested when the potential is kept in the lead oxide region, -400 to 950 mV against Hg/Hg_2SO_4 electrode, tet-PbO forms between the Pb electrode and the porous $PbSO_4$ layer as given in the **Figure 4.2**[70] which is similar to anodic product described by the Ruetschi and Angstadt[49].

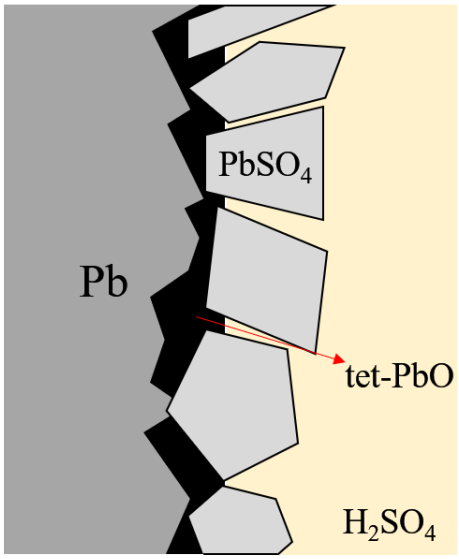

Figure 4.2. *Schematic of the anodic layer in the lead oxide potential region*[70].

Further formation of the tet-PbO depends on the oxygen transport through the formed tet-PbO layer similar to parabolic oxidation law. Hence the oxidation rate of the Pb determined by the ionic conductivity of the tet-PbO layer[70]. It stated that the main ion determining the oxidation is the

oxygen and Pb^{2+} do not affect the oxidation of the Pb electrode[71]. When the Pb electro oxidized in 7 N H_2SO_4 solution with to PbO_2 potential region α-PbO_2 is the main tetravalent lead compound up to 1530 mV vs Hg/Hg_2SO_4 then β-PbO_2 starts to form notice that the 1530 mV is more than the value given at **Table 4.1** reason for this is the higher acidity of the solution, according to E-pH diagram equilibrium potential between the $PbSO_4$/β-PbO_2 raises with decreasing pH[49]. Pavlov summarized to oxidation of the Pb to PbO_2 as follows; first, Pb oxidize to tet-PbO then tet-PbO oxidizes to α-PbO_2 is the formation is in solid state or β-PbO_2 if the formation reaction is dissolution precipitation[70].

Pavlov and Rogachev studies the effect of the anodic oxidation current density on the morphology of the anodic deposit. When the current density 0.4 $mA{\cdot}cm^{-2}$ is used for 48 hours the anodic product consist of needle like acircular particles and some spherical one coming together to form agglomerates. Instead, if current density increased to 19 $mA{\cdot}cm^{-2}$ needle like morphology seems to disappear and interconnected aggregates are formed[60]. They stated that the acircular morphology appeared when the current density 0.4 $mA{\cdot}cm^{-2}$ is used belong to the β-PbO_2 polymorph[60]. Again the similarity between tet-PbO and α-PbO_2 highlighted and stated that the this transformation occurs in solid state which facilitated by the oxygen species and concentration of these species determines the transformation rate[60].

Continuing his work on the electrochemical oxidation behavior of the PbO, Pavlov stated that there are numerous non-stoichiometric, assigned PbO_n, anodic oxidation product exists between the PbO-PbO_2 and this PbO_n forms in the tet-PbO lattice without nucleation[72]. Referencing the work by Lappe[73], Pavlov commented that the critical n value for the PbO_2 formation is about 1.4[72]. Also, this transformation appears to be starts (reaching the critical n value) when sufficient amount of charge passed through the system independent from the potential sweep rate[72]. Morphology of the anodic products investigated by the electron microscopy and large well shaped crystals identified as $PbSO_4$ while darker phase said to be PbO_2. Author state PbO_2 particles forms between the $PbSO_4$ pores[72] and almost none of the $PbSO_4$ effected by the formation of the PbO_2. This result can be interpreted as the formed PbO_2 most likely the α-PbO_2 because of two reasons; first, formation potential stated as 1050 mV vs. Hg/Hg_2SO_4 electrode and H_2SO_4 concentration used as 1 N, in these conditions, β-PbO_2 formation not likely according to E-

pH diagram for the $Pb/H_2SO_4/H_2O$ system. Second, $PbSO_4$ surface layer appears to be unaffected by the formation of the PbO_2.

Cong and Chartier investigated the charge-discharge characteristic of the α-PbO_2 and β-PbO_2 as well as the morphologies of these polymorphs. Interestingly, they stated that the electrodeposited α-PbO_2 had better recharge current compared to the electrodeposited β-PbO_2[35]. They attribute this behavior to the different formation morphology of the $PbSO_4$ on the PbO_2 samples. It is stated $PbSO_4$ film formed on the α-PbO_2 while $PbSO_4$ formed from the β-PbO_2 appeared more localized[35]. They stated, during cycling of the pure α-PbO_2 in H_2SO_4 electrolyte β-PbO_2 forms via α-PbO_2 to $PbSO_4$ to β-PbO_2 transformation. Surprisingly, they concluded formation β-PbO_2 lowers the capacity of the initially pure α-PbO_2 samples[35]. Point that authors did not mentioned the effect of the morphology of the α-PbO_2 and β-PbO_2 before the discharge. Their SEM images shows that α-PbO_2 appears to be much more porous compared to the β-PbO_2 even with the cycling, it can be said that the β-PbO_2 still less porous then the α-PbO_2 which can affect the charge-discharge characteristics of the sample[35].

Similar results shared by Ruetschi that is discharge performance of α-PbO_2 fund to be better[27]. However, here, author used chemically produced PbO_2 samples and finalized their statement by saying that the electrochemically produced β-PbO_2 yields higher capacities. These higher capacities in defective structures attributed to presence of Pb^{2+} cation in the PbO_2 structures[27].

Takehara and Kanamura deposited β-PbO_2 on to the gold plate and commented on the transformation of the $PbSO_4$ to β-PbO_2 in acidic environment[74]. Authors described three stage process;

"*(i) the formation of the thin lead dioxide layer at the interface between lead sulfate and the gold plate; (ii) the two-dimensional growth of the thick lead dioxide layer at the inner part of lead sulfate film; and (iii) the oxidation of lead sulfate near the interface between lead sulfate and a sulfuric acid solution."*[74]

Their description is similar to Pavlov's[70] yet results of these authors shows no α-PbO_2 formation. Schematic representation of their 3-stage formation given in the ***Figure 4.3***[74].

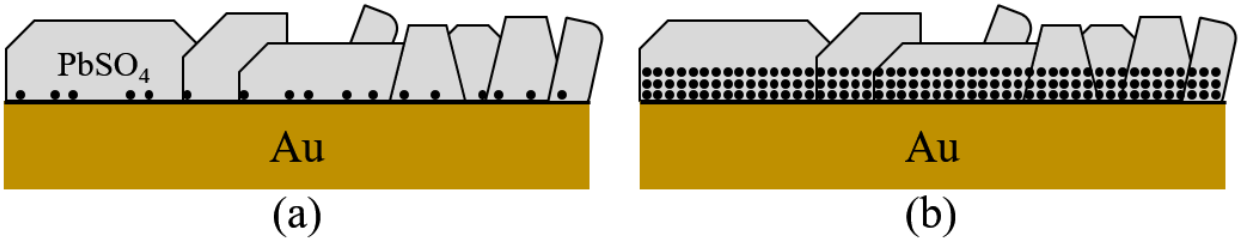

Figure 4.3. *(a) Active oxidation sites (black dots) at $PbSO_4$ gold interface (b) β-PbO_2 formation*[74].

Same authors also investigated the oxidation behavior of the $PbSO_4$ to PbO_2 and stated that the increasing the acid concentration results in the decrease in the crystal size of the PbO_2 deposit[75]. Note that this is in line with the E-pH diagram if we make the analogy that the potential and temperature equivalent and increasing the ΔT (equivalently ΔV) increases the nucleation. In this example the ΔV decreases if the applied formation voltage kept constant and acid concentration is increased since the equilibrium potential of the $PbO_2/PbSO_4$ electrode increases with decreasing pH (or increasing acid concentration).

Electrodeposition of PbO_2 on to titanium (Ti) substrate investigated by the Munichandraiah, and Sathyanarayana[76]. Even though these authors did not used H_2SO_4 solution, couple of helpful remarks are done. They stated that α-PbO_2 deposition efficiency is lower than the β-PbO_2 and deposition to same thickness takes longer time, once the α-PbO_2 deposited its firmly holds the Ti substrate if the solution stirred midly[76].They continue by saying;

"*in the absence of such a stirring formation took place of a loosely bound reddish brown oxide of lead which subsequently became detached from the anode*"[76].

Herron et. al. examines the $PbO_2/PbSO_4$ cycling with in-situ XRD. Additionally, authors stated it is in fact possible to deposit pure α- and β- polymorphs in acidic lead nitrate solution on to platinum (Pt) substartes[37]. The said to be α-PbO_2 best produced when the pH 4.3 with current density of 3.5 $mA{\cdot}cm^{-2}$ while β-PbO_2 prefers to form at lower pH and higher current densities. Authors mentioned their concerns with the lack of raw XRD data in the literature and question the purity claims. They investigate the how the composition of the anodic product changes depending on the pH, deposition time and deposition current density. **Table 4.2** summarized their results[37].

Table 4.2. *Summary of the XRD results from Ref.*[37]. *0.1 mol·dm^{-3} lead nitrate used for all samples*[37].

Constant Variables	Independent Variable		Result
Current Density 3.5 mA·cm^{-2} Charge 2.15 C·cm^{-2}	pH	4.3	As the pH drops β peak becomes more dominant also Pt peak intensity increases. Pure α and β deposition observed at pH 4.3 and 0, respectively.
		1.0	
		0.5	
		0	
Current Density 3.5 mA·cm^{-2} pH 4.3	Deposition Time (s)	0	Pure α-PbO_2 deposition, also, Pt peak intensity drops significantly. Apparently, α-PbO_2 forms as a surface layer on the Pt substrate.
		180	
		360	
		600	
pH 0.5 Charge 5.15 C·cm^{-2}	Current Density (mA·cm^{-2})	0.9	Increasing the current density greatly hinders the α-PbO_2 formation, at 7 mA·cm^{-2} no α-PbO_2 peak observed.
		3.5	
		7	
		14	

Alongside with the results above Herron *et. al*. investigated the reduction of the deposited α-PbO_2 with different voltage scan rates. As the scan rate increased several trends can be observed, first the reduction potential peak drops to lower values alongside with the charge associated with the reduction process, also peak current density increased as the voltage scan rate increased[37]. Following this work Herron *et. al*. investigated the transformation of the α-PbO_2 to β-PbO_2 upon cycling. Their XRD results clearly shows the gradual transformation of the α-PbO_2 to β-PbO_2, even though this result mentioned earlier raw XRD data presented in this paper makes the argument more compelling[36].

Effect of pH on the anodic product composition also investigated by the Monahov *et. al*. by cycling the Pb electrode in H_2SO_4 solution[77]. They stated pH of the H_2SO_4 solution also effects the oxidation/reduction kinetics as well as the composition of the anodic product. In dilute H_2SO_4 solution $PbSO_4$ dissolution is higher leads to faster oxidation while if the concentrated acid is used and $PbSO_4$ solubility deceased which leads to lower oxidation rate and some unoxidized $PbSO_4$. In this paper authors classified the anodic layer in to 3 sublayers namely, outer, middle and inner. As a function of solution pH composition of each layer differs with different characteristics.

For all sublayers when pH -1 α-PbO_2 and tet-PbO are dominant (as mentioned these phases quite similar with almost equivalent characteristic peak) and as the pH increases to 0 β-PbO_2 starts do dominate with the exception being the inner sublayer. However, one should take this α-PbO_2/tet-PbO peak dominance at the outer sublayer with a grain of salt since tet-PbO may form as a anodic product during potential sweeps[69], [70]. Even authors admitted by saying;

"*This outer sub-layer contains more α-PbO_2 than β-PbO_2. Such a phase composition of the anodic layer is rather 'strange'* "[77]

Rather interesting morphologies occurred when the cycling proceeded at pH -0.25 with different time frames. When sample cycled for 1 h oxidation product appears to be rectangular agglomerates which is somewhat similar to PAM produced from the 4BS pastes[17] but again note that these samples produce by cycling a lead electrode. However, when the electrode cycled for 16 hours more spherical morphology appeared[77]. Finally, authors stated the H_2SO_4 concentration influences the crystal/hydrated-surface/solution interfaces and if pH interval of -1 to 0 is used the hydrated zones dominates which lowers the crystallinity[77]. These interfaces structures explained more thoroughly in next chapter.

Devilliers *et. al*. conducted cyclic voltammetry experiments to shine a light on the PbO_2/$PbSO_4$ transformation[29]. Before that they deposited several PbO_2 samples in different mediums on to the Ebonex® substrates[29]. Authors stated all the samples were textured and the modification formed in the alkaline medium found to be highly non-stoichiometric[29], which is consistent with the literature that the α-PbO_2 is stable at high pH region and has lower oxygen content[25], [33], [44]. Also, in the alkaline mediums high amount of Pb^{2+} detected and it is stated that the non-stoichiometric nature of the deposited formed at the alkaline medium facilitated by these high amounts of Pb^{2+} cations[29]. By using the **Eq. 1** one can see that if the Pb^{2+} incorporated in to the PbO_2 crystals in order to reach the electro neutrality oxygen leaves the system. For convenience, similar form of **Eq. 1** given below.

$$Pb^{4+}_{1-\frac{x}{2}}\ Pb^{2+}_{\frac{x}{2}}\ O^{2-}_{2-x}\ (OH)^{-}_{x}$$

One of their samples deposited NaOH solution with pH > 13 yielded pure α-PbO_2[29]. Formation of PbO_2 produces H^+ ions hence reduces the pH around the formation region locally. It is found that the solubility of Pb^{2+} has a minimum at pH 9.3[48]. Hence when the α-PbO_2 starts to form pH

drops locally and decreases the solubility of the Pb^{2+} in return these ions incorporated to PbO_2 crystal causes non-stoichiometry.

Chen *et. al*. directly investigated the morphology of the α-PbO_2 on the aluminum substrates[78]. They found that morphology is a function both kinetic (current density, time) and thermodynamic (ion concentration and temperature) factors[78]. Well adherent layer on top of the substrate can be deposited with different parameters, with all other parameters kept constant; i) increasing the current density change the size of the α-PbO_2 crystals such that the at 3 $mA \cdot cm^{-2}$ α-PbO_2 start to appear as rod like structure and further increasing the current density results in the decrease of the rod diameter; ii) increasing the $HPbO_2^-$ ion concentration from 0.1 to 0.14 $mol \cdot L^{-1}$ morphology of the deposit changed and crystal size increased; iii) increasing temperature results in the increase in adhesion also it is important to note that at low temperatures rod like α-PbO_2 formed as the temperature increased well shaped crystals start to appear; iv) with increasing time size of the grain like structures increased it seem like these structures consists of smaller rod like α-PbO_2 crystals. At final note authors again highlighted the fact α-PbO_2 is non-stoichiometric[78].

Even though electrodeposition not directly explains the mechanism responsible for the PAM in lead acid battery there are some takeaways that can shine some light on the formation of PAM in the battery;

i) Discharge characteristics of α-PbO_2 and β-PbO_2 can vary from sample to sample.
ii) α-PbO_2 has higher defect content then the β-PbO_2 modification.
iii) When $PbSO_4$ form as an intermediate product alkalization takes place. Which leads to formation of α-PbO_2.
iv) formation of α-PbO_2 can occur via tet-PbO ➔ PbO_n ➔ α-PbO_2 mechanism.
v) Acid concentration and particle size has an inverse relationship.
vi) In dilute H_2SO_4 solutions $PbSO_4$ dissolution increases in return formation of PbO_2 increases.
vii) Formation of $PbSO_4$ from α-PbO_2 and β-PbO_2 is different, α-PbO_2 particles gets encapsulated by the $PbSO_4$ layer in return, hinders the discharge.

Next chapter focuses on the formation of PbO_2 from some form of paste material which more closely related to the morphology of the α-PbO_2 and β-PbO_2 appearing in lead acid battery.

4.2. Formation of Lead Dioxide

Burbank investigated the effect of the antimony on the positive plates and found that this element increased the α-/β- ratio of the positive plate[79]. In this investigation samples taken from the same supplier with same paste and process parameters only difference being the current collector. Effect of the antimony on the morphology also investigated, author stated that when the positive plate did not include antimony PbO_2 appear as *nondescript nodular particles* while addition of the antimony changes the particle morphology to more prismatic looking[79]. It is stated that the positive plates with antimony hence with the prismatic PbO_2 and higher α-/β- ratio leads to better performance and said that this results in line with the previous works[79]. However, one should be careful to attribute the increase in the cycle life to any parameters mentioned above i.e. antimony addition to positive plate, change in morphology and increase in α-/β- ratio, since, determining dominant parameter, if any, is almost an impossible task.

Simon *et. al*. studied the morphological changes of the positive electrode during cycling[80]. Authors obtained the commercial plates in the cured state then formed them in 1.11 s.g. acid with 1.5 A current for 27 hours then with 1 A for 20.3 hours[80]. Authors stated formed PbO_2 practically a pure β-PbO_2 and has *cell-like or reticulate* structure[80]. Their results show that $PbSO_4$ forms on the selected sites on the PbO_2 surface which is in contact to the electrolyte. Once $PbSO_4$ forms growth takes place further if the crystal has access to Pb^{2+} and SO_4^{2-} ions[80]. Recharged said to be facilitated by the remnant PbO_2 encapsulated by the $PbSO_4$ during discharge. It is highlighted if the conductive PbO_2 network is not completely disappeared during reduction to $PbSO_4$ can help the re-oxidation. Based on their observations discharge-charge process of the β-PbO_2/$PbSO_4$ system occurs via dissolution redeposition process and solid state transformation not likely for these materials[80]. They finalize their paper by saying that, the efficiency of the lead acid battery seems *puzzling* since one of the materials involved in the discharge-charge process is the highly resistive $PbSO_4$ thus, thus presence of the remnant PbO_2 network at discharged state not far reached for an argument[80]. Following that, Simon *et. al*. researched the microstructural changes in the PAM upon cycling[81]. Authors stated that upon certain cycling PAM develops *coralloid structure* and this transformation is facilitated by the *inactive PbO_2* that present in the system[81]. Furthermore, theoretically this coralloid structure is the perfect form for the PAM since it has large pores so that the acid can penetrate as well as the small joined PbO_2 particles with quite large surface area but their explanation later challenged since the time that perfect

coralloidal structure forms capacity of the PAM decreases[82]. Authors gave two explanation for this phenomenon, first, is the $PbSO_4$ passivates the active PbO_2 particles upon cycling, second, is the extremely dense and packed corralloid structure prevents the extensive electrochemical reduction of the PbO_2 (however this explanation discarded by the authors)[81].

Chang also investigated the structural changes in the PAM that formed from 3BS paste[83]. It is stated that the pore size characteristics for the cured and as-formed samples had the similar shape but shift towards the larger diameters which is expected since PbO_2 is denser the basic lead sulfates, upon formation leaves larger pores. authors states that this similarity shows the PAM morphology is similar to paste morphology[83]. Author suggested for a highly reactive PAM; pore size and distribution are important and stated the macropore diameter, which responsible for the ion transfer, should be 0.05 μm at the low end otherwise these pore will be plugged during the $PbSO_4$ formation[83]. Here coralloidal structure said to be non-beneficial to PAM performance since the formation of such structure leads to decrease in the macropore length in return the micropores become responsible for the ion transfer to the active mass. These micropores can be easily plugged in return lowers the discharge capacity[83]. This change in the pore characteristics is quite evident in the figure 5 and 9 in the Chang's paper[83]. These figures can be used the explain why the coralloidal structure described by the other authors has lower capacity[80]–[82].

Hill and Madsen investigated the battery failure in terms of morphology and the structure of the PbO_2[84]. Electrochemically produce β-PbO_2 more accurately represented by the **Eq. 1** and as the cycling proceeds the amount of O^{2-}/OH^- and Pb^{4+}/Pb^{2+} substitutions decline and structure become less defective. It was suggested this decline in the hydrogen content of the β-PbO_2 crystals may cause the capacity loss. However, author stated that the;

"*decline in battery capacity is not a function of the loss of a hydrogen species from the crystal structure of electrochemically active β-PbO_2*" [84].

Finally, it is stated that the large OH^- content can be associated with the surface hydration and/or amorphous regions. Later, this hydrogen species attributed to formation of the gel-crystal system by Pavlov[31]. In the context of morphology, it is said that the size of the β-PbO_2 crystals increase almost 4 fold if operation temperature set to be 50 ℃ but the size increase occur well before the failure hence do not play a part in the low performance[84].

Formation mechanism directly investigated by the Pavlov *et. al*. in this paper authors used a paste mostly consist of tet-PbO and some basic lead sulfates (3BS and 2BS)[46]. From their XRD and chemical analysis it is clear that tet-PbO and basic lead sulfates transforms in to $PbSO_4$ when they come in contact with the H_2SO_4 solution after 6 and 2 hours, respectively. It is also interesting to note up to 4 hours $PbSO_4$ not consumed in the system. Thus, one can argue PbO_2 formation is facilitated by the tet-PbO and basic lead sulfates. Authors stated the PbO_2 is the α polymorph and since only tet-PbO and basic lead sulfates transformed in to the PbO_2 one can conclude that the tet-PbO and basic lead sulfates facilitates the formation of the α-PbO_2. Increase in the β-PbO_2 and decrease in the $PbSO_4$ content in line with each other which supports the $PbSO_4$ to β-PbO_2 formation mechanism. authors claimed the formation can be separated in to two stages as follows[46];

"First stage (prior to the fourth hour). Chemical reactions between H_2SO_4 and tet-PbO and basic sulfates with $PbSO_4$ as a result; electrochemical reaction during which tet-PbO and basic sulfates are oxidized mainly to α-PbO_2 and partially to β-PbO_2.

Second stage (after the fourth hour). Lead sulfate is oxidized to β-PbO_2. No α-PbO_2 forms. The electro- chemical reaction takes place at high positive potentials at which OH^- oxidizes to O_2. During this time interval a considerable part of the current is consumed for the evolution of O_2." [46]

and continue by saying that such formation process proceeds by zones. Here, chemical reaction depends on the ionic diffusion of the H^+ and SO_4^{2-} ion diffusion towards the interior of the plate and starts from the acid paste interface, while, the electrochemical reactions depends on the available electronic contacts and exclusively starts from regions that is close to the grid since this grid is the only conductive component of the system at the beginning of the formation. Figure 3 in their paper shows this process beautifully[46]. Schematic of the zonal formation given at **Figure 4.4.**

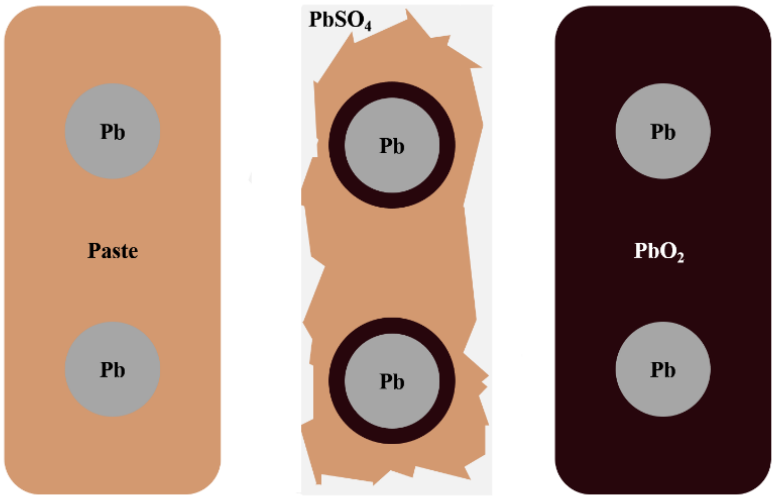

Figure 4.4. *Schematic of the zonal formation described in the Ref*[46].

There are some important points arises when above figure is investigated, first note that paste and the $PbSO_4$ is not conductive hence the electrochemical reactions hindered in those regions since there is no electronic contact hence when the especially $PbSO_4$ finds the electronic contact it can transforms to PbO_2 (mainly the β-PbO_2 polymorph). This schematic looks like describing the solid-state transformation but it can be applied to the dissolution preparation mechanism as well dissolved Pb^{2+} species (can be dissolved from PbO, $PbSO_4$ or basic lead sulfates) has to find electronic contact to oxidize to Pb^{4+} cation. Thus, in light of the above stages and earlier described alkalization several processes said to occurring simultaneously during the formation i.e. dissolution, ionic diffusion, neutralization, charge transfer, nucleation and growth[46]. Dissolution can be affected from the dissolved species stability in H_2SO_4 solution, temperature and even ionic diffusion; ionic diffusion and neutralization also depends on the temperature and ionic mobility as well as the pore characteristics of the paste; charge transfer depends on the current density and even the paste density and so on. Point is that the formation process is chaotic with several dependent and independent variables. Going back polymorph dependence to the process parameters, authors stated increasing the $PbO/PbSO_4$ ratio (PbO in the basic lead sulfates also counts) has a positive effect on the amount of α-PbO_2 produced. This is in line with the road map and driver analogy given in the **Figure 1.2,** because increasing the $PbO/PbSO_4$ contain is like shifting the starting point to the right side of our "road map" hence depending on the kinetic factor

one improves the probability the formation of the α-PbO_2. On final not authors gave an equation to determine the α-/β- ratio in the positive plate as follows[46];

$$\alpha/\beta = \frac{q^o_{PbO} - q'_{PbSO_4} - q'_{PbO}}{q^o_{PbSO_4} + q'_{PbSO_4} + q'_{PbO}} \quad \textbf{(30)}$$

Here superscript ^{o} represents the initial amount of the species while the q'_{PbO} and q'_{PbSO_4} represents the amounts of PbO transformed in o β-PbO_2 and $PbSO_4$ formed during the first stage (described above) of the formation. Following parameters said to effects the α-/β- ratio; i) H_2SO_4 concentration, ii) current density, iii) paste density, iv) soaking time, v) grid design and vi) temperature[46].

Following that Takehara *et. al*. studied the reduction of the PbO_2 samples prepared from paste under different discharge conditions[85]. Authors used combination of galvanostatic and potentiostatic discharges one after another. Points to be taken as follows; i) galvanostatic discharge left the Pb/PAM interface relatively unchanged while after the potentiostatic discharge large $PbSO_4$ crystals formed at the interface; ii) discharge starts at the interface and proceeds gradually[85]. especially the latter finding is a mirror opposite to the charging process described by the Pavlov *et. al*. (see previous paragraph)[46].

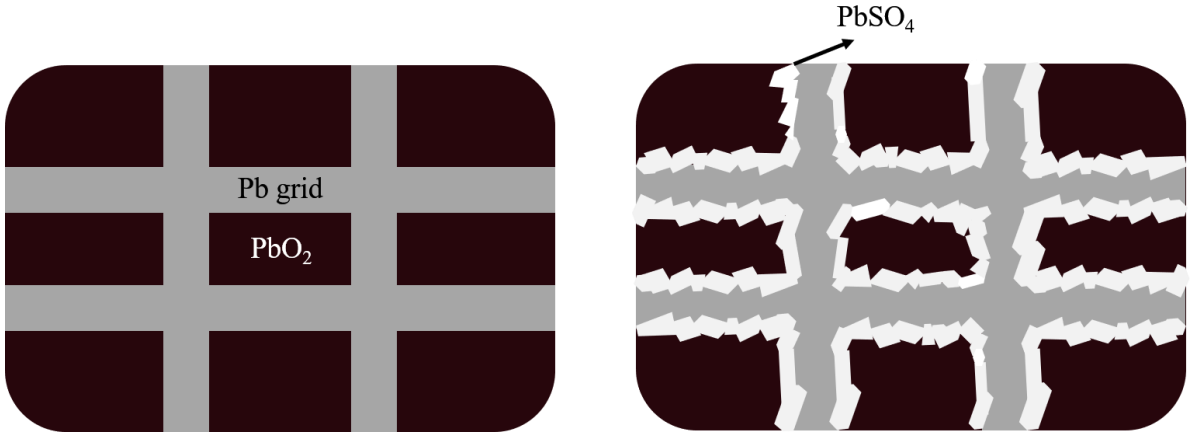

Figure 4.5. *Schematic of the overdischarge process*[85].

Zerroual *et. al*. analyzed the PbO_2 formation in lead acid battery with both XRD and chemical analysis from 3BS pastes. Chemical analysis is very useful when used in tandem with XRD since it allows identification between tet-PbO and α-PbO_2[86]. After 5 hours of formation main transformation is the $PbSO_4$ to β-PbO_2. Which means that the 3.12 Å peak can be attributed

to the α-PbO_2 alone. Interestingly final α-PbO_2 and β-PbO_2 amounts found to be corresponds to the Pb and PbO used in the LO for the paste production[86].

Grugeon-Dewaele *et. al*. investigated 3BS to PbO_2 transformation[87]. Authors stated neither PbO_2 nor intermediate sulfation product $PbSO_4$ formed from the 3BS did not maintain its precursor morphology[87]. It is stated that 3BS to $PbSO_4$ transformation is rather rapid and 3BS particles are completely transforms in to $PbSO_4$ in just 15 minutes. Authors concluded their study on the 3BS by saying[87];

"As a practical consequence of such a fundamental study, it can be anticipated that any attempt to control the Pb02 performances with a control of the 3BS morphology will be unsuccessful"[87].

Morphology of 3BS-based PbO_2 presented by Dimitrov and Pavlov. Here PAM consists of rounded PbO_2 particles which interconnected in a porous agglomerate network[88]. Size of the individual PbO_2 particles said to be 30 to 200 nm. As this structure cycled it converts to branches of agglomerates called aggregates. Authors established a morphology map for the PAM structure based on 3BS paste, see **Figure 4.6**[88]. It is also stated that the keeping the crystallite size below 60 nm is advantages for the electronic contact between particles hence improves cycle life via facilitating better charging[88].

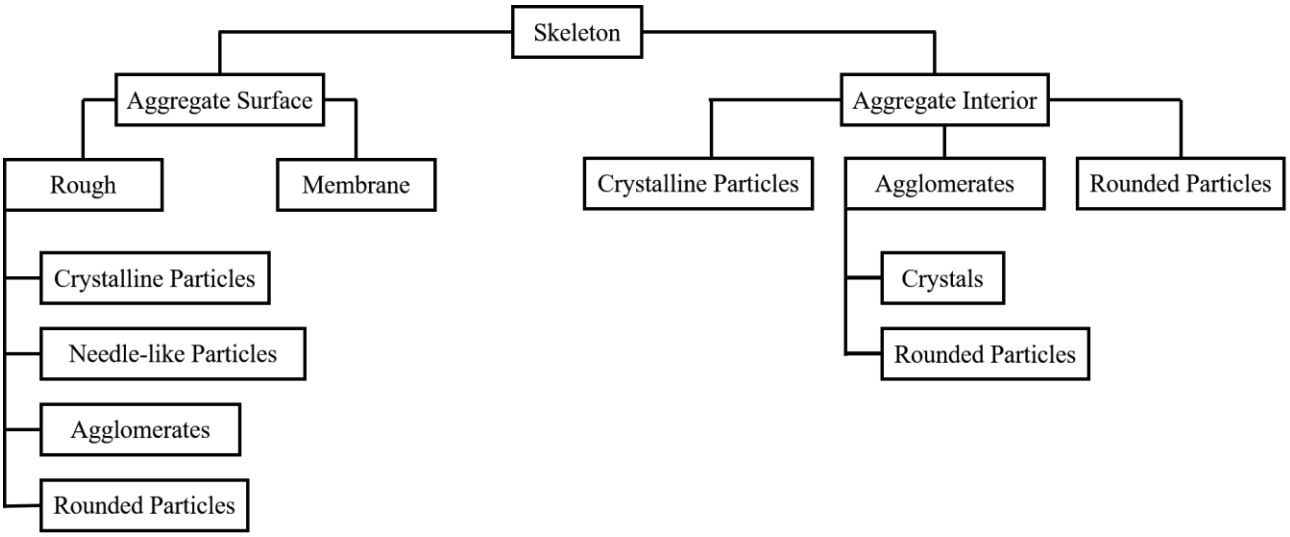

Figure 4.6. *PAM structure evolution scheme*[88].

Pavlov and Kapnov used 4BS pastes to see the effect of the paste material on the PAM characteristics as well[23]. PbO_2 formed from 4BS metasomatically and preserve the shape of the 4BS particles in the macrostructure level. Addition to that authors stated the cycle life is improved significantly by the usage of 4BS ad decreased capacity can be compensated with use of Pb_3O_4[23]. PbO_2 formation from the 4BS pastes later investigated more thoroughly by Pavlov and Bashtavelova[17]. Here morphology of the samples with different oxidation times are investigated. By examining the provided SEM images one can state that during formation both electrochemical oxidation and chemical sulfation simultaneously occurs. Some of the 4BS convert to $PbSO_4$ during formation and some oxidize to PbO_2[17]. When PAM treated with ammonium acetate solution it is very clear that the PbO_2 forms on the surface of the 4BS metasomatically that is dissolved Pb^{2+} ions precipitate as PbO_2 on the sites they originated. Agglomeration of two type also can be observed one is similar to 4BS while other resembles the $PbSO_4$ particles formed from the sulfation o the 4BS particles[17]. As mention that initially the it is though that the usage of the 4BS leads to formation of the α-PbO_2 but, this comment later dismissed by the literature[43]. Lam *et. al*. investigated these claims more in depth and conclusively find that the 4BS not particularly promotes the formation of the α-PbO_2 by using the XRD analysis[89].

Lam *et. al*. studied the pulsed-current effect on the formation of the 4BS pastes[90]. Authors also published information about the soaking of the 4BS electrode. This information can be critical because, the PbO_2 tends to maintain the morphology of its precursor, stated by the Pavlov and Bashtavelova[17], thus, different morphologies can emerge as function of the precursor. Lam *et. al*. stated[90];

"*4BS crystals become covered by compact films of $PbSO_4$ immediately the formation acid is introduced*."[90]

thus different morphologies can be expected to form and proposed two different formation mechanism for the plates that soaked for a long and short time[90]. Morphology, especially the size of the PbO_2 seems to be effected by the soaking time based on their model[90].

Figure 4.7. *Sulfation and oxidation mechanism for 4BS*[90].

Grugeon-Dewaele *et. al*. followed that and stated if soaking is applied o 4BS pastes $PbSO_4$ crystals with two different morphologies, first is the larger polyhedras, 2 μm in diameter, and smaller interconnected $PbSO_4$ particles, 0.2 μm in diameter, forms[91]. Latter said to be form metasomatically and PbO_2 particles formed from these $PbSO_4$ mainly originated from the smaller $PbSO_4$ particles[91]. Authors stated that the PbO_2 formation is a *double metasomatic process*, is that, first 4BS chemically transform in to $PbSO_4$ then smaller $PbSO_4$ particles electrochemically oxidize to PbO_2[91]. From their results it can be seen that the sulfation of the 4BS paste levels of roughly after half a hour[91], this might be caused by the relatively large size of the 4BS particles. As stated in the **Section 4.1** when $PbSO_4$ forms as an intermediate product it tends to cover the surface of the present materials which can be either basic lead sulfates or the substrate. In contrast 3BS soaking i.e. formation of $PbSO_4$ via sulfation of the 3BS particles occurs much rapidly[91]. It is also stated that as the thickness of the 4BS particles decreased capacity of the battery increased, this expected but important since it is shown that the morphology of the 4BS is retained by the PbO_2 which means the morphology of the precursor, precursor PbO_2 transformation mechanism and the precursor type have an interconnected effect on the battery performance[87].

Clear difference between the PbO_2 morphologies produced by 3BS and 4BS pastes presented by Pavlov[32]. It can be said that the shape memory effect more pronounced in the PAM formed from the 4BS pates. Morphology developed from the formation on 3BS paste shows some sign of metasomatic $PbSO_4$ transformation[32]. Also, it is evident that the 4BS-based PAM has larger agglomerates compared to 3BS-based PAM which is result of the size of the 4BS being larger than the 3BS particles[32]. This size difference, also, leads to lower initial capacity of the 4BS-based electrodes due to full transformation cannot be achieved, see **Figure 4.7**.

Pavlov and Bashtavelova investigated the PAM produced from different types of pastes and as expected different morphologies emerged, as a consequence, authors proposed a two level structure for PAM[92].

"first-level microstructure, which consists of small crystals with the form of grains, prisms, plates, and needles organized in porous agglomerate, and a second-level macrostructure. The individual agglomerates (with a screw-like, spherical, prismatic or rock-like shape) are linked in a macroporous skeleton, which supports mechanically the active material, conducts the electric current, and serves as memory, where the conditions for the preparation of the paste, the curing, and the formation of the active material are coded."[92]

Resulting morphologies from the experiments of the investigation is summarized at **Table 4.3.**

Table 4.3. *Summary of the Ref*[92].

Paste Composition	**Structure levels described by Pavlov and Bashtavelova**	**Morphology of PAM**
majority tet-PbO minority 3BS	*microstructure (crystal)*	Tightly linked grain like crystals
	macrostructure (agglomerate)	Rock like interconnected agglomerates, similar to paste structure
majority 3BS minority tet-PbO and ort-PbO	*microstructure (crystal)*	Spherical tightly connected crystals.
	macrostructure (agglomerate)	More spherical agglomerates, dissimilar to paste structure
majority 4BS minority tet-PbO and ort-PbO	*microstructure (crystal)*	Both needle like and prismatic crystals
	macrostructure (agglomerate)	Long prismatic agglomerates, similar to paste structure
majority 1BS and 3BS minority tet-PbO	*microstructure (crystal)*	Well grown prismatic crystals
	macrostructure (agglomerate)	Highly porous agglomerates, dissimilar to paste structure

Effect of paste density investigated with the paste composition of "majority 3BS and minority tet-PbO and ort-PbO" pastes with 3.7, 4.2 and 4.75 $g \cdot cm^{-3}$. Authors stated paste density highly influential o both of the structure levels[92]. For 3.7 $g \cdot cm^{-3}$ needle like crystals formed came

together to form porous macrostructure. When density 4.2 $g \cdot cm^{-3}$ used for paste material, more prismatic crystals dominates the microstructure and these crystals merges in a more spherical orientation. 4.75 $g \cdot cm^{-3}$ leads to increase in particle size compare to the 4.2 $g \cdot cm^{-3}$ also appears that the macrostructure becomes more discontinuous[92]. Following that study same authors describe the "breathing" of the positive electrode while cycling. It is stated that the both pore volume and the surface area of the positive electro decline during discharge due to the formation of the $PbSO_4$[93]. Note that discharge capacity of the electrode depends on the available reaction regions which is correlated by the available PbO_2 surfaces as well as the acidic medium ability to reach those PbO_2 surfaces. In this context pore characteristics and the surface area of PAM's that formed with different pastes investigated. Even though authors stated their results scattered, general pattern shows that surface area and the capacity is positively correlated as expected. Interesting result, however, comes from the correlation between the pore volume and the capacity. According to their results micropore volume do not affects the capacity of the plates[93]. Actually, these results are in line with Chang's findings which described earlier[83]. One may interpret these results such that the micro and macro structure of the PbO_2 is dependent on each other also the pore characteristics has slightly more complex effect on the performance.

Winsel and Bashtavelova developed a so-called agglomerate-of-spheres, in German Kugelhaufen-Modell, model to describe the behavior of the electrochemically created networks[94]. It is stated that model can be for powder metallurgy as well. As name suggests structure forms from individual spherical particles coming together to form large agglomerates, actually model developed mainly considering the PAM of the lead acid battery. Here authors treat particles and necks as their thermodynamically different from each other. Model leads to conclusion that the there is a relation between the formation polarization and the particle size. They stated;

"(I) Small over-voltage favors the formation of large spheres particles. (II) Above of 10 mV over-voltage the sphere's radii are in the observed range. (III) A larger coordination number reduces the sensitivity against the over-voltage."[94].

Yet it seems that the effect of the polarization on to the size can be seen if quite large current densities are used, see figure 8 in the article[94].

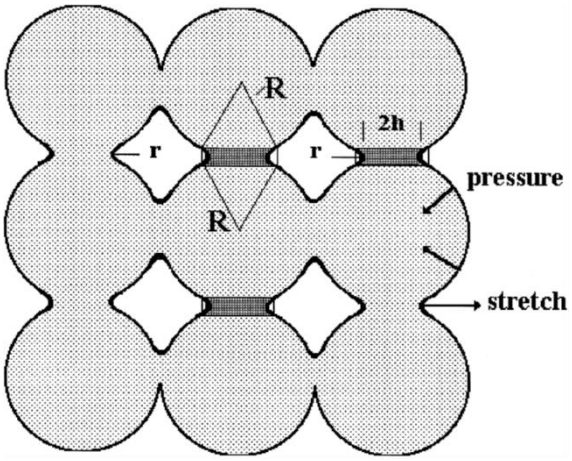

Figure 4.8. *Schematic of agglomerate-of-sphere model*[94].

Pavlov *et. al*. investigated the PbO_2 formation mechanism from the $PbSO_4$ crystals[95]. Again, two main mechanism emerged; i) metasomatic transformation of the PbO_2 from the $PbSO_4$ starting from the surface and move towards the interior of the $PbSO_4$ particle ii) dissolution of the $PbSO_4$ to Pb^{2+} and SO_4^{2-} and oxidation of the Pb^{2+} to Pb^{4+} cation. Metasomatic formation said to yield both needle like and grain shaped crystals. Authors stated second mechanism occurs if the PbO_2 nucleation do not occur at the $PbSO_4$ surfaces[95]. Figure below gives the schematic of the mechanisms described.

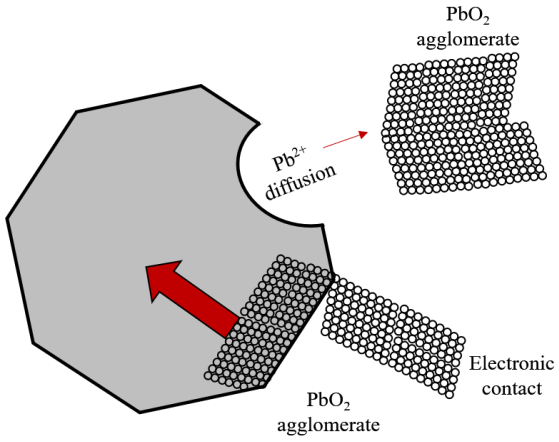

Figure 4.9. *Metasomatic and diffusion-based formation of PbO_2 from $PbSO_4$*[95].

Notice the electronic contact between the already existent PbO_2 particles and the metasomatically produces ones. This contact provides the electrons to the Pb^{2+} dissolved just on the $PbSO_4$ surface upon formation also micropores developed due to the volumetric difference between the $PbSO_4$ and the PbO_2.

Pavlov *et. al*. investigated the effect of the fast charge on the battery performance[96]. Even though it is only highlighted with a single paragraph, morphology of the PbO_2 particles near the current collector and the surface of the electrode are mentioned. Both morphology appears to be agglomeration of spherical particles no distinct feature between them[96].

Up to now PbO_2 morphology described in term of micro and macro structure however no clear definitions made for the polymorphs. Pavlov *et. al*. investigated the structure of the individual PbO_2 particles under both SEM and TEM[30]. They stated individual PbO_2 particles consist of α-PbO_2 and β-PbO_2 crystal regions as well as an amorphous region (again going back to gel-crystal system and assuming amorphous region is hydrated)[30]. It seems that the PbO_2 morphology is needle like and contains amorphous regions. Also, aspect ratio of the β-PbO_2 seems to be smaller compared to the α-PbO_2 counterpart, that being said there is not clear cut distinction between the α-PbO_2 and β-PbO_2 can be seen[30]. Also, some crystals shown in the authors work contains both of the crystal polymorph as well as the amorphous regions. Later, authors described three zones;

"1. Highly transparent for the electron beam of the microscope. They can be assumed to consist of lead (IV) hydrate. The latter has formed a "cloud" with high water content.

2. Zones with growing mass density. Probably, a dehydration reaction proceeds at many places therein resulting in condensing of the substance and its transformation into lead (IV) hydroxide. These sites form the zones with different structure within the PbO2 particle. It can be expected that both the hydrate and part of the hydroxide are amorphous.

3. Compact zones. They are illustrated by the darkest zones in the particle, since the density of lead and oxygen ions there is the greatest. This happens when the structure is organized in a crystal lattice. Consequently, the process of dehydration and substance condensing is almost completed. These crystal zones have a different orientation because the conditions of their formation in the particle are different."[30]

According to this zone description formation process for PbO_2 proposed as follows; initially $PbSO_4$ dissolves and Pb^{2+} concentration in the solution reaches a level, these Pb^{2+} ions oxidize to Pb^{4+} at the conductive PbO_2 surface, yet, since the Pb^{4+} is not stable in the solution Pb^{4+} hydrates and forms $Pb(OH)_4$. Later by dehydration PbO_2 particles forms with both crystalline and amorphous regions[30]. They also stated the SO_4^{2-} concentration increases the amorphization of the crystals.

Hence one can expect there is an equilibrium between the ions in the solution and the PbO_2 particles as well.

Later Pavlov proposed a more comprehensive model for the structure of the electrochemically produced PbO_2 and gave a general expression for the structure that contains both crystalline and the amorphous regions[31].

$$\overbrace{PbO_2}^{\text{crystal}} + H_2O = \overbrace{PbO(OH)_2}^{\text{amorphous}} \quad \textbf{(31)}$$

This model named as gel-crystal system, gel zone comprise of the this hydrated species that can conduct protons and localized in the surfaces of the PbO_2 particles[31]. Pavlov and Balkanov presented further prove that the PbO_2 surfaces are hydrated by heating the samples inside the TEM and also discovered that these hydrated surfaces exchange ions with the electrolyte[97]. They again highlighted the fact chemically produced PbO_2 is more ordered[97]. Pavlov also stated that the amorphous PbO_2 also satisfies the requirements of being good proton conductor, like other metal oxides with good proton conductivity, PbO_2 also holds on to water at relatively elevated temperatures[6], [31].The amorphous hydrated regions said to be similar to polymer chains of hydrated octahedra which allow them to conduct electrons. The electron transport mechanism for the gel-crystal system is similar to the crystal PbO_2 that is electrons “hops” between the Pb cations[31]. Upon dehydration gel structure integrated by the crystal structure and crystallinity is improved. For simplicity one can see the crystal and gel zones responsible for the electron and proton conduction, respectively. However, note that the hydrated regions also possess electron conductivity[6], [31]. **Figure 4.10** is the schematic of the gel-crystal system that proposed by the Pavlov[31] and the conductive hydrated region which has a polymer like structure. Note that gel system is conductive, in terms of both electron and proton, see **Figure 4.10b**. When the fraction of the gel regions diminishes upon dehydration electronic conductivity of the structure improves however, proton conductivity just as important for the electrochemical oxidation to occur.

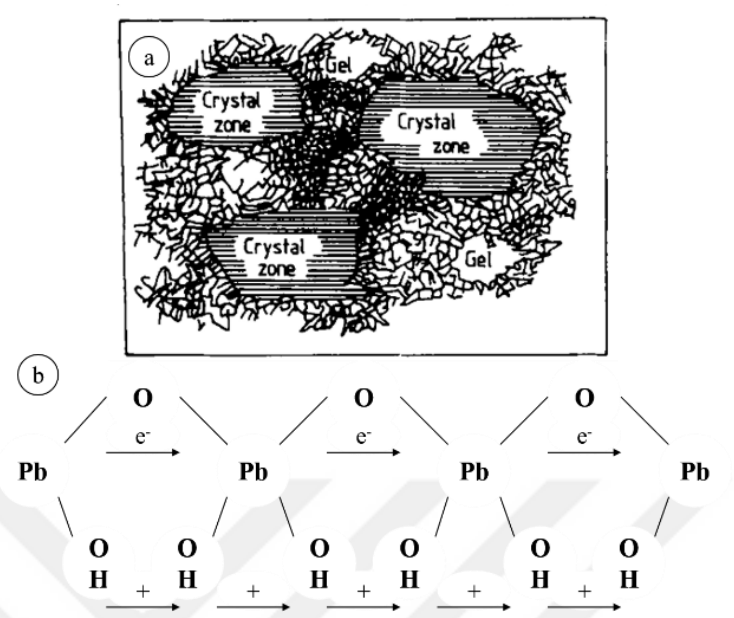

Figure 4.10. *(a) Gel-crystal system and (b) conduction mechanism of the polymer chains*[30].

High-resolution TEM proved that the gel zones consist of hydrated and linearly arranged polymer chains[32]. Monahov and Pavlov stated the PbO_2 layer that electrodeposited from the Pb electrode comprise of 10% of these hydrated zones while for the PAM structure this value reaches 30%[64]. When such electrode placed in a H_2SO_4 solution initially $PbSO_4$ layer forms by reaction of Pb^{2+} and SO_4^{2-} ions at the surface of the Pb electrode, this $PbSO_4$ layer tightly packed and hinders the SO_4^{2-} and HSO_4^- ions to reach the Pb surface. This causes the Pb^{2+} ion accumulation and in order to maintain neutrality H^+ ions go to bulk of the solution hence the interiors of the oxidation product alkalized which leads to formation of hydrated forms of tet-PbO and α-PbO_2 according to oxidation potential[64]. This mechanism later discussed more detail and importance of the balance between the sulfation and the oxidation is highlighted in terms of their effect formation of the PbO_2 polymorphs. It is also considered that these hydrated regions might play a role in the oxygen evolution during the anodic polarization of the positive electrode[64]. According to Pavlov and Monahov oxygen evolution originate from some active sites that located in the hydrated (gel) regions of the PbO_2. Their explanation considers the conductive gel structure and proposed reaction later proved by other authors[98], [99]. Amadelli *et. al*. stated that the O_2 evolution takes place in the both crystal and hydrated (gel) regions where the O_2 evolution at elevated potentials mostly facilitated at the gel region[58]. Cao *et. al*. used the mechanism proposed by Pavlov and Monahov[100] and stated that the longer the oxidation lesser the PbO_2 activity due to oxygen

atoms migration towards the electrode which this oxygen atoms layer recombine and evolve as O_2 gas[99]. It is also said that this gel-crystal system is in equilibrium with the solution. Thus, depending on the ionic concentration of the solution equilibria between the crystal/gel/solution changes. This change can favor both increase in crystal or gel region which in return changes the properties of the PAM[32].

While investigating the ort-PbO formation during discharge, Pavlov *et. al*. presented morphological analysis for two polymorphs that formed from 4BS paste[101]. Authors findings suggests α-PbO_2 has a nonuniform shape and β-PbO_2 appears as needle like shape with small aspect ratio. In the paper, lack of characteristic peak of the α-PbO_2 sample attributed to the incomplete formation of the material[101].

5. EXPERIMENTAL METHOD

5.1. Sample Preparation

In order to analyze the existent morphologies inside the operational batteries, all samples provided by commercial battery manufacturer. Samples taken from the same batch, applied different formation procedure to investigate the both α-/β- ratio as well as the morphologies of the PAM. In order to avoid industrial rights violation only formation acid density and ampere·hour (Ah) values are shared. One should note that the formation profiles applied to the plates are not the same procedure applied to the commercial batteries. LO materials and the cured but not formed plate also investigated for the thesis but the mass fractions will not be shared. These parameters especially effect the performance of the lead acid battery but, believed to be not create a significant difference when it comes to the individual α-PbO_2 and β-PbO_2 morphologies.

5.2. Sample Characterization

All the samples including the cured plate investigated under the SEM. XRD analysis done to determine the phase distribution of the samples. TEM investigations conducted to shine light on the phase composition of the individual particles encountered in the PAM structure, in order to investigate the distinct morphologies, if any, of the PbO_2 modifications.

For the SEM imaging Zeiss brand Leo Supra 36VP Field Emission model microscope is used. XRD analysis conducted by using Bruker D2 phaser (AXS GmbH) with Cu-K_α (λ=1.54 Å). Finally, JEOL brand JEM-ARM200CFEG UHR-TEM is used for TEM investigations.

6. RESULT AND DISCUSSION

Table below summarized the samples were used in the thesis. Samples with varying acid concentration and formation Ah values investigated.

Table 6.1. *List of the samples being investigated.*

Sample #	Acid density (s.g.)	Formation Condition	Final Voltage (V)	e^- (10^{22})	Average Current (A)	Formation Time (h)
P1	1.28	1 Ah	2.05	2.25	0.25	4
P2	1.28	4 Ah	2.12	9	0.25	16
P3	1.28	Cut-off below 2.7 V	2.13	—	—	—
P4	1.28	No V cut-off (probably above 2.7)	2.15	—	—	—
P5	1.16	1 Ah	1.94	2.25	0.25	4
P6	1.16	4 Ah	2.02	9	0.25	16

Note that the Ah values for the samples P3 and P4 is not given. Purpose for these samples was to find out the effect when the formation continued without any voltage and/or current control on the plate morphology.

6.1. X-ray Diffraction

XRD patterns from the P1, P2, P5 and P6 are given below. Samples reduced to powder form before the analysis. All analysis done with the 0.01 step size and 5 seconds intervals to avoid noise. Also, one can clearly see the several possible peak overlap can occur in the XRD analysis. Note that vertical marker position of the individual phases also represents the relative intensities of those diffraction lines, see

Table 3.1. Especially for the separation of the tet-PbO from α-PbO_2, ratio of the diffraction lines is used. As mentioned these two crystals has the same characteristic peak. Note that the intensity ratio of the 2θ = 23.25° and 2θ = 28.47° is 1:5 for the α-PbO_2.

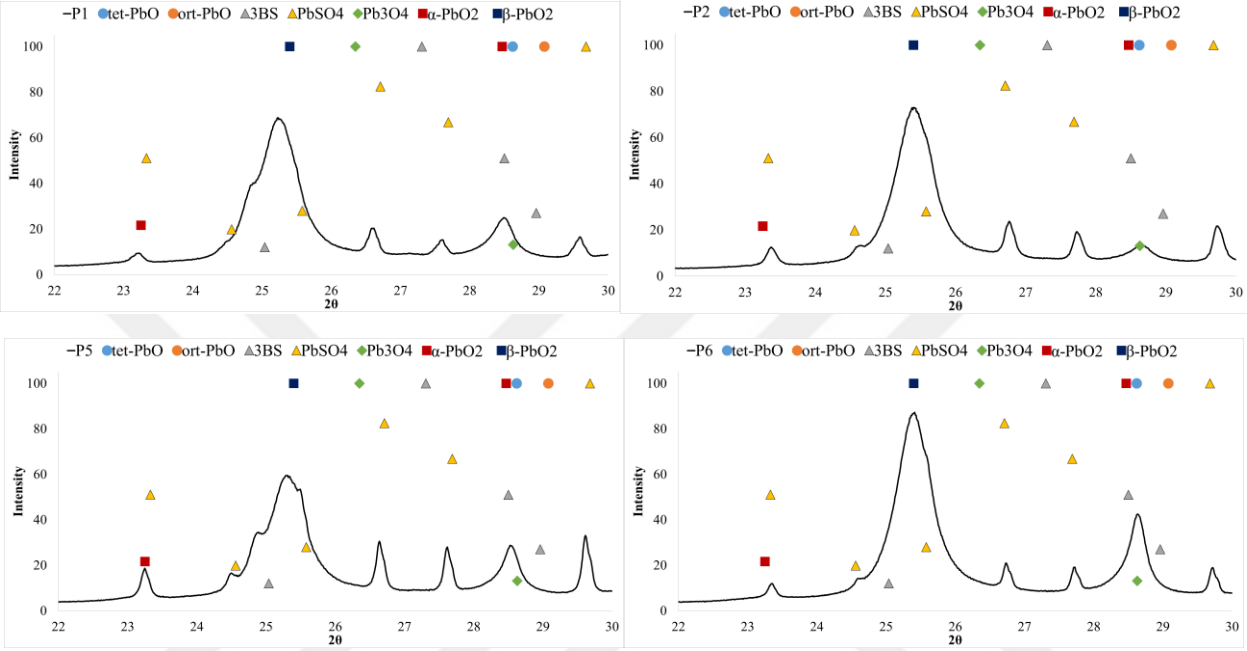

Figure 6.1. *XRD patterns of the P1, P2, P5 and P6 samples.*

Notice that the P3 and P4 patterns not shared since the formation profile for these samples are unknown, which, makes it impossible compare them with rest of the samples.

6.1.1. Effect of formation time with acid density 1.28 s.g.

Figure below give the superimposed XRD patterns of the P1 and P2. Note that these plates formed in the acid with 1.28 s.g. density and P2 has 4 times higher formation time.

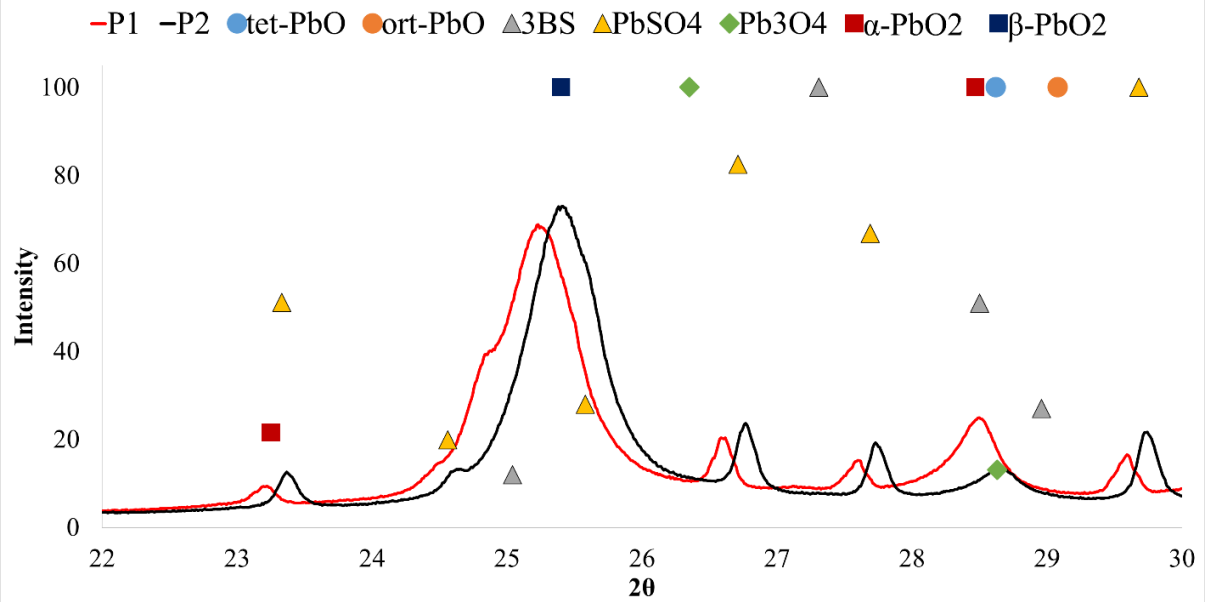

Figure 6.2. *Phase composition of the P1 and P2 samples.*

First thing to notice that the α-PbO_2 did not survive the high acid concentration as the formation proceeds since the peak at the 2θ = 28.47° is completely gone. This also shows that the amount of tet-PbO also converted to the β-PbO_2 via tet-PbO to $PbSO_4$ to β-PbO_2 mechanism, rather than converted to α-PbO_2 via solid state oxidation. These patterns show that if the sulfation rate increased with high acid concentration formation of α-PbO_2 can be hindered completely. One can make the argument that if the larger acid concentration is used the basic lead sulfates transforms in to $PbSO_4$ at the surface of the PAM and further sulfation is limited, alkalization process, which explained in the **Section 4.1**, takes place hence the α-PbO_2 formation becomes favorable. Yet these results show that even though surface is sulfated to $PbSO_4$, this phase starts to form in to β-PbO_2 in return acid density increased and if, the rate of the α-PbO_2 formation is low system do not find the change to produce this phase. Which means there is a certain acid concentration which makes the sulfation completely prevail against α-PbO_2 formation.

It is also evident that the all the peaks shift to the right and slightly becomes narrower, since all peaks shift to one direction this could be due to a wrong zeroing of the goniometer. Crystals formed and gets larger as the formation proceeds. Surprisingly, $PbSO_4$ content increased for the P2 sample. This might be coming from the tet-PbO to $PbSO_4$ transformation, some of this $PbSO_4$ did transformed to the β-PbO_2, hence the increase in the β-PbO_2 peak intensity, yet some of them stayed as they are hence the increase in the $PbSO_4$ peaks. Another interesting fact is the

protrusion around the 2θ = 25° for the P1 sample, this peak is completely gone if the formation proceeds, this peak appears to be not corresponding any common phases presents in the lead acid battery production, 4BS included[16]. It is obvious that both ort-PbO and 3BS not survived from the acid attack and sulfated to $PbSO_4$ by chemical means and most of the $PbSO_4$ oxidize to β-PbO_2. At the end, P2 sample phase composition is mainly the β-PbO_2 and $PbSO_4$ phases, addition to these phases P1 also contains some tet-PbO.

6.1.2. Effect of formation time with acid density 1.16 s.g.

Superimposed XRD patterns for the P5 and P6 are given in **Figure 6.3**. More intuitive results are obtained with those samples compared to the high acid samples.

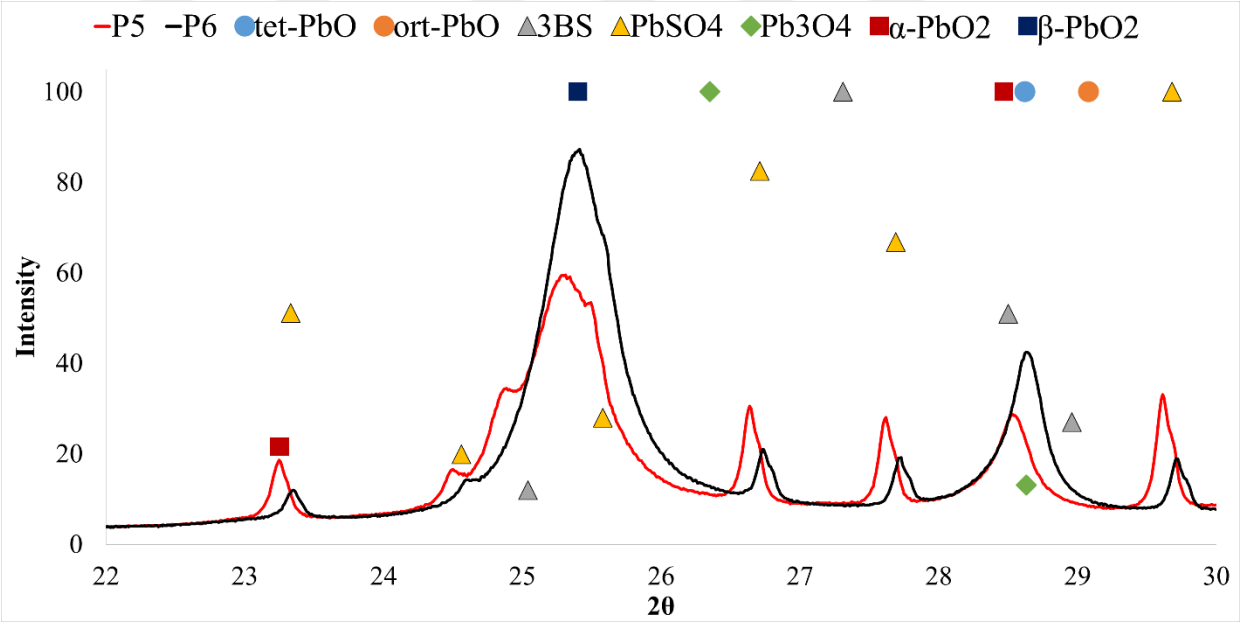

Figure 6.3. *Phase composition of the P5 and P6 samples.*

Again, P5 can be treated as the initial stages of the formation and P6 is the final stage. Here, initial increase and later decrease in the $PbSO_4$ content is visible. Also, for these samples tet-PbO transformed in to α-PbO_2 since the both α-PbO_2 peak exist and the intensity ratio close to 1:5. It is believed that the peak at 2θ = 23.25° correspond to $PbSO_4$ for the P5 sample. Interestingly increase in the 2θ = 28.47° peak shows that α-PbO_2 produced from another mechanism addition to the solid-state oxidation form the tet-PbO. Similar to **Figure 6.2**, it can be said that ort-PbO and 3BS did not survived from the acid attack and peak shift occurred as the formation proceeds. $PbSO_4$ lower for these samples this fact can be attributed to the lower acid density. Protrusion around the 2θ = 25° is even more pronounced yet again completely disappears for longer formation. There is much

larger increase in the β-PbO_2 peak intensity compared to the higher acid concentration samples, P1 and P2, this can indicate the acid concentration and the oxidation rate has a positive relationship. Also, it can be said that formation of α-PbO_2 slows down the oxidation process. If we assume there is no α-PbO_2 formation in P1 and P2 samples all of the oxidation product is β-PbO_2, this is logical since P2 has no indication of α-PbO_2 modification and $2\theta = 28.47°$ peak can be attributed to tet-PbO for P1, even with the shorter formation time most of the β-PbO_2 oxidation is completed in high acid samples. And high acid samples contain no α-PbO_2. Which these statements indicate that the formation rate/amount of β-PbO_2 formation is a function of $PbSO_4$ content with a certain maximum. Normally all of the $PbSO_4$ should transformed in the β-PbO_2 but since lead acid battery is an extremely heterogeneous system some sulfated regions can be excluded from the oxidation process due to lack of electronic contact and large Pb^{2+} ions which produced from the $PbSO_4$ dissolution might fail to find these contacts as well. Thus, neither metasomatic nor the dissolution-precipitation oxidation mechanism can be activated during the formation.

6.1.3. Effect formation acid density with 1 Ah

XRD spectrum for P1 and P5 samples presented together in the **Figure 6.4**. Formation acid density for the P1 and P5 samples taken as 1.28 s.g. and 1.16 s.g., respectively and both samples subjected to 1 Ah formation.

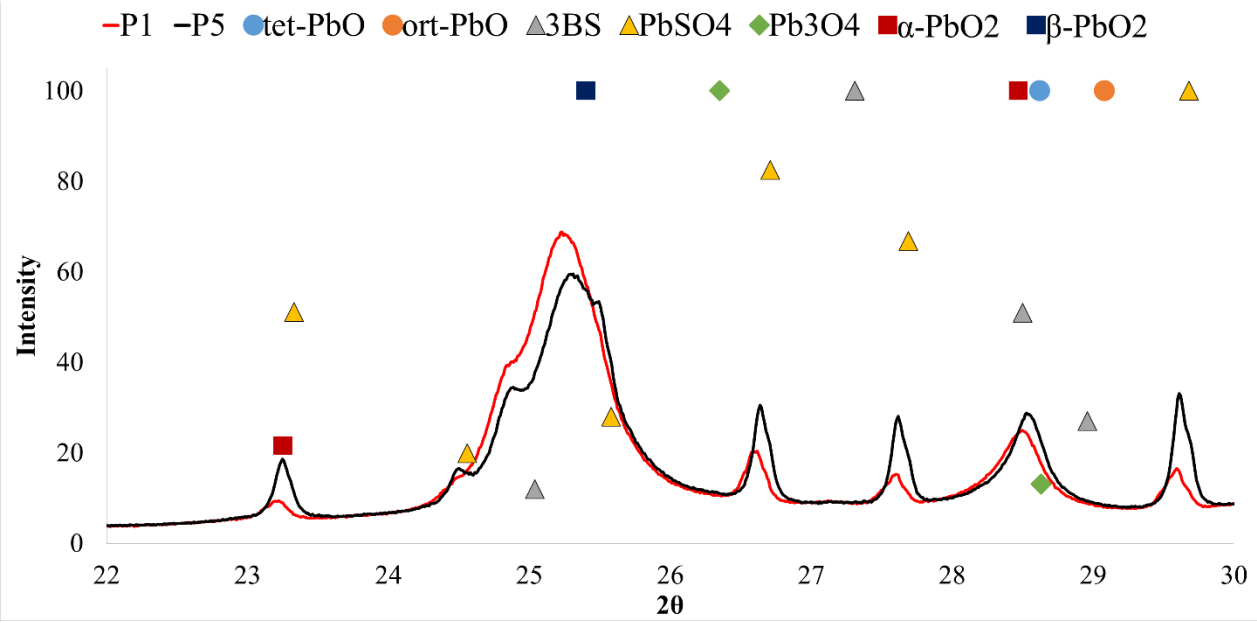

Figure 6.4. *Phase composition of the P1 and P5 samples.*

Right away two significant difference is evident. First is the larger $PbSO_4$ content of the low acid density sample, P5, and the larger higher intensity of the characteristic β-PbO_2 peak in sample P1. Miniscule peak shift also observable indicating that P5 slightly further in the formation process yet P1 has larger β-PbO_2 content. What is the reason for these phenomena?

It is believed that the sulfation rate increases with the acid concentration as expected. In return, formation of the β-PbO_2 increases due to following reason. When higher acid concentration is used the $PbSO_4$ amount and thickness at the surface increases. Note that here, term "surface" used for the regions which is away from the current collector, which is the only conductive part at the beginning of formation. This $PbSO_4$ region gets closer and closer to the current collector hence probably of finding an electronic contact increase. Since when the $PbSO_4$ oxidize to PbO_2 those regions also become electronic contacts which the expense of increasing the acid concentration, see **Figure 1.1** and **Table 1.3**. For the low acid concentration sample P5 probability to find electronic content is lower since the $PbSO_4$ thickness on the surface is smaller. Sample P5 needs to formation of the "inside", regions closer to current collector, takes place so that the oxidation at the surface can take place.

6.1.4. Effect formation acid density with 4 Ah

Phase composition for the samples P2 and P6 given in the XRD spectrums below. Similar to P1 and P5, P2 and P6 has 1.28 and 1.16 s.g. acid densities, respectively, with the 4 Ah formation.

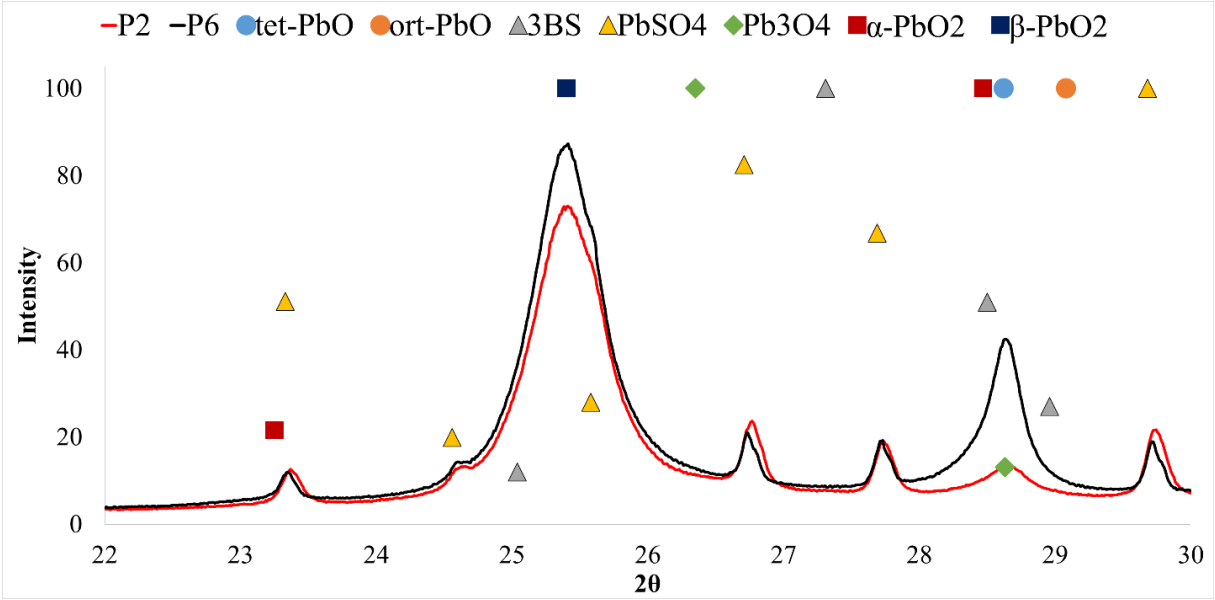

Figure 6.5. *Phase composition of the P2 and P6 samples*

One can see that for both samples $PbSO_4$ content is similar. For both sample main materials are PbO_2 and $PbSO_4$, as well as, very small amount of tet-PbO. Yet there is drastic change for the PbO_2 polymorph distribution, which, P6 has large amounts of α-PbO_2. Reason for this difference depends on oxidation and sulfation mechanisms simultaneously being activated during the formation. Following the statements in the previous chapter, it can be said that the rate of the oxidation and sulfation effects the α-/β- ratio. Proposed model for the formation process is as follows;

(i) at time equal zero, current collector, paste and acid solution separated. When the formation process starts, the surface of the paste rapidly sulfated to $PbSO_4$. We shall call this region $PbSO_4$ region. The extend of this $PbSO_4$ region mainly depends on the acid concentration. Note that both metasomatic or dissolution-precipitation oxidation can be facilitated by this $PbSO_4$ region. Two scenarios can emerge:

(a) For the case of high acid concentration, $PbSO_4$ region is large and closer to the current collector. Probability of the metasomatic and/or dissolution-precipitation $PbSO_4$ oxidation mechanisms to occur is high. As this $PbSO_4$ region oxidize, acid concentration rejuvenate itself, see **Figure 1.1** and **Table 1.3**. Recall that alkalization mechanism facilitated when the Pb^{2+} and H^+ ions increased the positive charge density of the certain region resulting the H^+ ions dissipate to maintain electroneutrality, this phenomenon explained in detailed in the **Section 4.1**. Effect of alkalization in the paste drops because of the shorter distance between the Pb^{2+} ions created at the $PbSO_4$ region/paste interface and the current collector, see **Figure 6.6c**. This phenomenon cannot efficiently occur in high acid samples since Pb^{2+} quickly oxidizes to Pb^{4+} and then PbO_2 decreasing the positive charge density due to shorter distance. Hence, the only oxidation product is the β-PbO_2.

(b) In the case of low acid concentration, $PbSO_4$ region is smaller, hence the probability of finding an electronic contact for the Pb^{2+} to Pb^{4+} oxidation decreases and distance increases. This leads to enough alkalization. As the time progress, paste oxidizes mainly to α-PbO_2. Since in the $PbSO_4$ region oxidation takes place further in the formation process, alkalization effect can stay dominant for a long enough time that α-PbO_2 modification can be produced. **Figure 6.6** represents the schematic of the proposed model. Note that both

$PbSO_4$ region and the paste are porous structures which allows ionic diffusion in some extent.

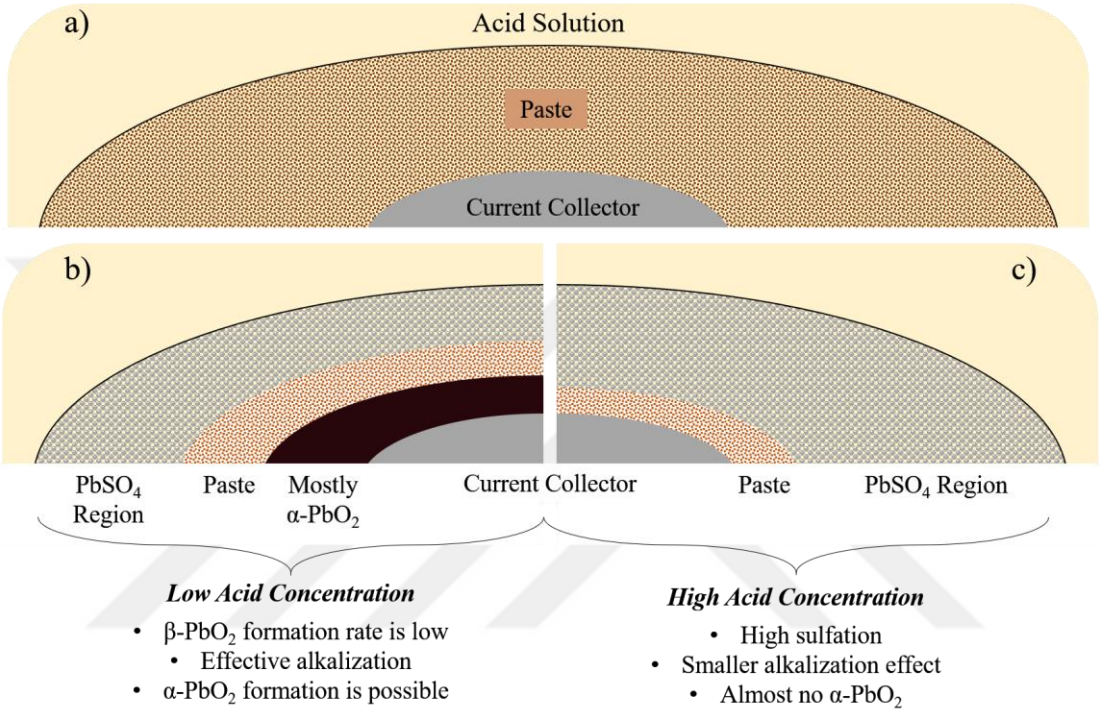

Figure 6.6. *Schematic comparison of high and low acid concentration on the formation characteristics. a) instant that plate submerged in H_2SO_4 solution, regional changes in; b) low acid concentration and c) high acid concentration*

Assuming that the dissolution-precipitation oxidation is dominant and ionic diffusion of Pb^{2+} excepted equally limited for both high and low acid samples. For low acid concentration samples, distance for the Pb^{2+} to travel is larger which leads to effective alkalization and α-PbO_2 formation. As the conductive PbO_2 starts to form close to current collector, electronic contact gets closer to $PbSO_4$ region hence β-PbO_2 formation starts. However, for high acid concentration, Pb^{2+} dissolved from the $PbSO_4$ region reaches the electronic contact before alkalization occurs which hinders the α-PbO_2 formation.

6.2. Scanning Electron Microscope (SEM) Results

In this section the morphologies of each plate will discussed in orderly fashion to understand the formation mechanism of the lead acid battery plates. Before starting, one should

remember that surface and inside terms used in context of away from and closer to the current collector grid, respectively. Samples produced on a grid that is similar to schematic at **Figure 4.5** which gives an idea for the surface and inside terms. In the following section will discussed several morphologies emerged during investigation.

6.2.1. Sample P1 (1.28 s.g. and 1 Ah)

Surface of the P1 sample appears to be consist of large $PbSO_4$ crystals in the shape of prisms in a PAM matrix. It is also noticed that these $PbSO_4$ prisms not effected from the formation step did not oxidize at all. This can be expected since this is the region that further away from the grid. See **Figure 6.7**.

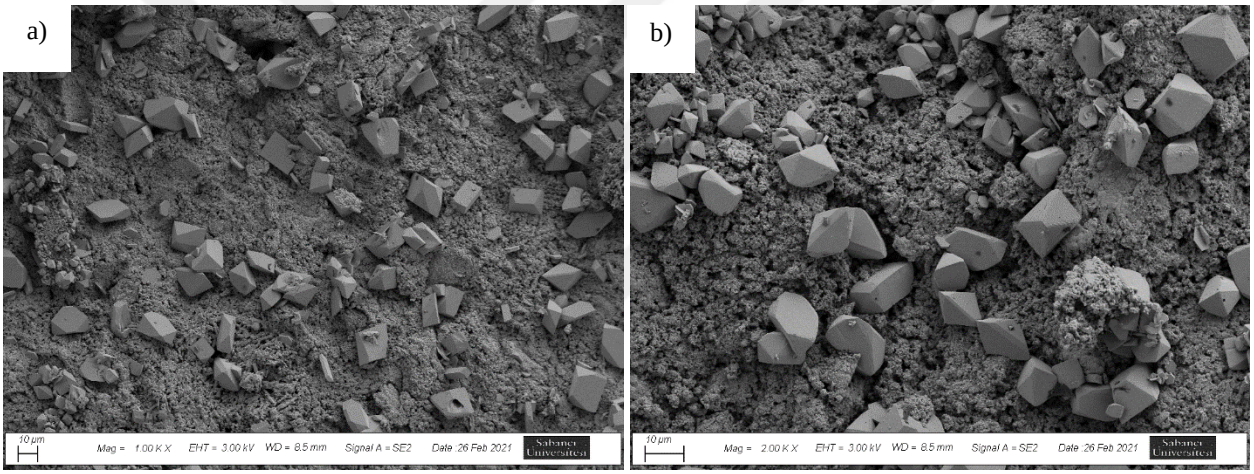

Figure 6.7. *Surface morphology of the P1 sample. a) 1000x and b) 2000x magnification.*

Further investigation reveals several reveals several interesting results. First the particle size of the $PbSO_4$ is not uniform which may interpret as some of the formed $PbSO_4$ grows to a certain size during formation. Also, well-shaped hexagonal structures also formed alongside the prismatic $PbSO_4$.

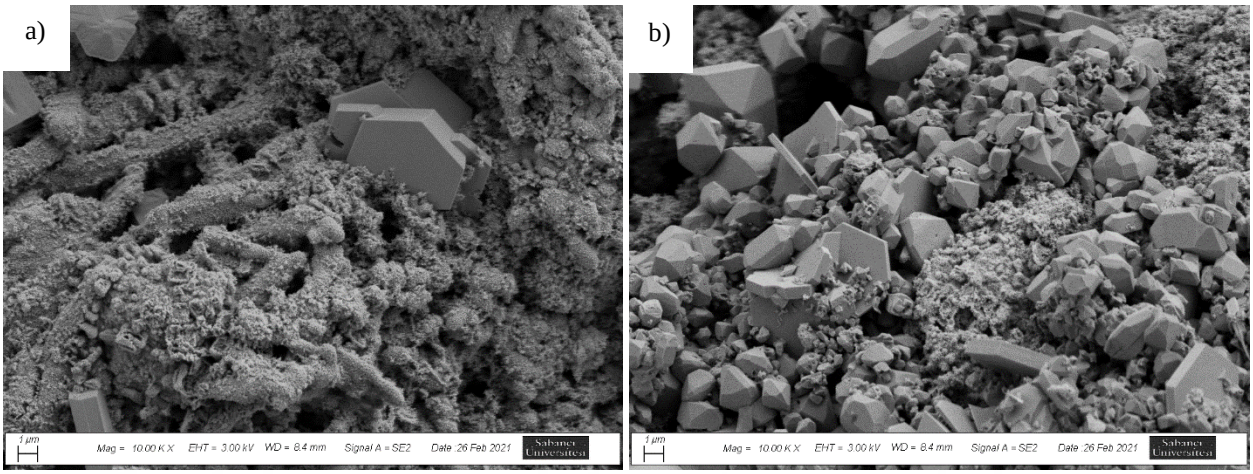

Figure 6.8. *Surface morphology of the P1 sample at 10000x magnification. $PbSO_4$ prisms with various sizes as well as the hexagonal morphologies are apparent.*

For the PAM structure, some of the PbO_2 appears to be formed on the long needle like morphologies, see **Figure 6.8a** and some created agglomerated structure, see **Figure 6.8b**. These long needle-like structures resemble the 3BS crystals that found in the plate at cured state, see **Figure 6.9**. It is interesting the observed these morphologies however they seem to occupy a small volume compared to the rest of the system.

Figure 6.9. *3BS crystals found in the cured plate.*

When the PAM structure at the surface of the electrode examined deeply one can see that the PbO_2 appears as a needle like morphology.

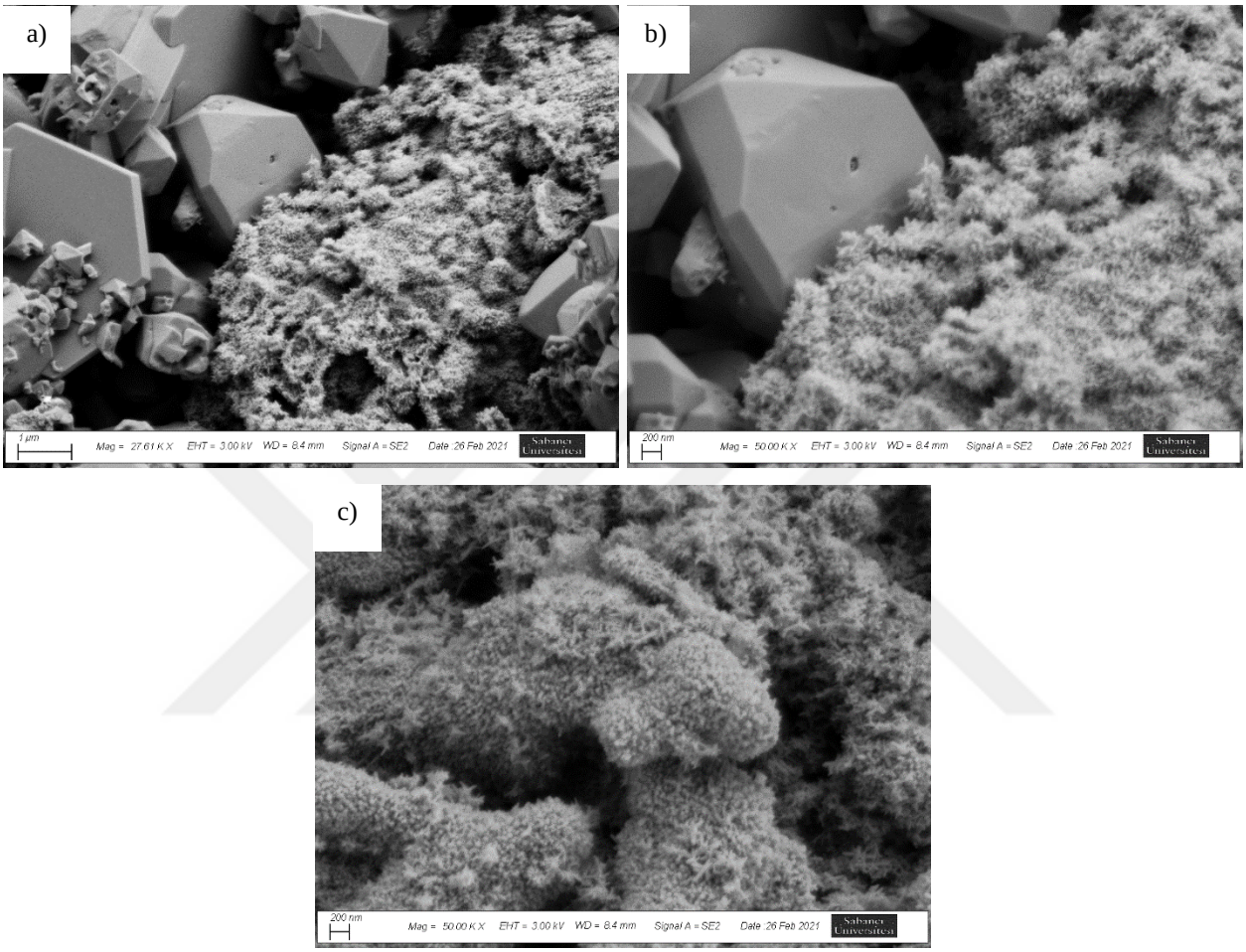

Figure 6.10. *Morphology of the PAM structure in P1. a) Needle like PbO_2 particles, b) larger magnification of a and c) needle like morphology from some other location.*

One should notice that in **Figure 6.10a** and **Figure 6.10b** it is apparent that the large $PbSO_4$ particles completely isolated from the PAM structure. This is not illogical since solubility of the larger particles are lower since which in return hinder both metasomatic and dissolution-precipitation mechanisms.

Interior regions of the P1 also investigated. Several different regions can be identified from the SEM images presented in the **Figure 6.11**. At **Figure 6.11a** one can see the $PbSO_4$ crystals starts to dissolve and lose their shapes regardless of their size. For PAM, metasomatic needle formation also present, see **Figure 6.11d**, and interestingly there is region where the PAM structure

appears to be much denser, **Figure 6.11c**. This region seems to formed form the agglomeration of these morphologies.

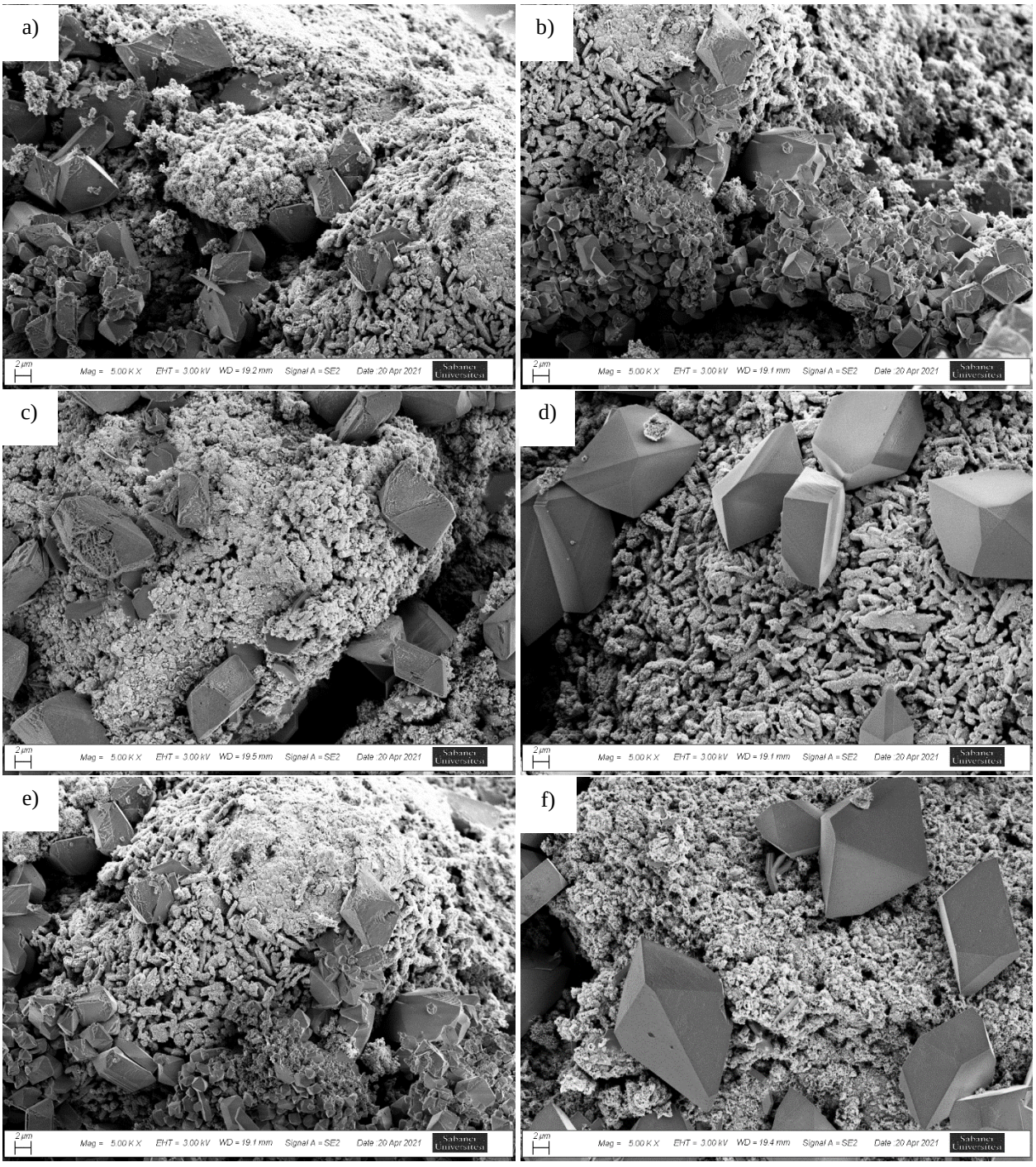

Figure 6.11. *Several morphologies emerged at the interior of the P1.*

Figure 6.11b shows similar regions but the $PbSO_4$ particles with various shapes seem to more connected to each other, especially smaller ones protect their shapes. This type of regions expected

to be inactive since the $PbSO_4$ is an insulator and supplied current cannot pass through this region because of it. **Figure 6.11c** to **Figure 6.11f** is very interesting since they appear to be complementing to each other. If the $PbSO_4$ particles did not grow, and instead, dissolved the needle like metasomatic morphology transformed in to denser PAM structure. But, if the $PbSO_4$ particles gets larger in size they completely isolated and needle like morphology stayed as is. In terms of PAM, again, several different structures observed. Figure below presents micrographs that taken from the several locations with 20000x magnification.

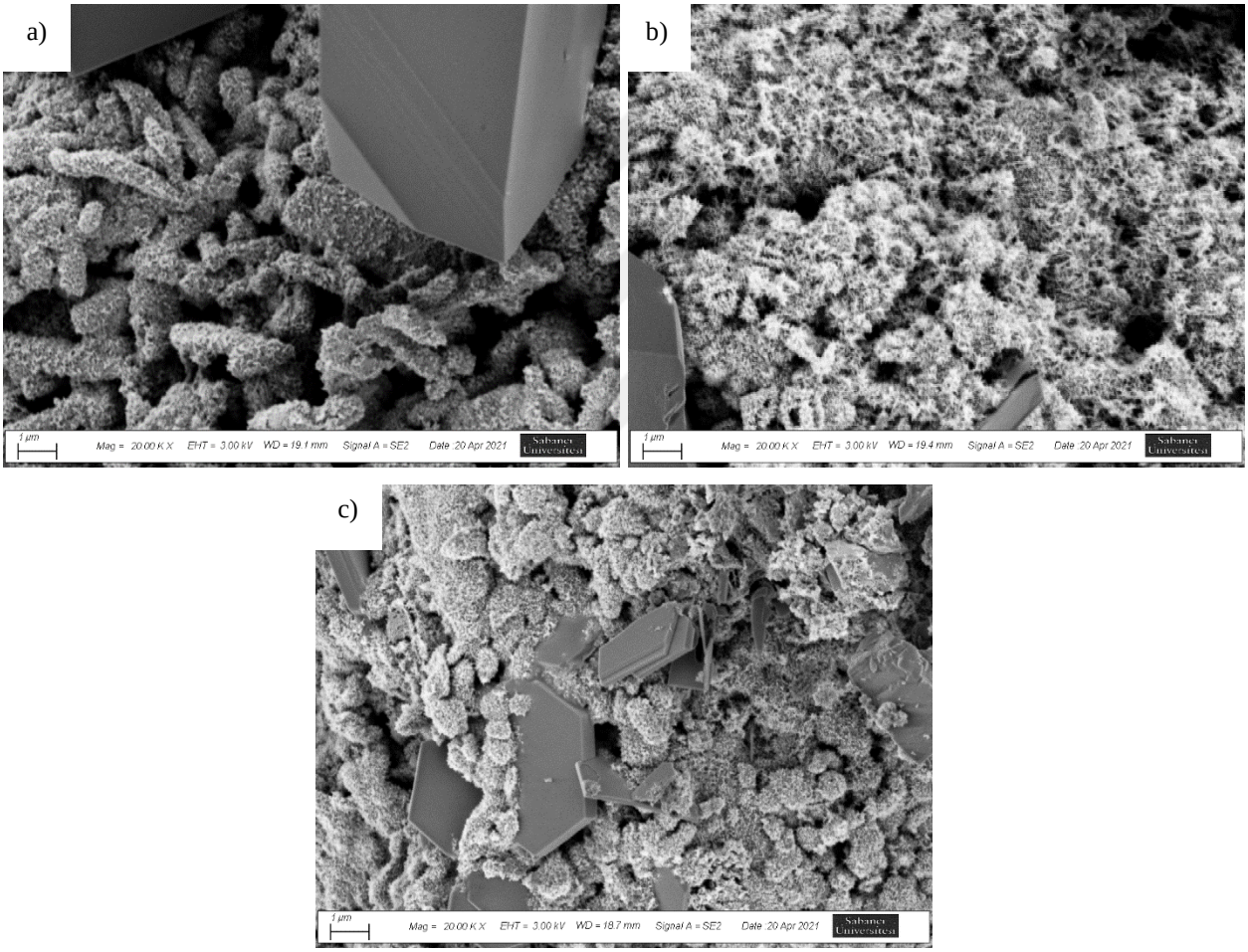

Figure 6.12. *Different PAM structures of the P1 sample.*

Figure 6.12a again shows the needle like morphologies precipitated on top of the 3BS like structure, PAM **Figure 6.12b** consist of agglomerates that consist of needle like particles that creates porous network, **Figure 6.12c** also similar to **Figure 6.12b** however agglomerates in this case rounder. Also, there is glimpse of the formation of the hexagonal morphology in the **Figure 6.12c**. See that, the hexagons grow on top of each other to get their final form. Main morphological

difference between the surface and the interior is the state of the $PbSO_4$ particles. $PbSO_4$ particles at the inside seems to be more damaged compared to the surface. Yet main takeaway would be the chaotic nature of the formation process that results in the heterogenous phase distribution and several morphologies for the PAM structure.

6.2.2. Sample P2 (1.28 s.g. and 4 Ah)

Surface of P2 is given in the figure below.

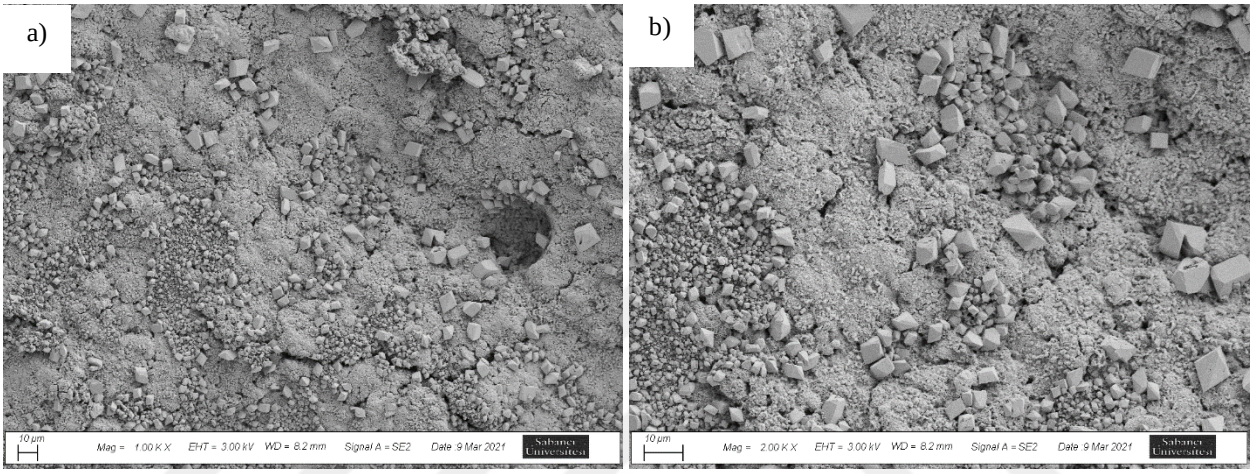

Figure 6.13. *Surface morphology of the P2. a) 1000x and b) 2000x magnification.*

Some $PbSO_4$ crystals still present at the surface even after 4 Ah of formation. Closer look reveals that the these $PbSO_4$ crystals are deforming and losing their well shapes. PAM macrostructure appears to be consisted of spherical agglomerates in porous network with varying pore structures, see that in **Figure 6.14a** porosity is higher compare to **Figure 6.14b**. needle like PbO_2 particles are more visible in **Figure 6.14b**, however closer look to the **Figure 6.14a** proves that this structure also consist of needle like PbO_2 particles, see **Figure 6.15**.

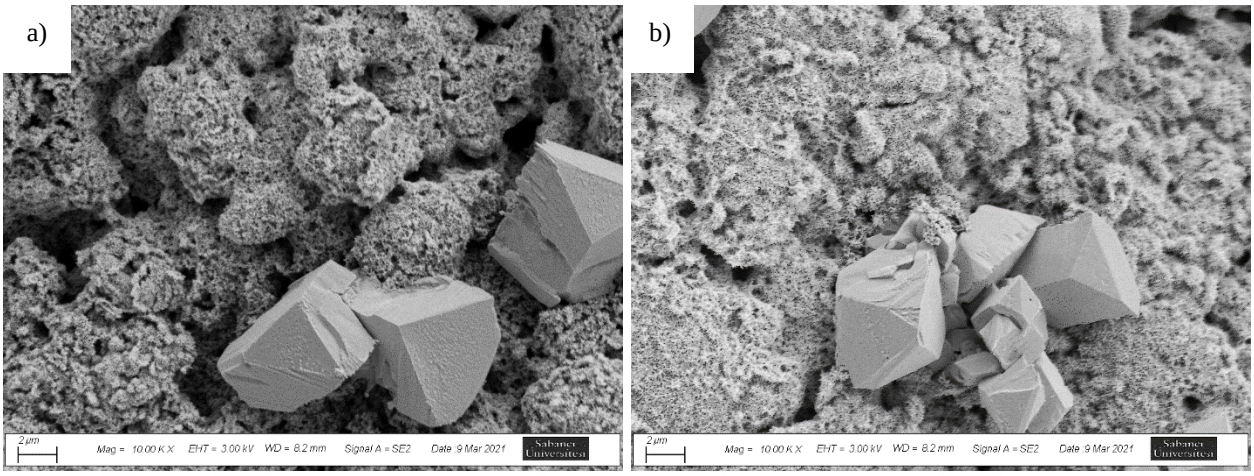

Figure 6.14. *PAM structure of P2 and remnant $PbSO_4$ particles.*

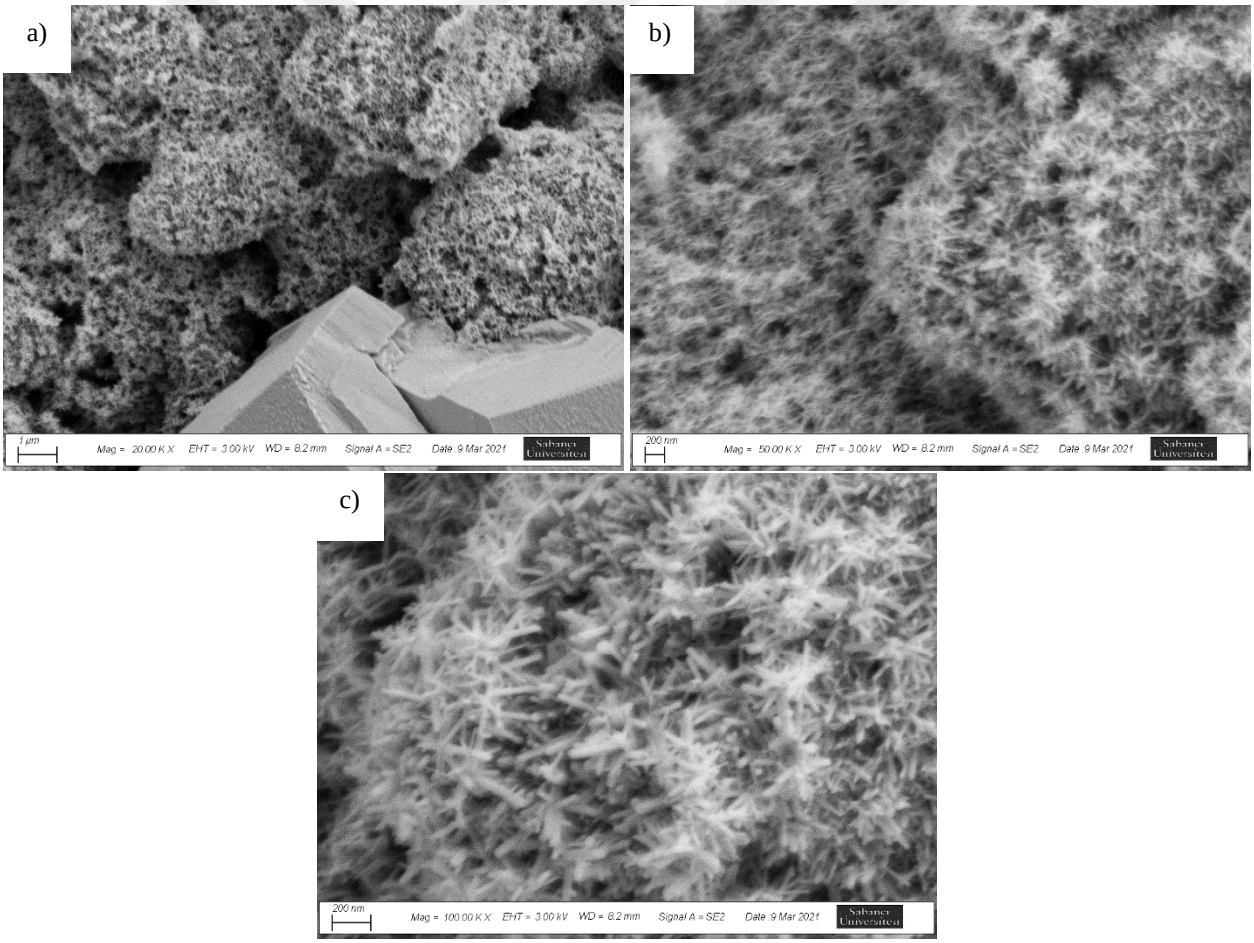

Figure 6.15. *Needle like PbO_2 particles. a)20000x, b) 50000x and c)100000x magnification.*

Interestingly enough the one branch of the agglomerate in the **Figure 6.15a** appears to be connected to the $PbSO_4$ crystal however rest of the crystal seems to be not affected from this condition. Size of the PbO_2 needles observed to be around 200 nm. Structure similar to samples at

Figure 6.15 observed by Pavlov *et. al*. when 3BS paste with 3.7 $g \cdot cm^{-3}$ density formed at 1.05 s.g. H_2SO_4 solution, see figure 6 in the article[92]. Their needle like morphology appeared when low paste density and low acid density is used, while, in this study similar microstructure formed when high paste density and high acid density samples are used. Notice that acid density used in this study is quite large, however, the paste density of our samples is larger than 4 $g \cdot cm^{-3}$. This is actually in line with the explanation given in the **Figure 6.6** since either higher acid density (for high paste density) or low paste density (for low acid density) can facilitate the increase in the $PbSO_4$ region given in the **Figure 6.6**. For high acid and high paste density, driving force for sulfation increased due to increased chemical potential of the sulfate ions. For low acid and low paste density movement of the sulfate ions becomes easier due to increased porosity of the paste. This shows that morphology of the PAM structure is a function of many production parameter and these parameters equally responsible for the resulting PAM morphology. Pavlov *et. al*. also showed that as the paste density increased the PAM morphology became more spherical, see figure 6 and 7 in their article[92].

Interior of the P2 appears to be completed its formation. Only, little amount of the volume not effected from the formation mechanisms. **Figure 6.16** is a micrograph taken form the interior of the P2 sample. Almost no $PbSO_4$ crystal survived from the formation. Yet some isolated $PbSO_4$ crystals can be found when deeper analysis is conducted, see **Figure 6.17**. Fully formed PAM structure and isolated $PbSO_4$ agglomerate can be seen in the **Figure 6.18** as well. One thing to notice as well, is that the hexagonal morphology is not obverse in P2. Which indicates it's an intermediate oxidation product, probably $PbSO_4$.

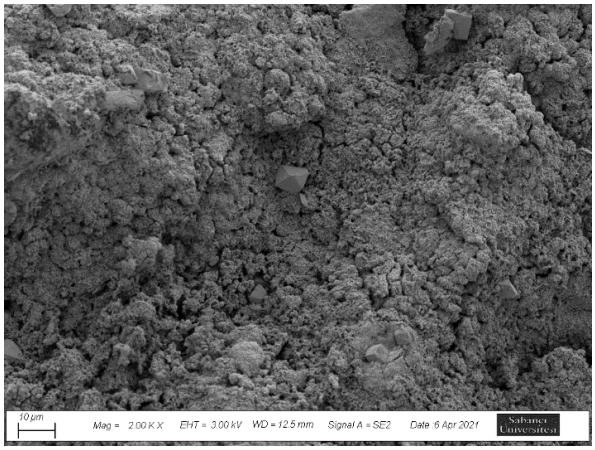

Figure 6.16. *Interior of the P2 sample.*

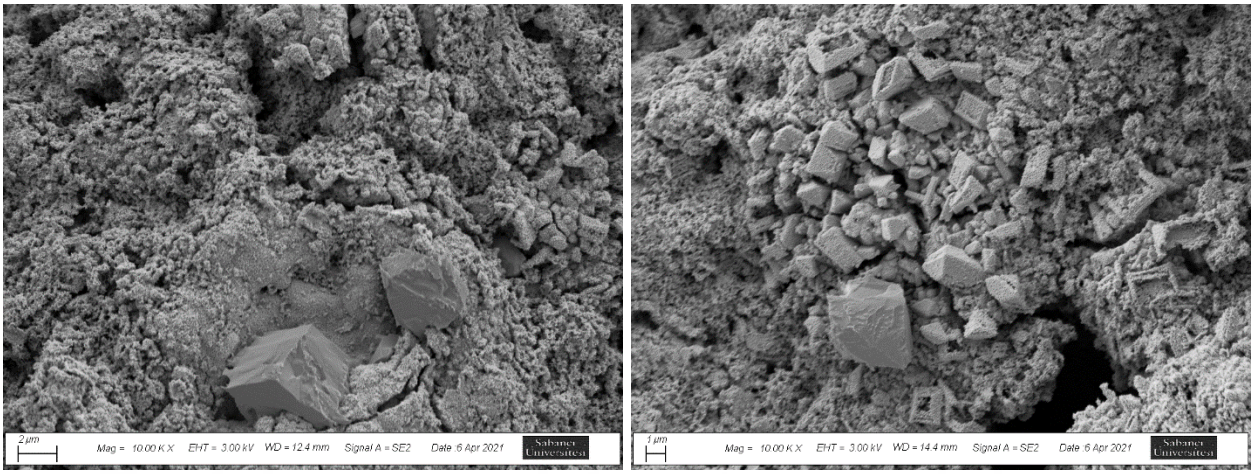

Figure 6.17. *$PbSO_4$ regions that not effected from the formation.*

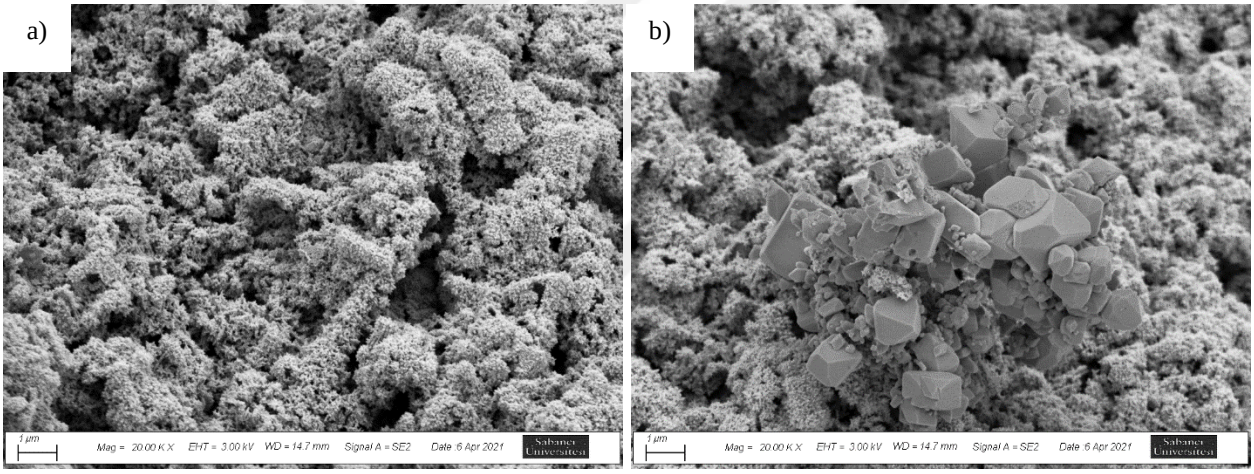

Figure 6.18. *a) PAM and b) $PbSO_4$ agglomerate structures.*

6.2.3. Sample P3 (Cut-off below 2.7 V)

Formation process of this sample stopped when potential is just below 2.7 V. Ah values are not supplied, however, similar to P1 and P2 1.28 s.g. acid is used.

Surface of the P3 observed SEM imaging. Morphology appears to be similar to P2 with smaller $PbSO_4$ prisms are visible.

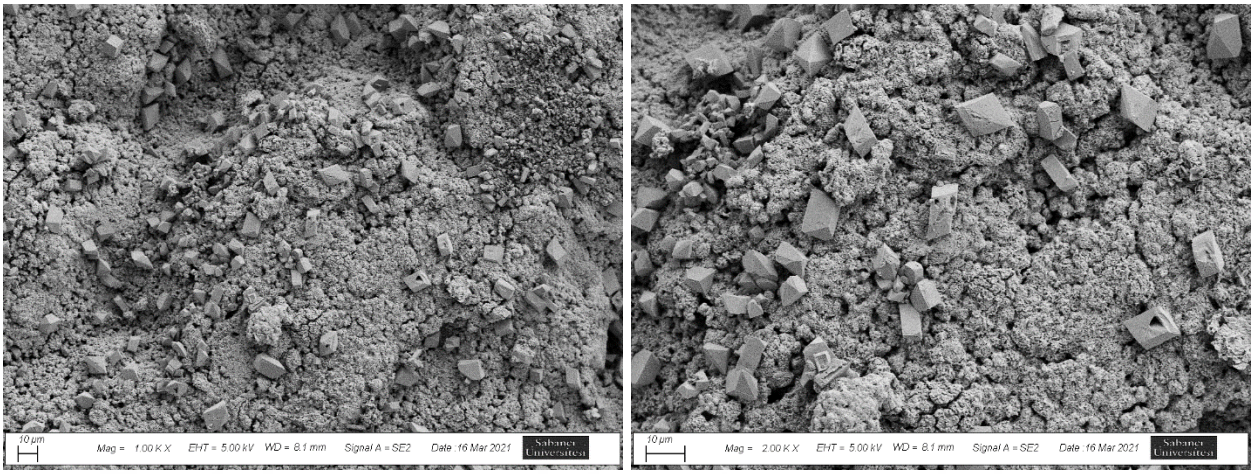

Figure 6.19. *Surface morphology of the P3 sample.*

It is clear that some of the $PbSO_4$ crystals are started to dissolved, see **Figure 6.20** and there is no indication of the needle like metasomatic transformation similar to **Figure 6.8a**, **Figure 6.11d** and **Figure 6.12a** that appeared in P1 sample.

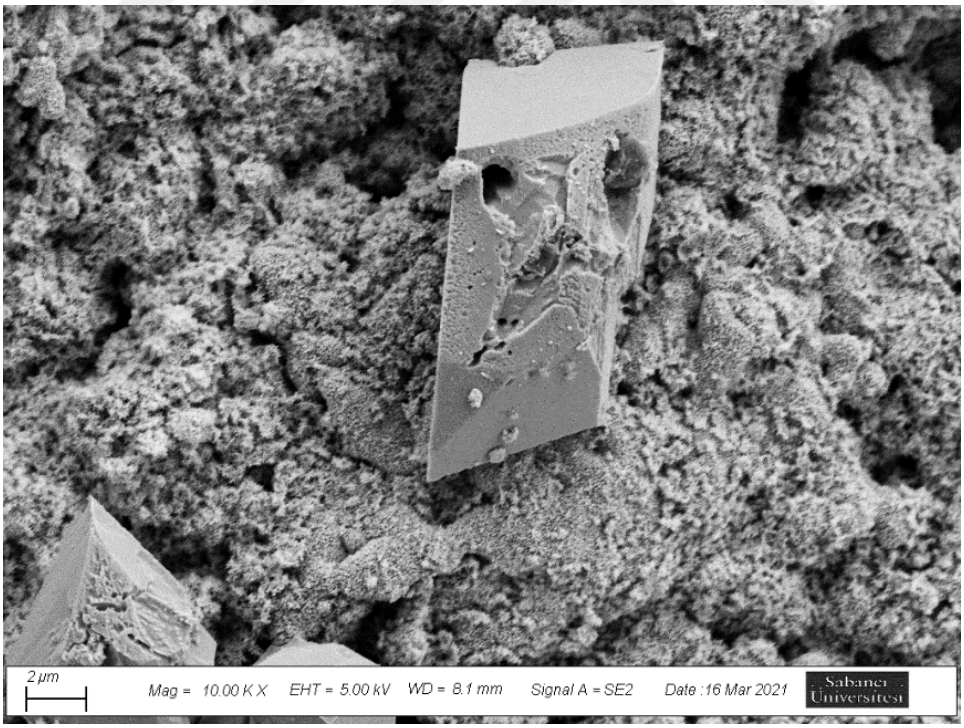

Figure 6.20. *Dissolved $PbSO_4$ crystal.*

PAM structure consists of agglomerated needle like PbO_2 crystals, see **Figure 6.21**.

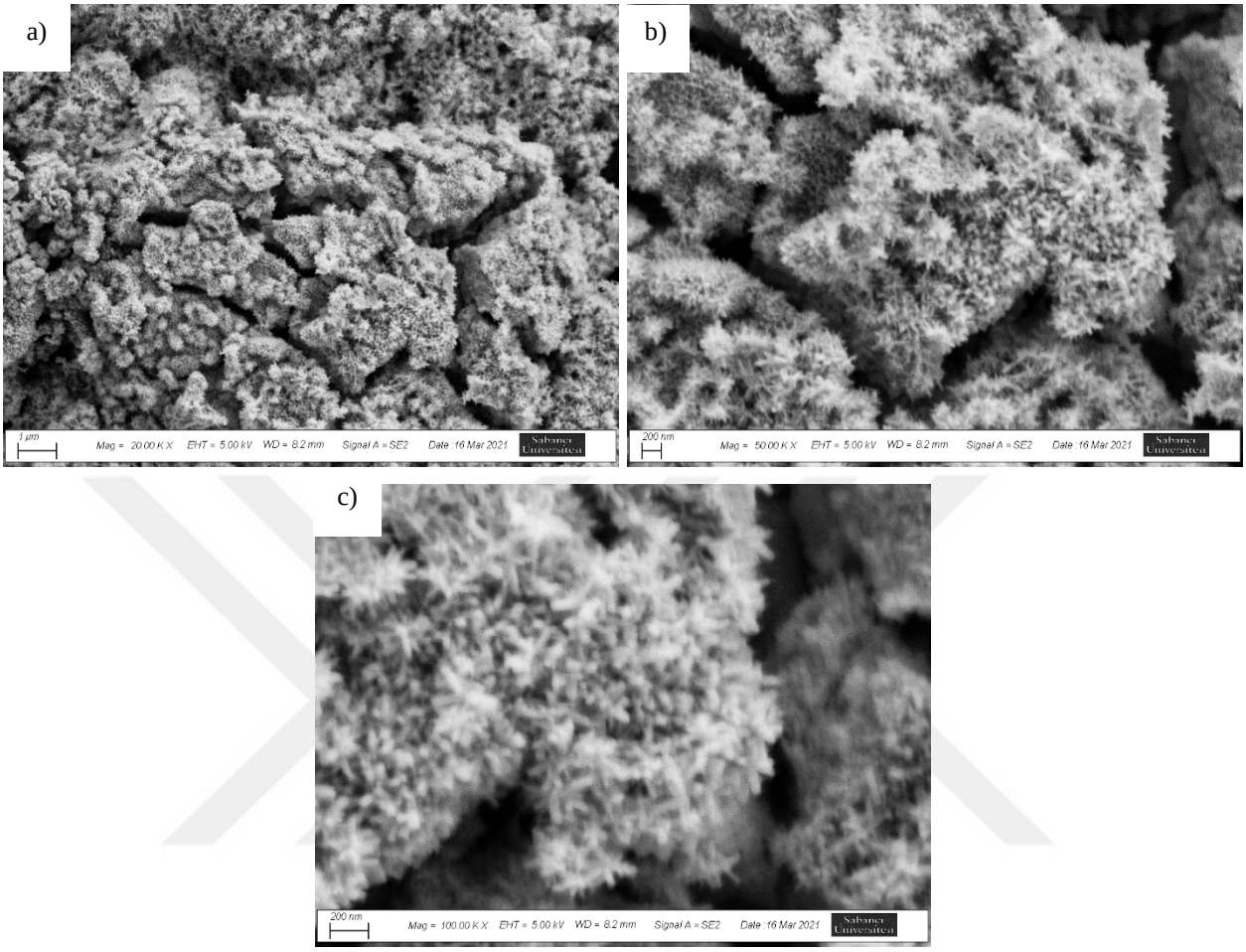

Figure 6.21. *PAM structure of the P2 sample. a) PbO_2 agglomerates, b) higher magnification of a and c) needle like PbO_2 particles.*

6.2.4. Sample P4 (No voltage cut-off)

Similar to P3 formation Ah did not given, this sample subjected to a formation without any potential cut-off criteria with 1.28 s.g. acid density.

Surface micrographs of the sample shows that the sample is further in to the formation process, see **Figure 6.22**. $PbSO_4$ crystal fraction as well as the size of these crystals appears to be low. Some $PbSO_4$ clearly damaged, and since the metasomatic transformation appears to be limited it can be said that these dissolved $PbSO_4$ crystals oxidize to PbO_2 via dissolution-precipitation mechanism. However, some metasomatic needle like formation can be observed for the PAM. But the extend of such reaction is small at least in the electrode surface, see **Figure 6.22b**.

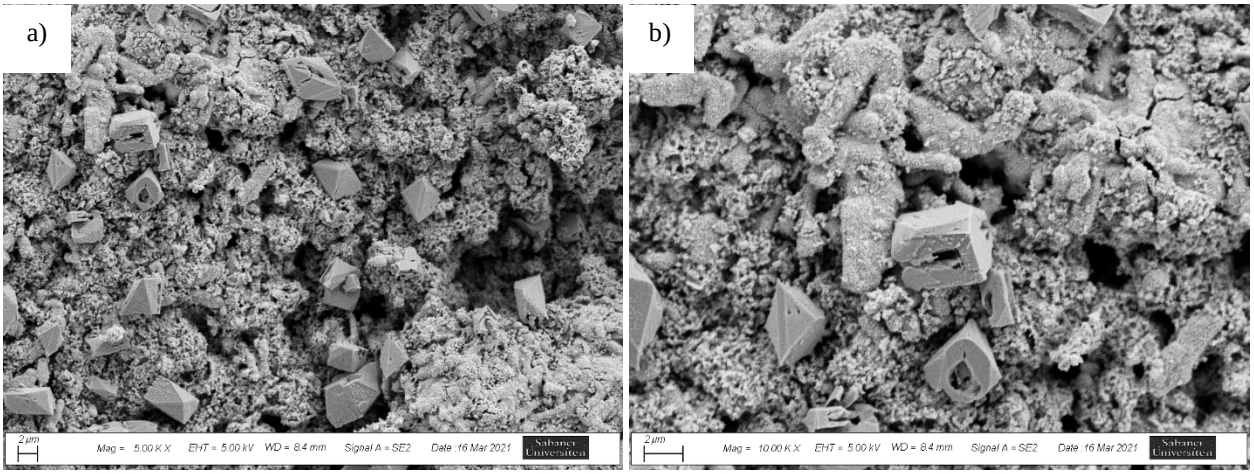

Figure 6.22. *Surface morphology of the P4 sample.*

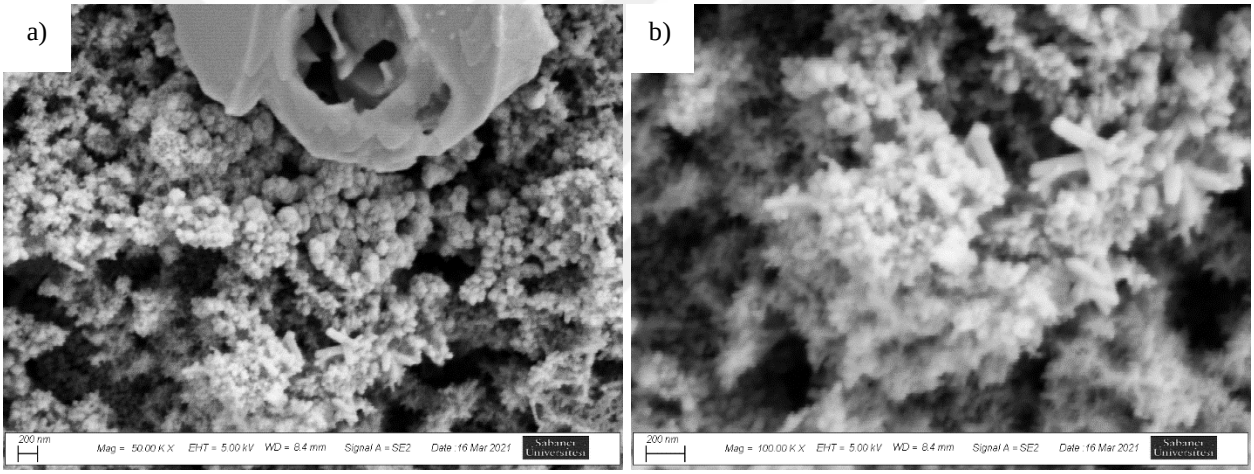

Figure 6.23. *PbO_2 particles with a) spherical (50000x magnification) and b) needle like (100000x) morphology.*

Interestingly some spherical PbO_2 particles are present addition to the needle like particles. **Figure 6.23** represent both of the morphologies.

Interior of the P3 and P4 is not investigated since it is not possible, our healthy, to used them in comparative study since the Ah values are unknown and the voltage profile not shared as well.

6.2.5. Sample P5 (1.16 s.g. and 1 Ah)

Surface SEM images for this sample reveals no $PbSO_4$ prisms at the first glance, see. **Figure 6.24**. One can see that there is no indication of the sulfate phase at 1000x, 2000x and 5000x magnifications.

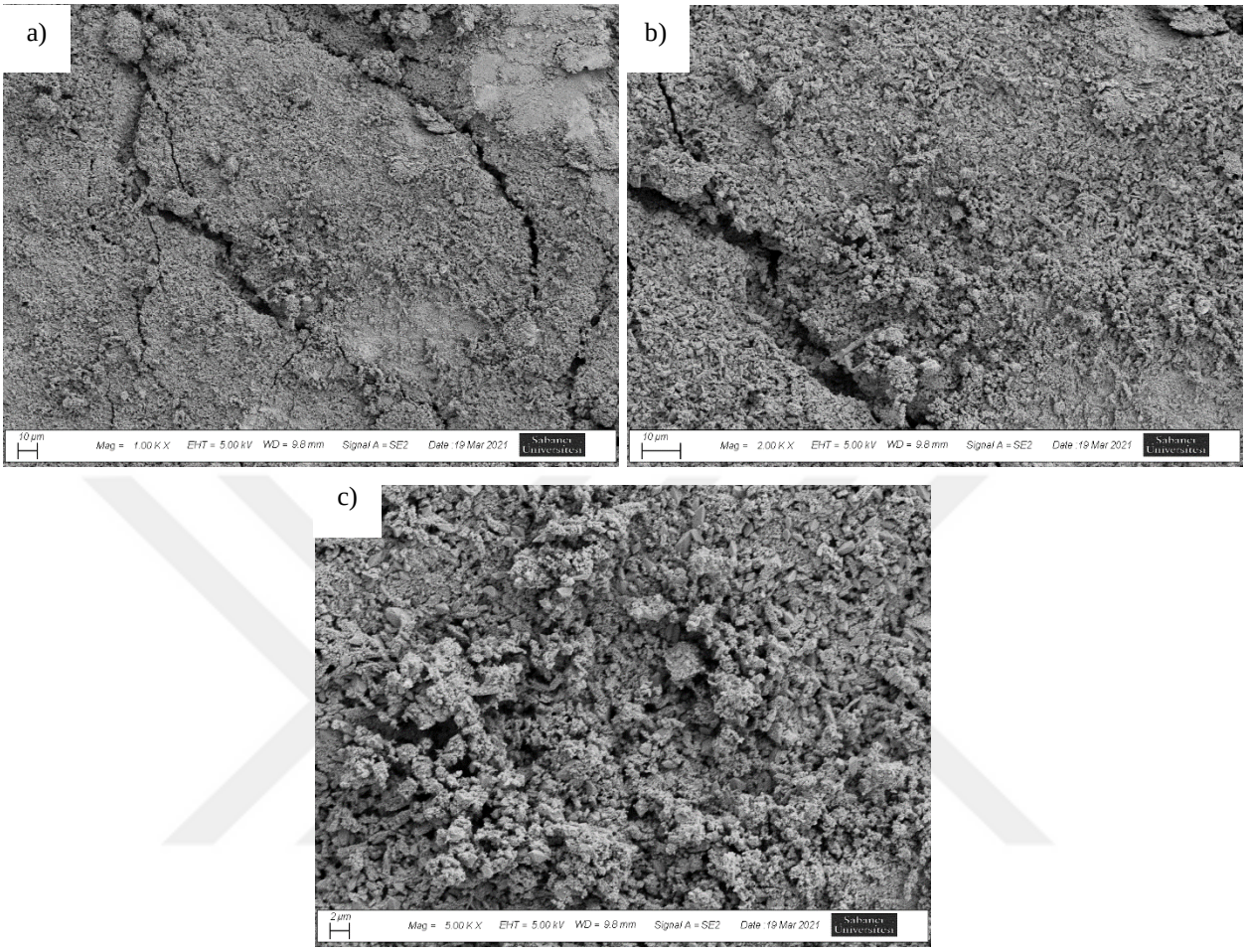

Figure 6.24. *Surface morphology of the P5 sample.*

However, larger magnifications reveal that there is large number of $PbSO_4$ crystals with smaller dimensions. **Figure 6.25** shows the morphology of the $PbSO_4$ crystals on the surface of the sample.

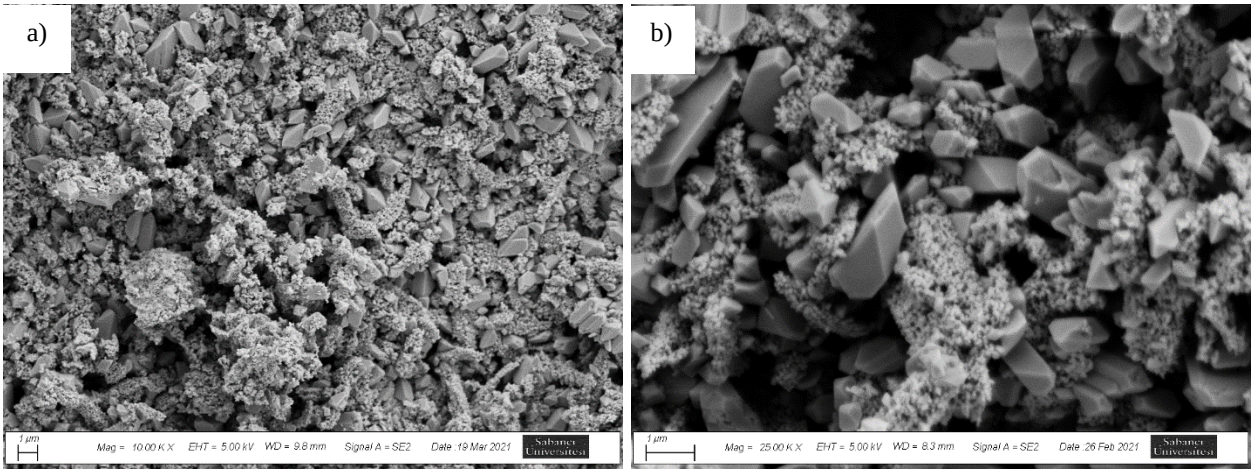

Figure 6.25. *$PbSO_4$ crystals at the surface of the P5 sample. a) 10000x and b)25000x magnification.*

These interesting features of this sample reveal itself with higher magnifications. Figure below is for shows the PbO_2 particles present at the surface.

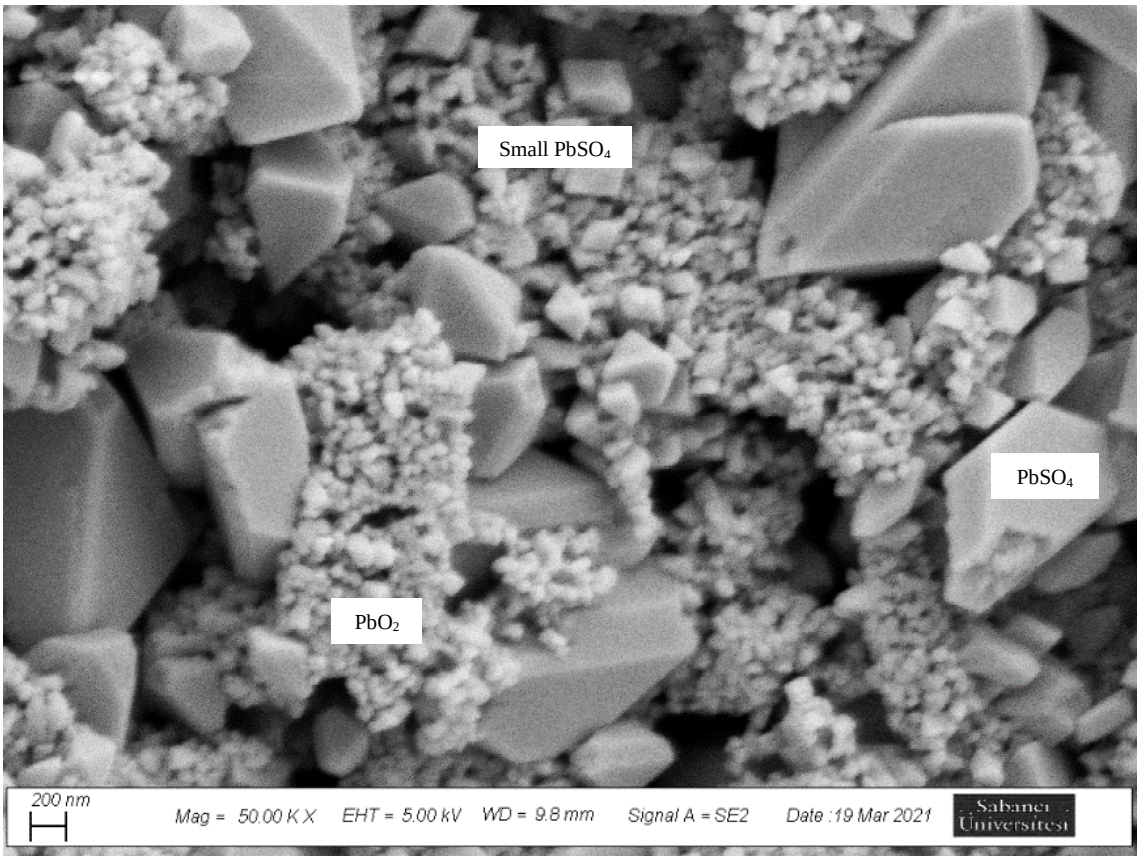

Figure 6.26. *PbO_2 crystals at the surface of the P5 sample.*

Notice the dissolved $PbSO_4$ crystal at the right side and the PbO_2 crystals at the left side of the **Figure 6.26**, pointed out in the figure. One of the morphologies assign to the PbO_2 crystals since it is clear that these particles lacks the clear-cut face and edges compared to the smaller $PbSO_4$ particles.

Interior of the sample, like the surface, lacks large $PbSO_4$ particles. at 2000x magnification $PbSO_4$ particles with 10 μm size starts to appear. These sulfate particles damaged and most probably material that leave from their surfaces oxidized via dissolution-precipitation mechanism. These particles are embedded inside the PAM, see **Figure 6.27.** Damaged PbSO4 particles at the interior of the P5 sample. **Figure 6.27**.

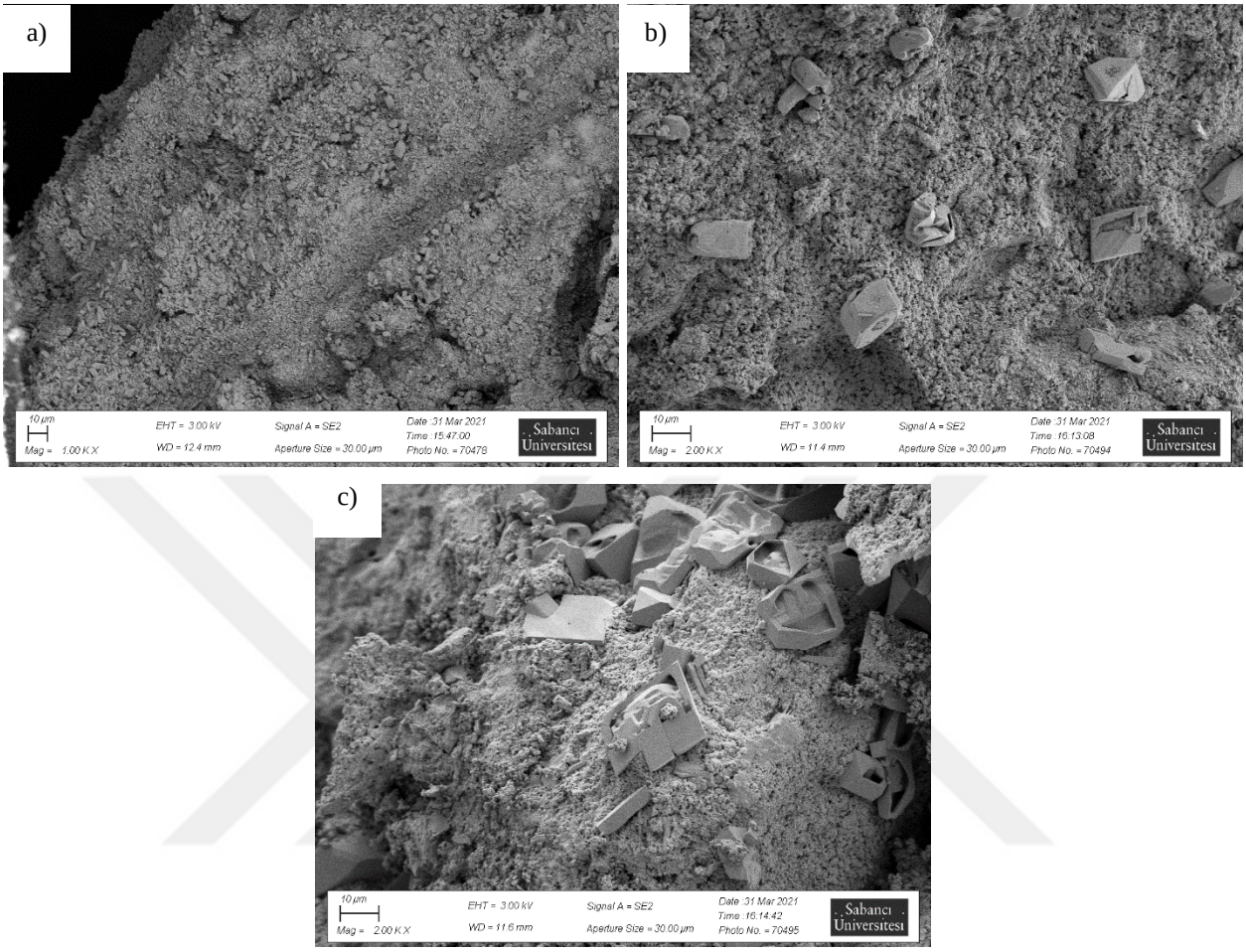

Figure 6.27. *Damaged $PbSO_4$ particles at the interior of the P5 sample.*

Images taken at same magnification but from different locations shows severely different morphological characteristics. Figure below presents two images taken with 5000x magnification.

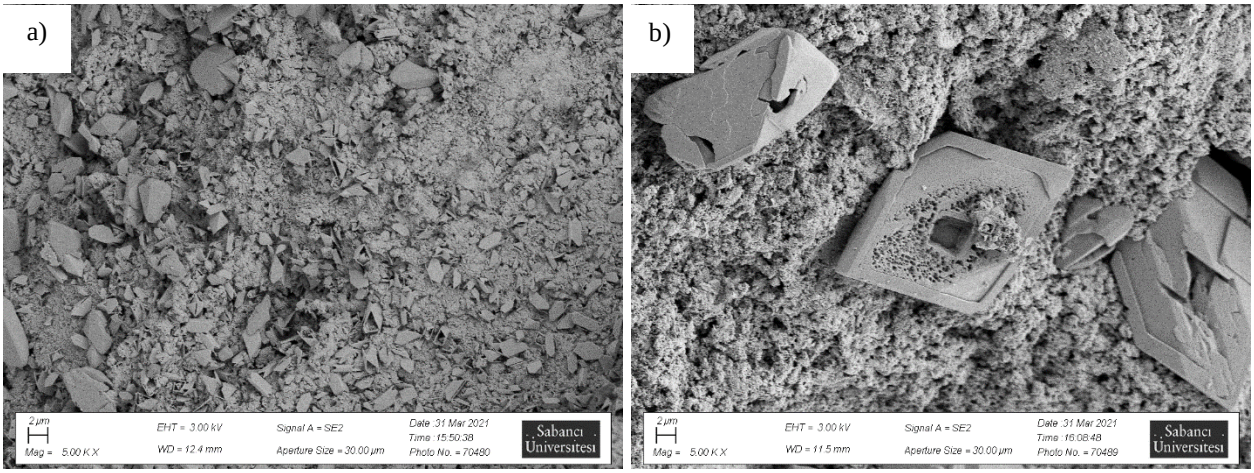

Figure 6.28. *Different morphologies appear in the P5 sample.*

Notice, at **Figure 6.28a** smaller $PbSO_4$ particles and some examples for the metasomatic $PbSO_4$ to PbO_2 transformation present. Yet in **Figure 6.28b** large, damaged $PbSO_4$ particles embedded in PbO_2 matrix. Even closer look at 10000x reveals regions with different morphologies.

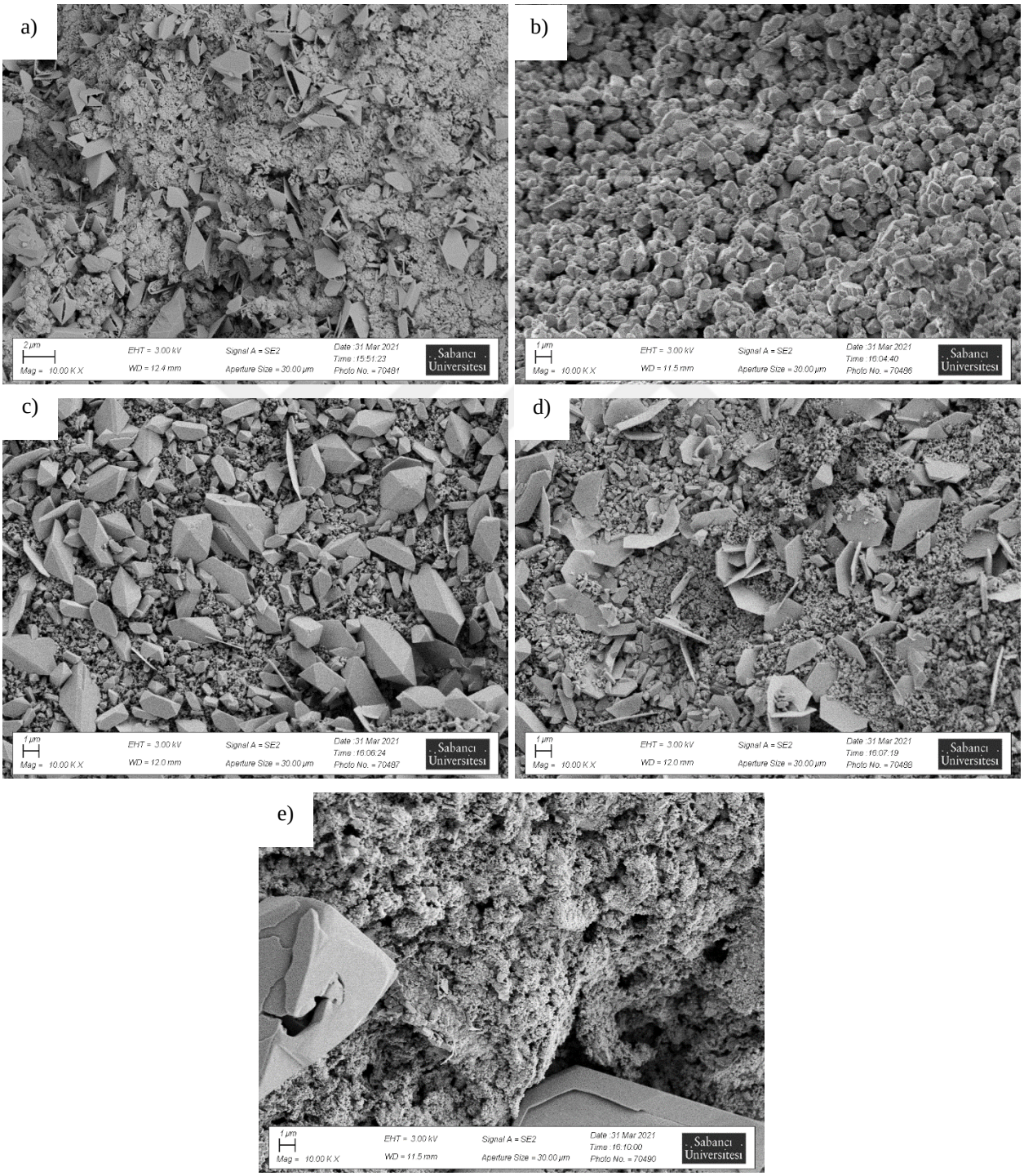

Figure 6.29. *Regional changes in PAM morphology for P5 sample.*

Figure 6.29a to **Figure 6.29e** taken in a successive manner in different locations, see the dates and photo numbers. In **Figure 6.29a** metasomatic PbO_2 transformation is more visible, these PbO_2 particles are spherical. As the metasomatic process proceeds $PbSO_4$ particles completely breaks, since the P5 can be considered as intermediate formation step, metasomatic transformation can be observed. **Figure 6.29b** also quite strange, this region appears to dominated by the smaller $PbSO_4$ particles such that taking the image was challenging due to charging. **Figure 6.29c** and the **Figure 6.29d** seems are close to each other in terms of formation condition. Many thin hexagonal plates in the **Figure 6.29d** is visible as well as the small $PbSO_4$ crystals. Finally, **Figure 6.29e** shows large $PbSO_4$ crystals which isolated from the PAM structure. Overall, **Figure 6.29** shows how complex the formation process is with several different mechanism occurring simultaneously with different extent in different regions. Metasomatic transformation mentioned a lot in the section. **Figure 6.30** shows clear evidence for the metasomatic $PbSO_4$ transformation. Notice the structure at the right end side of the **Figure 6.30b**, it can be said that the $PbSO_4$ crystal with well-defined surfaces starts to transformed in to PbO_2, transformation proceeds towards the inside of the $PbSO_4$ crystal in a similar manner described in the **Figure 4.9**. Eventually, since the PbO_2 has lower molar volume, $PbSO_4$ particles break in to pieces.

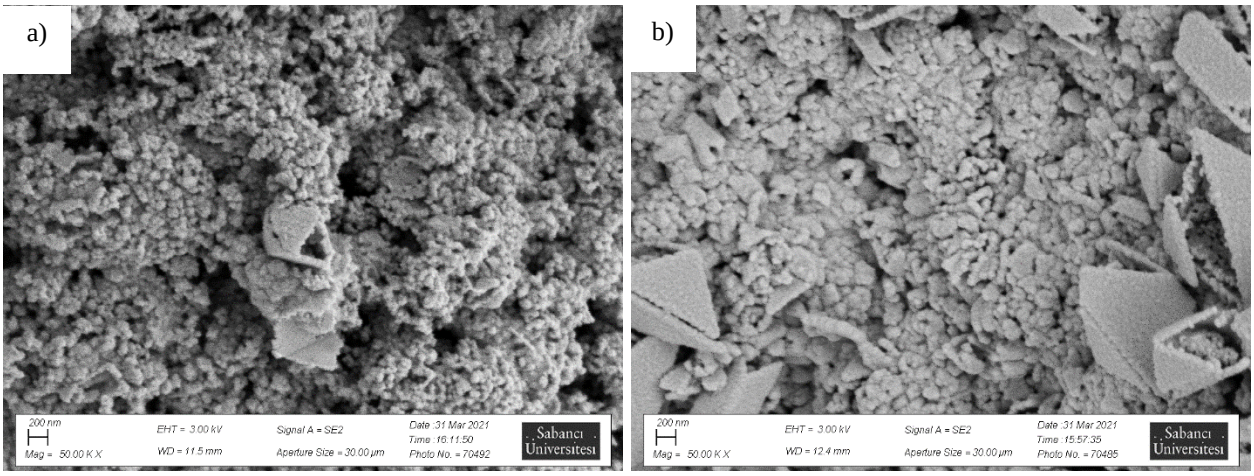

Figure 6.30. *Metasomatic transformation observed in the P5 sample.*

Note that even the transformation of $PbSO_4$ to PbO_2 is metasomatic in some cases, shape of the $PbSO_4$ did not retained, unlike the 4BS metasomatic transformation. Reason might be the change in the molar volumes during the metasomatic transformation. Molar volume of PbO_2 almost half the value of $PbSO_4$, 24.4 and 48.2 cm^3·mole, respectively[6], [8].

6.2.6. Sample P6 (1.16 s.g. and 4 Ah)

Surface of the P6 most consist of PbO_2 network. Some deformed/damaged $PbSO_4$ particles also can be observed, see **Figure 6.31**.

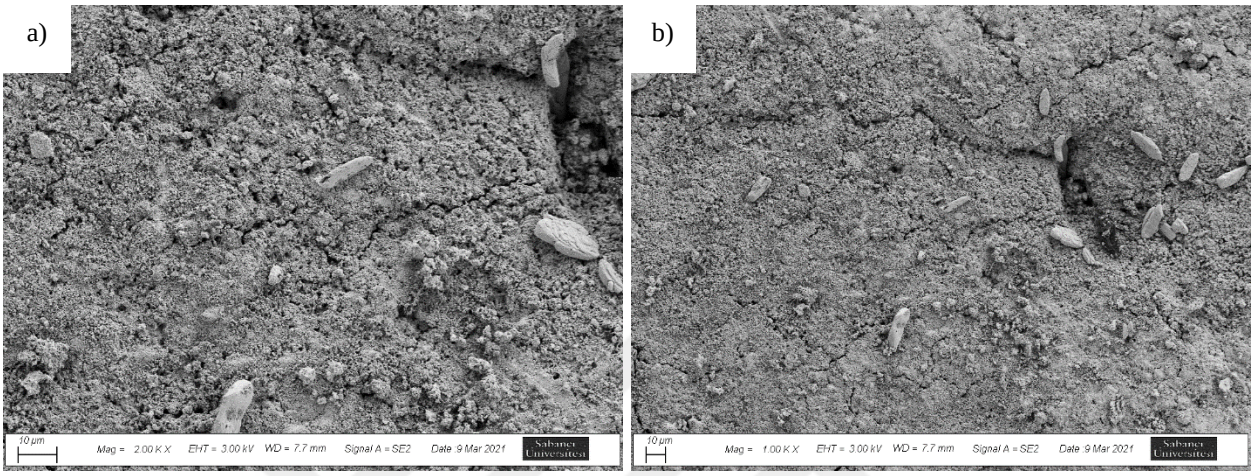

Figure 6.31. *Surface morphology of the P6 sample.*

Closer look reveals perfectly formed porous network of PbO_2 agglomerates, and these agglomerates consist of individual PbO_2 particles.

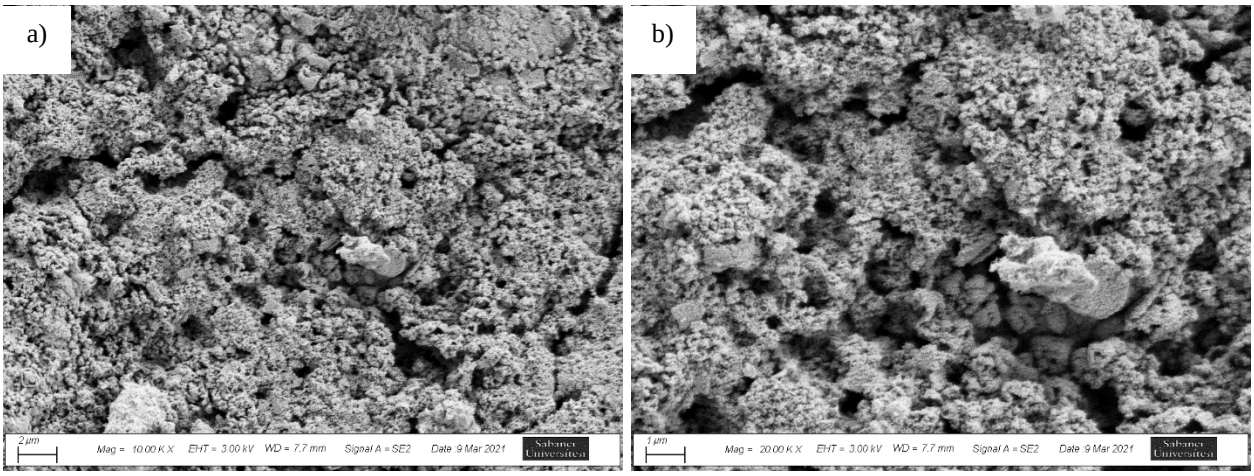

Figure 6.32. *PAM structure of the P6 sample at the surface.*

It can be said that at the surface PAM is rather dense and large pore density is relatively low. In terms of PbO_2 morphology, two different structure is observed. Pavlov et. al. presented similar structure to **Figure 6.32**, see figure 5 in their article[92]. Sample in **Figure 6.32** also consists of mainly spherical particles which forms the agglomerates. Compared to the microstructures presented in Pavlov *et. al*. **Figure 6.32** appears to be denser which is probably a result from the fact that the initial paste density being higher for the P6 sample.

Figure 6.33a show the rounder, more spherical PbO_2 particles coming together to form agglomerates, while **Figure 6.33b** shows needle like PbO_2 morphology.

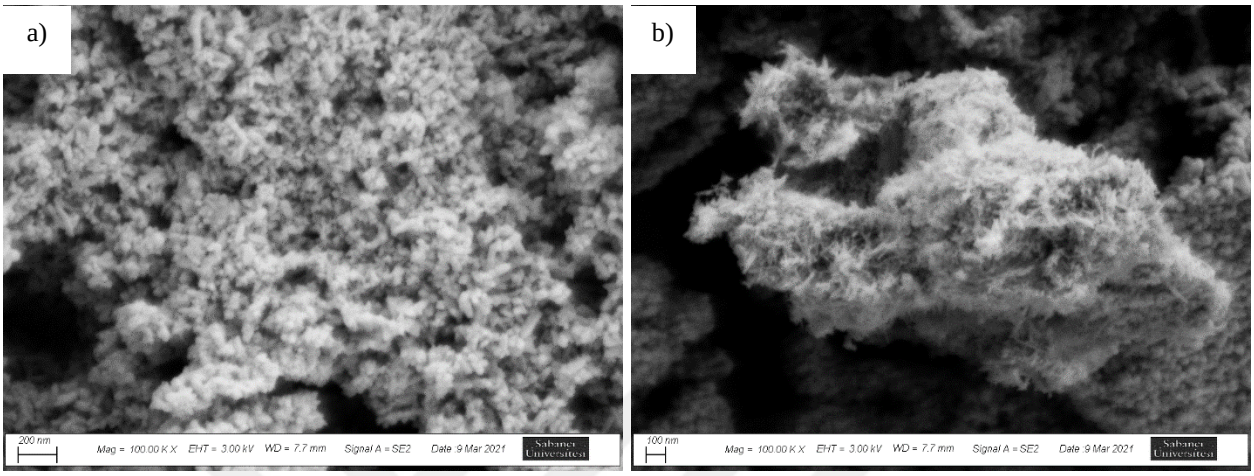

Figure 6.33. *PbO_2 particles at the surface of the P6 sample. a) spherical and b) needle like morphology.*

Interior of the sample, however, shows some large unformed $PbSO_4$ particles, most of them again about 10 μm in size, see **Figure 6.34**. This rather puzzling since one can expect formation efficiency of these regions to be better.

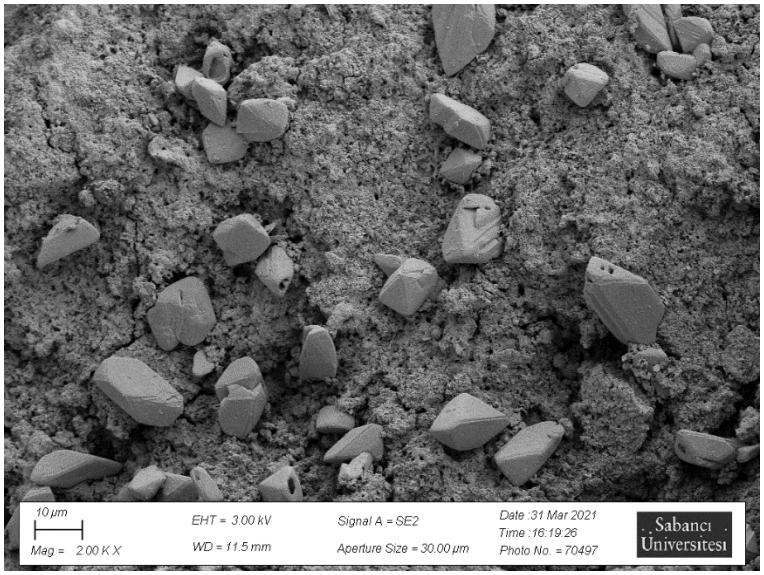

Figure 6.34. *Interior of the P6 sample.*

Again, it is possible to see differences in phase content and subsequent morphology differences in the different regions. These results show that formation some remnant $PbSO_4$ particles cannot be

avoided. **Figure 6.35a** show the some of those ppbso4 particles and **Figure 6.35b** shows the PAM structure at the interior of the P6 sample.

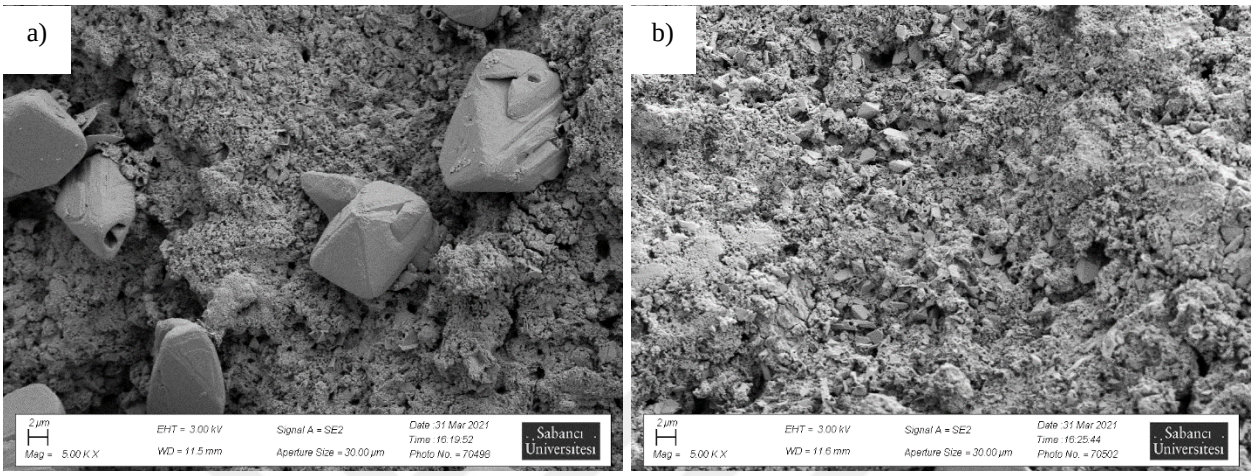

Figure 6.35. *a) Remnant $PbSO_4$ particle, b) PAM structure.*

More metasomatic transformation can be observed for the P6. **Figure 6.36** shows the mechanism with two different magnification.

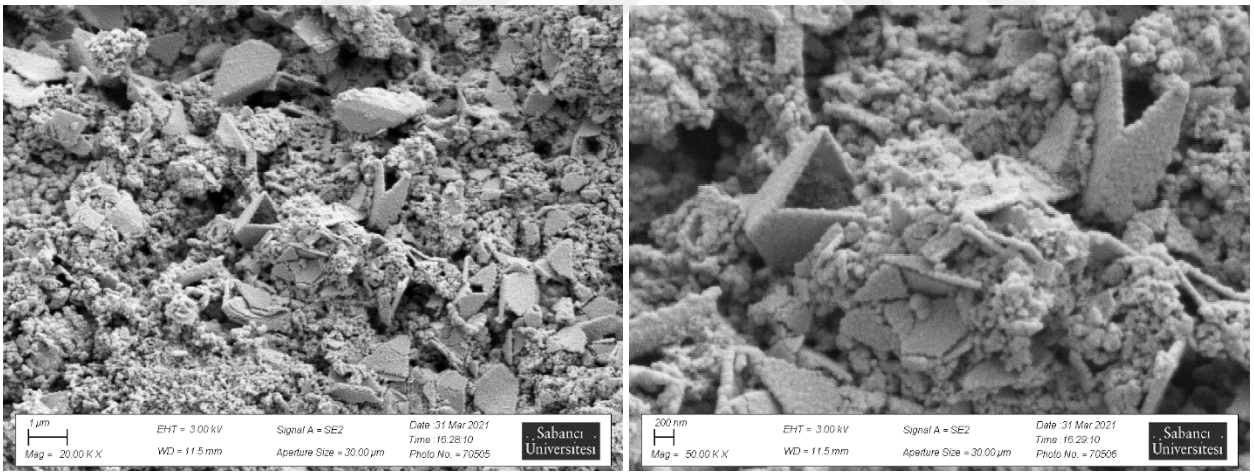

Figure 6.36. *Metasomatic PbO_2 formation at the interior of P6 sample.*

Results presented here quite in line with the PAM description made by Pavlov *et. al*[88]., see ***Figure 4.6***.. They also described a PAM structure that consist of aggregates (here term agglomerates used) made up from needle like and/or spherical particles[88]. Since this study mainly focuses on the PbO_2 polymorph morphology it is therefore necessary to comparatively investigate the effect of the formation parameters like Ah and acid density on the PAM.

Before examining the effect of the formation profile (Ah) and the acid density on the morphology, observed structures for the samples P1, P2, P5 and P6 are listed below.

Table 6.2. *Encountered phases and morphologies in the sample.*

	P1		P2		P5		P6	
	Surface	Interior	Surface	Interior	Surface	Interior	Surface	Interior
$PbSO_4$ Prisms	✓	✓	✓	✓	✓	✓		✓
$PbSO_4$ Hexagons	✓	✓			✓	✓		
$PbSO_4$ Dissolved		✓				✓		
$PbSO_4$ Metasomatic						✓		✓
PbO_2 on 3BS	✓	✓						
PbO_2 Needles	✓	✓	✓	✓			✓	
PbO_2 Spheres			✓		✓	✓	✓	✓

This table just presents the dominant phase and morphologies observed in samples, not all the morphologies observed in the samples. Given the chaotic nature of the formation process, especially for the P1 and P5, it is convenient to have a more general view.

6.3. Comparison of the SEM Results

Effect of the Ah and the acid density on the phase composition is commented earlier, in the following sections, effect of these parameters on the morphology will be discussed.

6.3.1. Effect of formation time of the morphology

6.3.1.1. P1 vs P2

Surface images shows that the as the formation proceeds $PbSO_4$ particles size decreases, as expected. For the P1 sample (1 Ah) many 10 μm size $PbSO_4$ particles are observable $PbSO_4$ particle size distribution rather uniform compared to the P2 sample (4 Ah). for the P2 sample $PbSO_4$ decreases as well as the standard deviation of the particle size distribution becomes larger, **Figure 6.37**. This result is expected since as the formation continues large $PbSO_4$ particles in the P1 will transforms in to PbO_2 since under the applied potential PbO_2 is the stable phase. It can be

said that for the P1, $PbSO_4$ particles appears to be better shaped and their surfaces are smother compared to the $PbSO_4$ particles encountered in P2 sample. This may indicate the dissolution of these particles with time and subsequent oxidation to PbO_2.

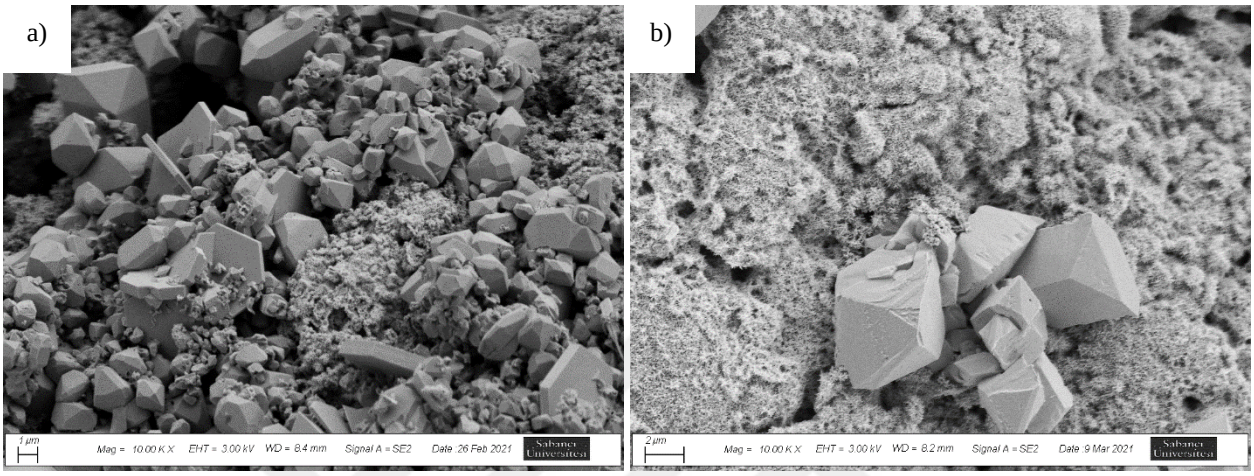

Figure 6.37. *Comparison between $PbSO_4$ particles encountered in a) P1 and b) P2 surfaces.*

In terms of the PbO_2 morphology dominant structure appears to be same for both samples. The difference, as expected, increase in the PbO_2 content in the P2 sample. **Figure 6.38** shows the comparative images between P1 and P2 samples. One can argue that needle like spikes of the P2 sample is slightly larger those P1 also, in **Figure 6.38a** initiation of the needle like PbO_2 is observed.

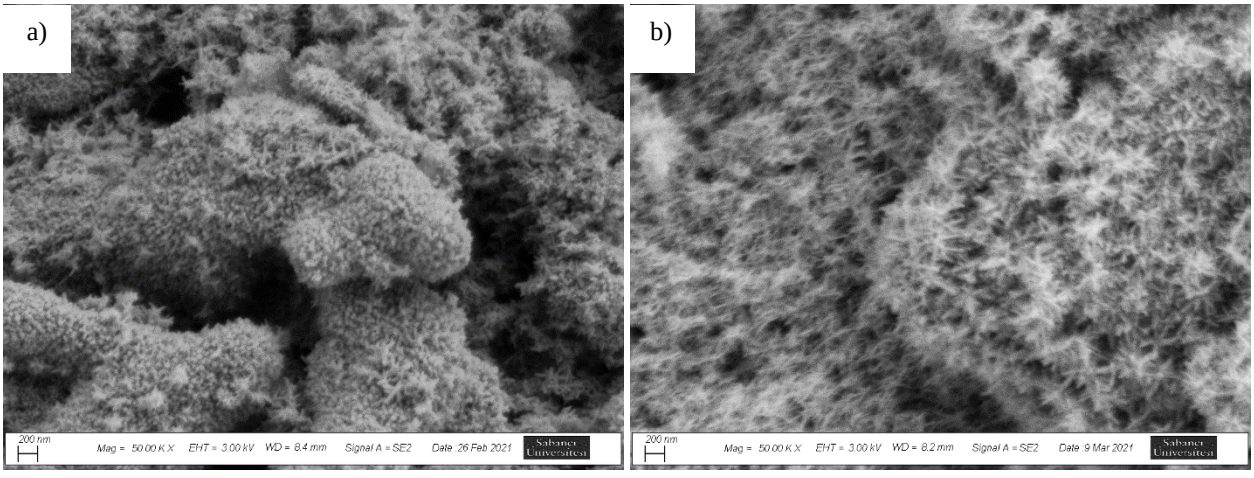

Figure 6.38. *Comparison between PbO_2 particles encountered in a) P1 and b) P2 surfaces.*

For the P2 sample some spherical PbO_2 particles observed located on the surface of some remnant $PbSO_4$ particles. These structures clearly different form the needle like formations. It can be speculated that these spherical particles formed metasomatically form the smaller $PbSO_4$ particles.

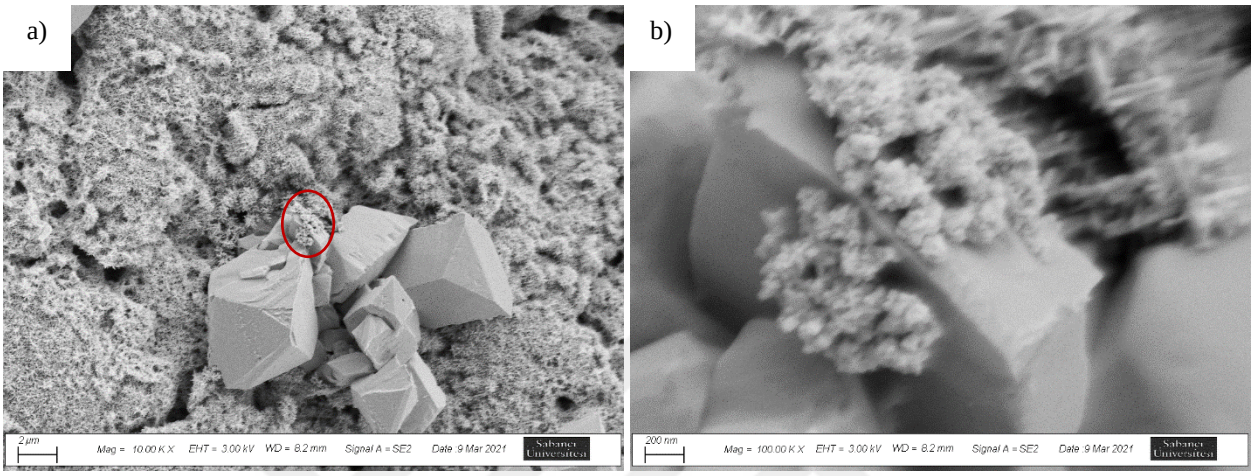

Figure 6.39. *Spherical PbO_2 particles encountered in P2 surface. a) 10000x and b)100000x magnification.*

Figure 6.39a show the location of the spherical PbO_2 particles and **Figure 6.39b** shows the larger magnification image of the particles.

Interior of P2 sample practically shows no sign of remnant $PbSO_4$ particle except some isolated sites. For the P1 however many 10 µm size $PbSO_4$ particles are visible. It appears to be 10 µm somewhat critical size for the stable $PbSO_4$ particle, see **Figure 6.40**.

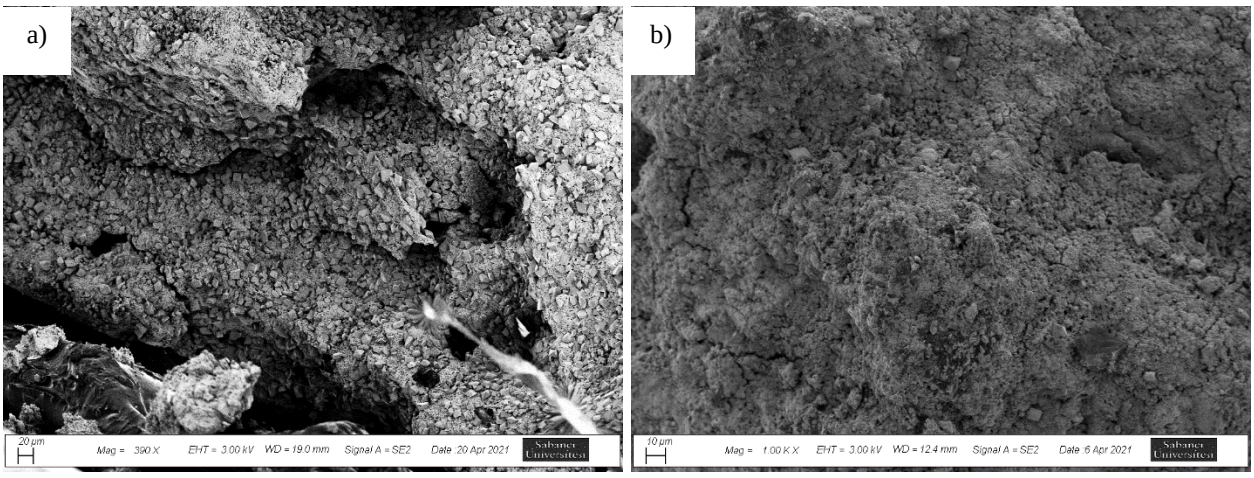

Figure 6.40. *Comparison between PbO_2 particles encountered in a) P1 and b) P2 interiors.*

Such that, closer look at the $PbSO_4$ particles at the P1 interior shows particle size distribution with little standard deviation from the 10 μm. **Figure 6.41** shows these particles, note that images taken from different locations close to the current collector.

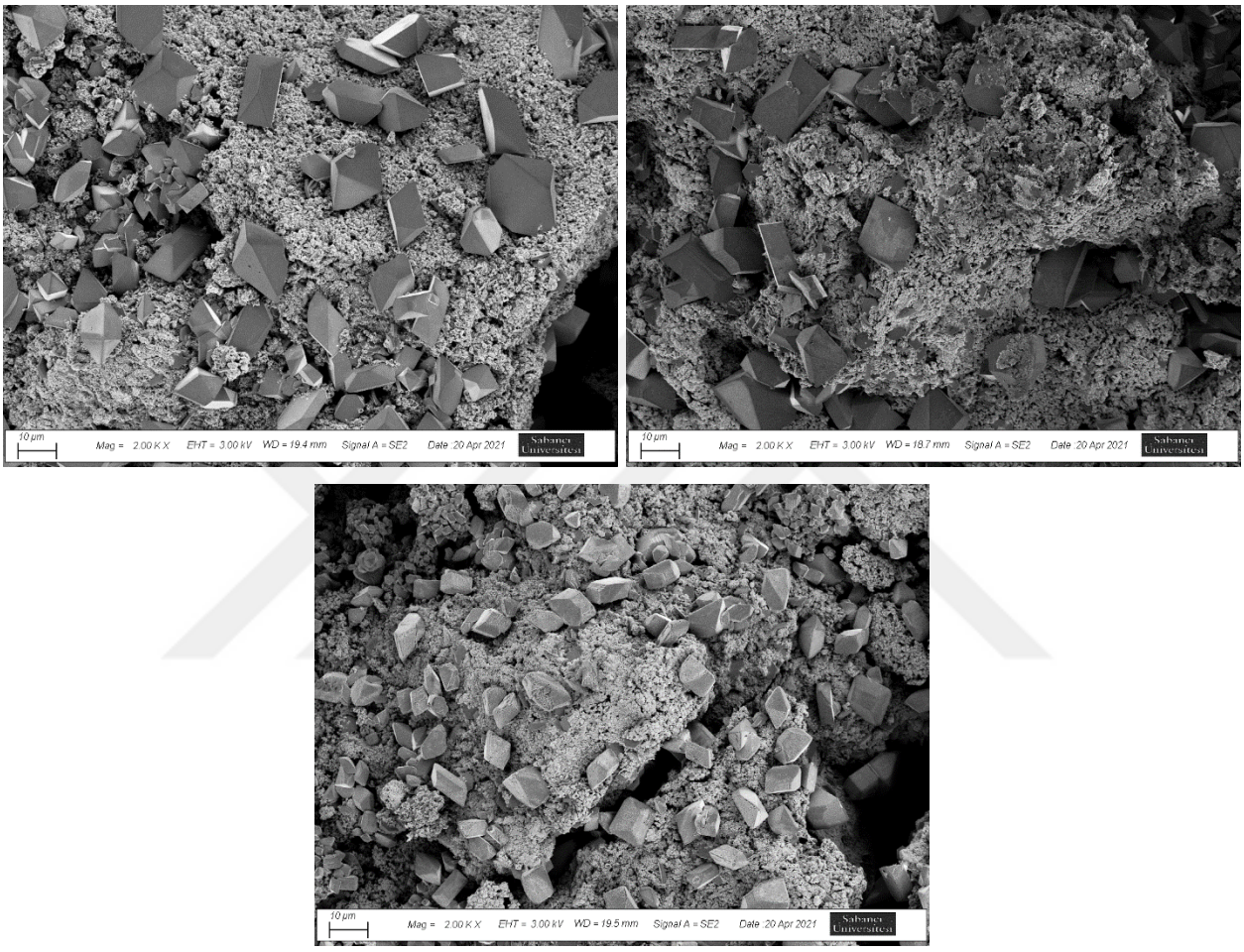

Figure 6.41. *$PbSO_4$ particles encountered in P1 sample interior. Large majority of the particles are 10 μm in size.*

It seems that, PbO_2 needles gets longer and thicker as the formation proceeds from P1 to P2 and agglomerates surface becomes covered by these needles, see **Figure 6.42**.

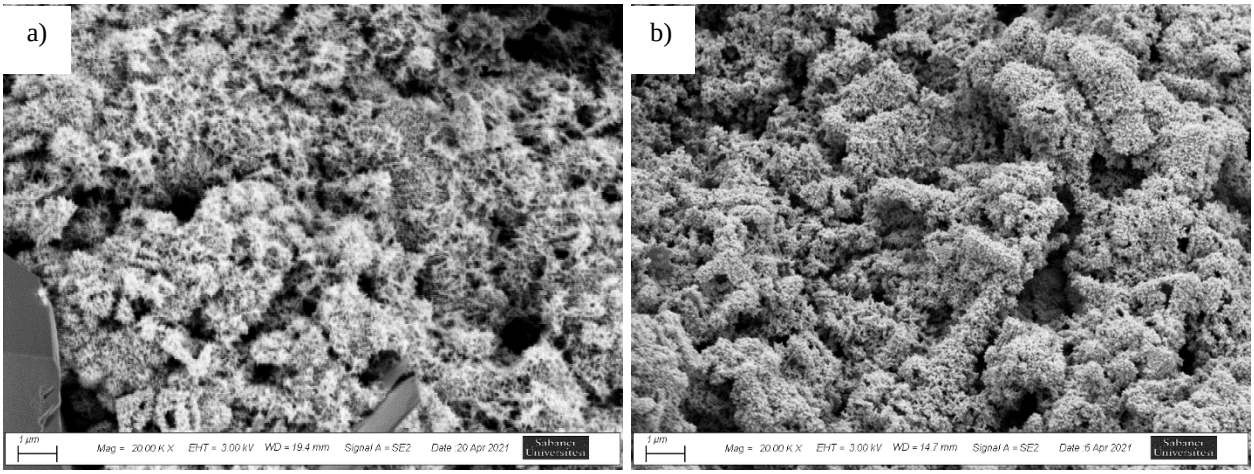

Figure 6.42. *PAM morphology of a) P1 and b) P2 interiors.*

Further investigation of the P2 reveals some metasomatic $PbSO_4$ transformation and subsequent spherical PbO_2 morphology, see **Figure 6.43**, which is not observed in P1. In **Figure 6.43a** there are a $PbSO_4$ particles, not yet destroyed by the metasomatic transformation (highlighted by red enclosure) and, in **Figure 6.43b**, there is $PbSO_4$ particle which destroyed by the metasomatic transformation process.

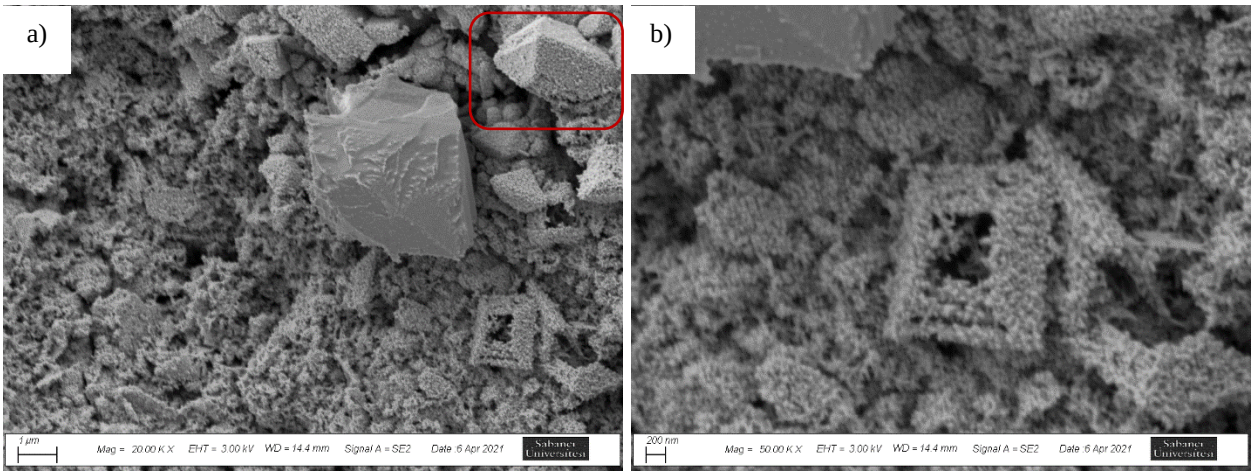

Figure 6.43. *Metasomatic $PbSO_4$ transformation in P2 interior.*

Also notice that in **Figure 6.43a**, relatively large $PbSO_4$ particle dissolved instead of transformed in to PbO_2 metasomatically. Thus, one can argue that size of $PbSO_4$, which depends on the acid concentration, also determines the oxidation mechanism.

6.3.1.2. P5 vs P6

Surface of the low acid samples investigated comparatively. Large amount of small $PbSO_4$ particles observed at the surface of P5 but practically no $PbSO_4$ particle observed in the P6 surface. $PbSO_4$ particles at the P1 surface around 1 μm size. **Figure 6.44** shows the surface SEM micrographs of the P5 and P6 samples.

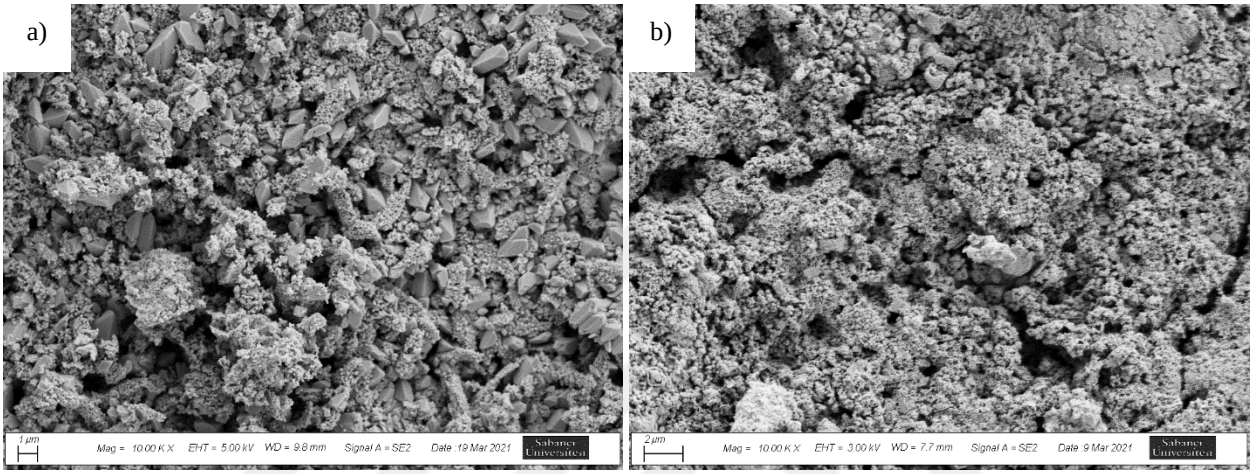

Figure 6.44. *Comparison between $PbSO_4$ particles encountered in a) P5 and b) P6 surfaces.*

In terms of PbO_2 morphology there is no significant difference between the samples. Both samples dominantly showcase spherical PbO_2 particles. Interestingly PbO_2 size appears to be larger, see **Figure 6.45a**, in the P5, this however, should not be commented as "size decreases as the formation proceeds", results most probably arises from the heterogenous structure of the PAM.

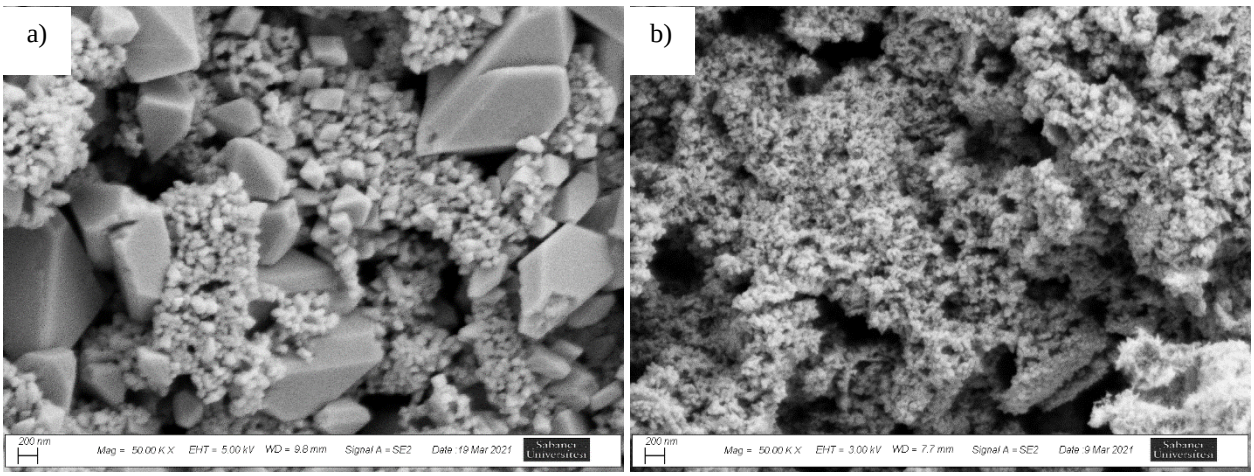

Figure 6.45. *Comparison between PbO_2 particles encountered in a) P5 and b) P6 surfaces.*

Agglomeration however, seems to be in final stages at the P6. For the P5 there are several PbO_2 agglomerates are visible and these structures are not well connected compared to P6, see **Figure 6.46a**.

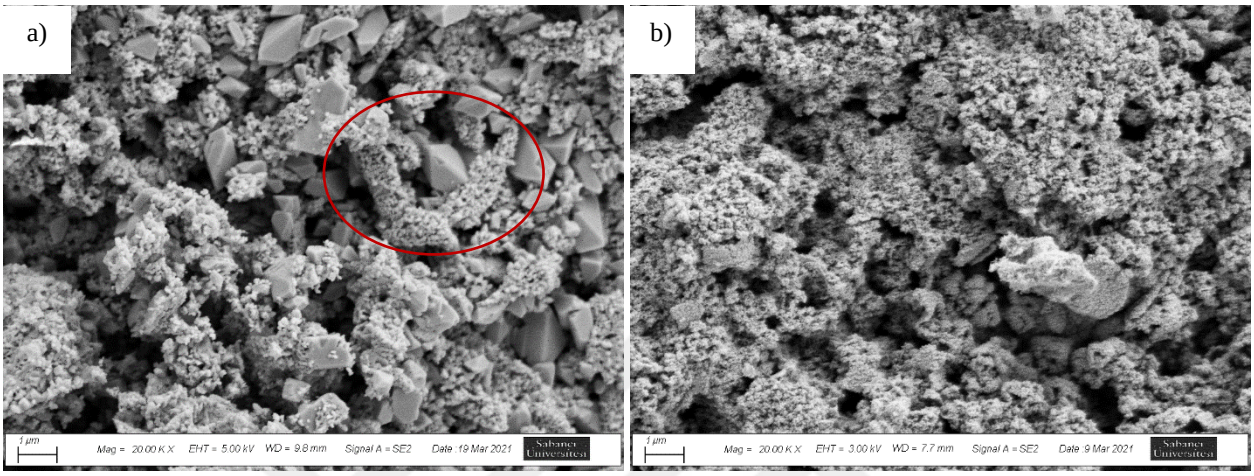

Figure 6.46. *Agglomerates observed in the surface of a) P5 and b) P6.*

One interesting feature of the P6 is the presence of the agglomerate that consist of needle like PbO_2 particles. This structure seems to isolated from the rest of the PAM.

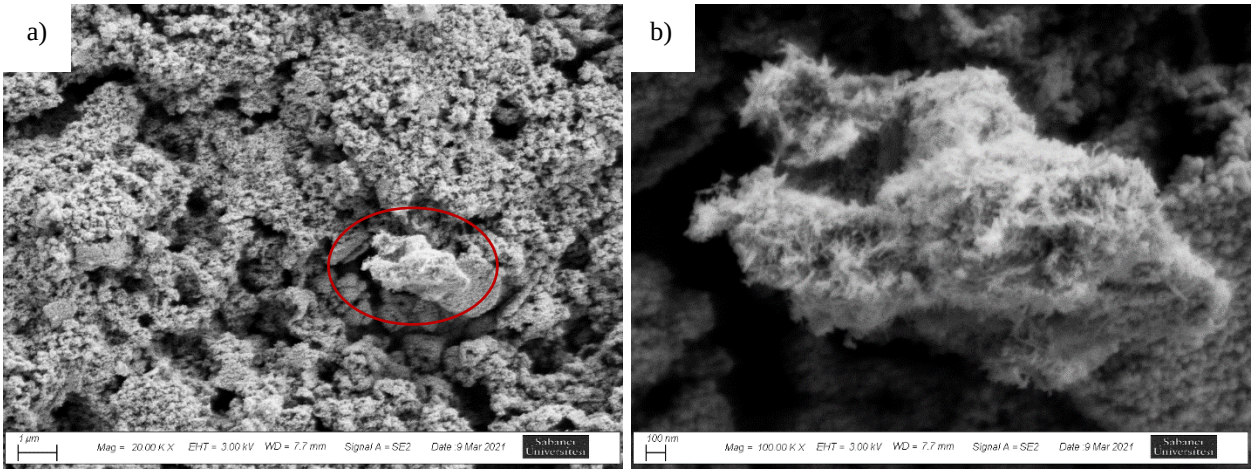

Figure 6.47. *Agglomerate that consist of needle like PbO_2 particles encountered in P6 surface. a) 20000x and b) 100000x*

Remaining PAM of the P6 surface appears to be consists of spherical PbO_2 particles. Except the for the structure presented in **Figure 6.47a**.

At the *interior* of the P5, $PbSO_4$ crystals with various morphologies encountered, see **Figure 6.29**. Comparison between P5 and P6 shows that variety in the $PbSO_4$ morphology

disappears and remnant $PbSO_4$ particles appears as prisms with damaged surfaces become dominant morphology for P6.

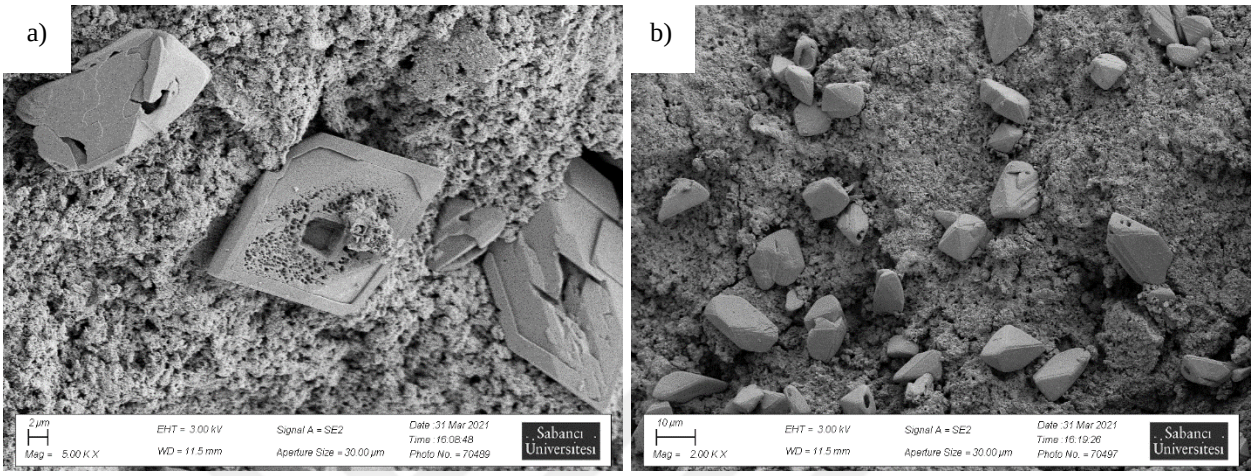

Figure 6.48. *Comparison between $PbSO_4$ particles encountered in a) P5 and b) P6 interior.*

Figure 6.48a show some damaged crystals in the P5 and **Figure 6.48b** shows $PbSO_4$ damaged $PbSO_4$ particles in P6. The particles in the **Figure 6.48a** might be some 3BS. In the process of $PbSO_4$ formation crystals dissolves hence the damaged shapes depicted in the **Figure 6.48a** emerges. PbO_2 morphology is dominantly spherical for both samples. Many examples of metasomatic $PbSO_4$ transformation are evident.

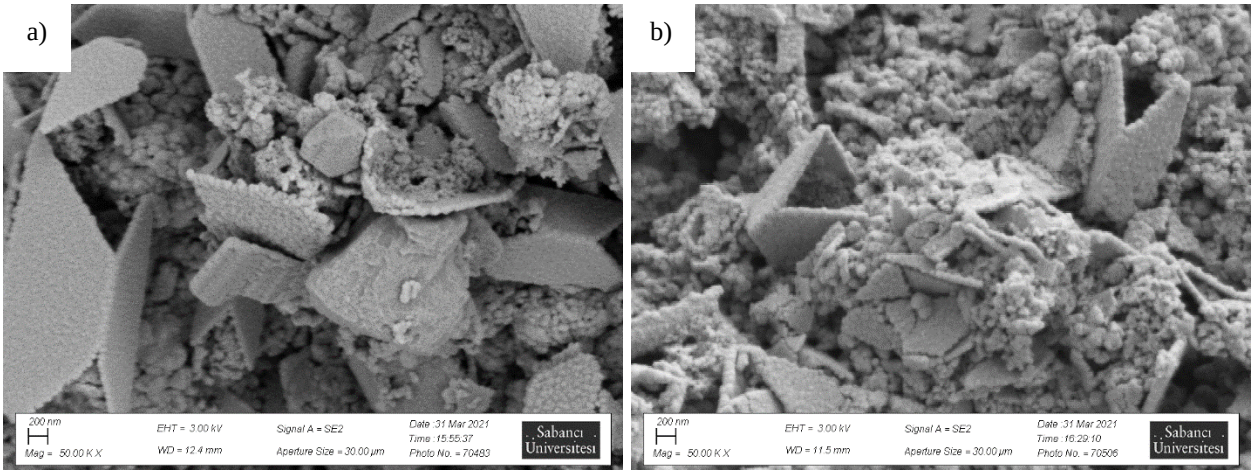

Figure 6.49. *Comparison between PbO_2 particles encountered in a) P5 and b) P6 interior.*

It appeared that in the low acid concentration metasomatic oxidation is an important mechanism. $PbSO_4$ particles metasomatically transforms in to PbO_2. However, they transform their shapes unlike the metasomatic 4BS transformation. Among possible reasons are the difference in molar

volumes of the PbO_2, $PbSO_4$ and 4BS structures. Molar volumes of PbO_2, $PbSO_4$ and 4BS are roughly 24.5, 48.2 and 147 $cm^3 \cdot mole^{-1}$, respectively[6], [8]. If the metasomatic transformation occurs directly from the $PbSO_4$ to PbO_2 decrease in molar volume cannot be compensated and inevitably $PbSO_4$ structure collapses. However, if transformation takes the 4BS ➔ $PbSO_4$ ➔ PbO_2 route similar to he one described by the schematic at **Figure 4.7**, structure first expands ($PbSO_4$ forms) then shrinks (PbO_2 forms). However, when $PbSO_4$ particles form they form on the surface of 4BS therefor mimic the morphology. Later, when the oxidation to PbO_2 takes place the metastable $PbSO_4$ *layer* decomposes but since there is a sublayer of 4BS below this layer PbO_2 find sites to hold on to[17], [23]. It can be speculated that the size of the 4BS particles plays a role in the shape retention as well, since larger size of these particles prevents complete sulfation to $PbSO_4$ during formation which ensures the existence of possible sites that PbO_2 crystals to hold on[17], [23].

6.3.2. Effect of the acid density of the morphology

6.3.2.1. P1 vs P5

At the <u>*surfaces*</u>, major difference between the $PbSO_4$ particles encountered in P1 and P5 samples is the size. P1, sample formed with higher acid contact (1.28 s.g.), shows significantly larger $PbSO_4$ particles compared to the P5 sample (acid density 1.16 s.g.).

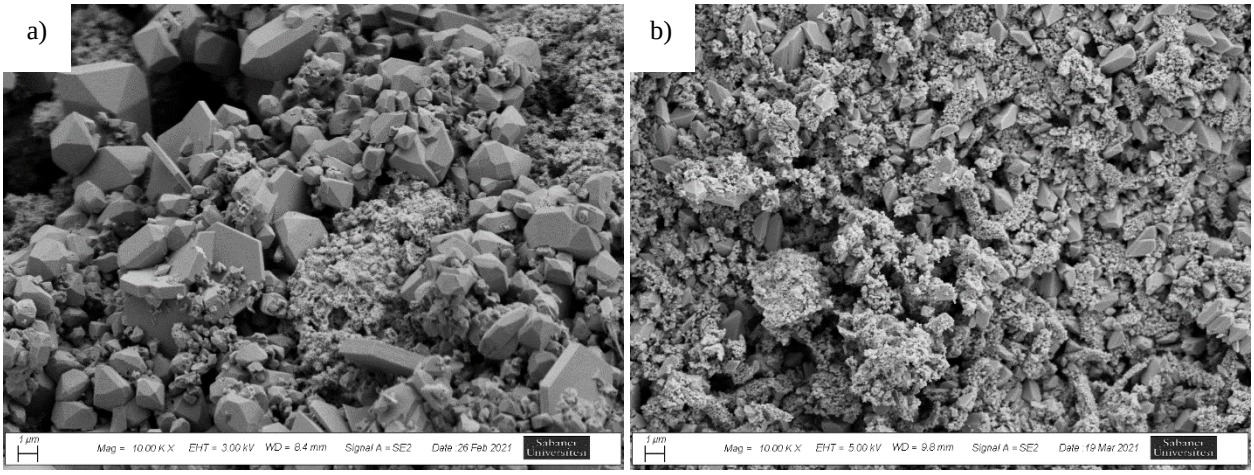

Figure 6.50. *$PbSO_4$ morphology in a) P1 (large) and b) P5 (small) surfaces.*

In the light of this result, it can be said that the larger acid density increases the driving force for the $PbSO_4$ growth. for the case of PbO_2 particles however condition is reversed. PbO_2 particles in

the low acid sample relatively larger compared to the P1. **Figure 6.51** gives PbO_2 morphologies encountered at the surfaces for the P1 and P5 samples.

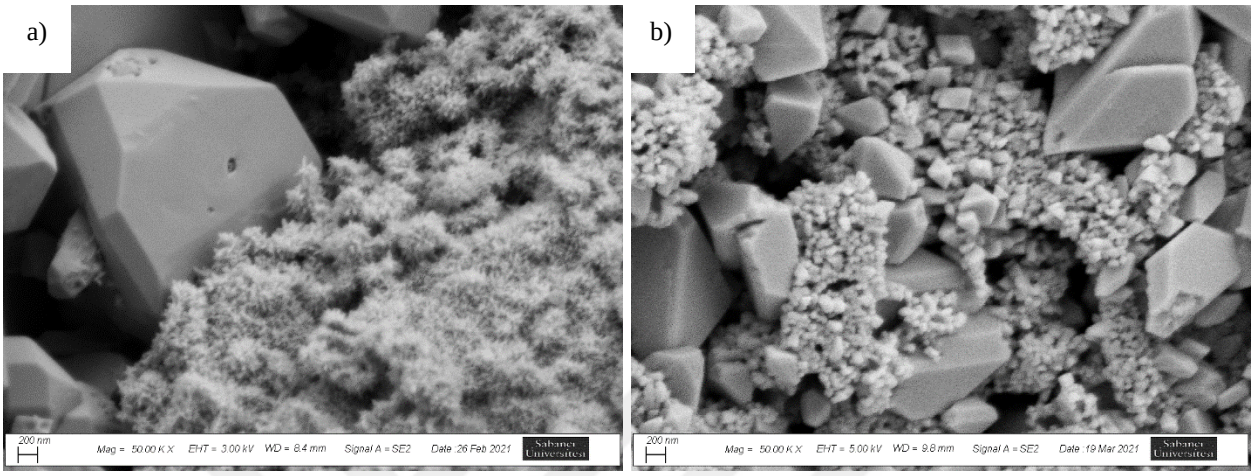

Figure 6.51. *a) Small needle like PbO_2 particles and b) larger, more rounder PbO_2 particles encountered in P1 and P5 surfaces, respectively.*

Reason for the different PbO_2 morphologies at the surfaces of the P1 and P5 samples might be explained by the following; $PbSO_4$ solubility depends on the acid concentration and given by the Danel and Plichon[20], also, as a common knowledge one can argue that smaller $PbSO_4$ crystals have better solubility.

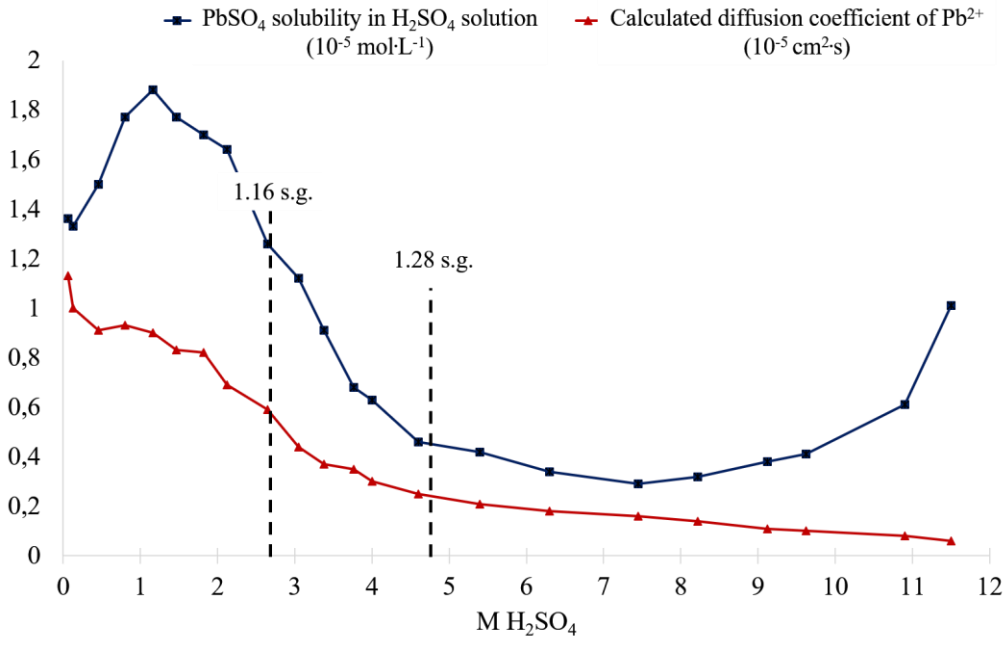

Figure 6.52. *$PbSO_4$ solubility and Pb^{2+} diffusion coefficient in H_2SO_4 solution by Danel and Plichon*[20].

Notice the dashed lines represents the P1 and P5 samples[102]. By using the **Figure 6.52**, one can see smaller $PbSO_4$ particles on the surface of the transforming paste, in the low acid (1.16 s.g.) sample P5 can have much better solubility. This can lead to larger PbO_2 formation. On the other hand, high acid concentration (1.28 s.g.) solubility of the $PbSO_4$ particles are low hence growth process hindered simply due to lack of material.

This trend repeats itself at the ***interior*** of the plates as well, see **Figure 6.53**. Notice majority of the PbO_2 content of the P1 has small needle like morphology originating from some larger structure. Also, almost no metasomatic $PbSO_4$ transformation is observed for this sample. However, for the P5 many regions that exhibit metasomatic transformation is observed.

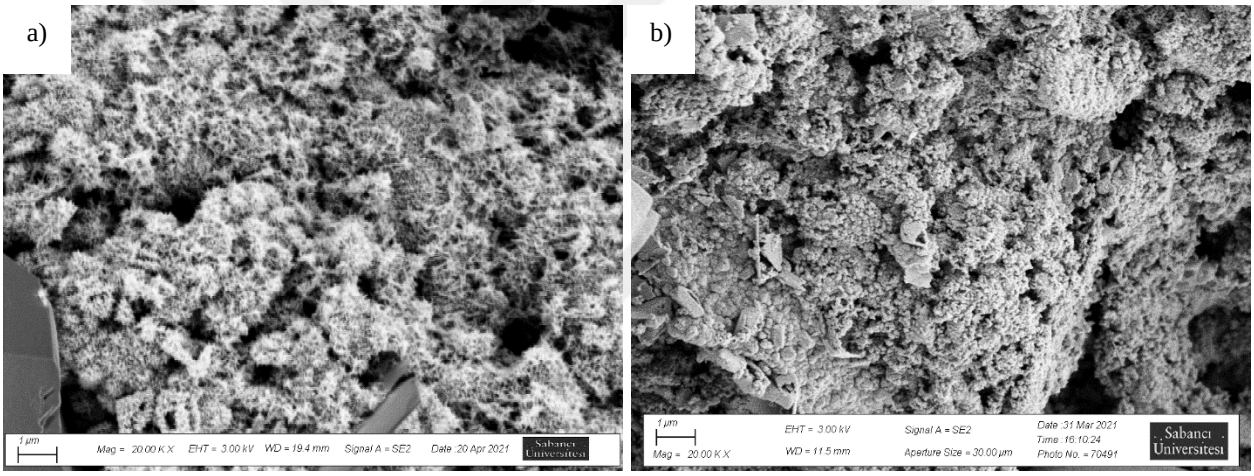

Figure 6.53. *a) Small needle like PbO_2 particles and b) larger, more rounder PbO_2 particles encountered in P1 and P5 interior, respectively.*

Utilizing the **Table 6.2**, one can say that the higher acid concentration leads to small needle like PbO_2 particles, while, lower acid content results of the formation of slightly larger, spherical PbO_2 particles. Also, it is evident that $PbSO_4$ particles in P5 sample metasomatically to PbO_2. It can be expected see such structures at the interior of the P5 since in order to metasomatic transformation to occur there should be electronic contact near by the oxidize Pb^{2+} cations to Pb^{4+} cations. No metasomatic transformation is observed at the surface of P5. $PbSO_4$ morphology at the interior of the samples shows similarities as in both cases size of the remnant $PbSO_4$ about 10 µm, with the exception of some regions of P5 like given in the **Figure 6.29d**. Figure below showcases the $PbSO_4$ crystals observed at the interior of the P1.

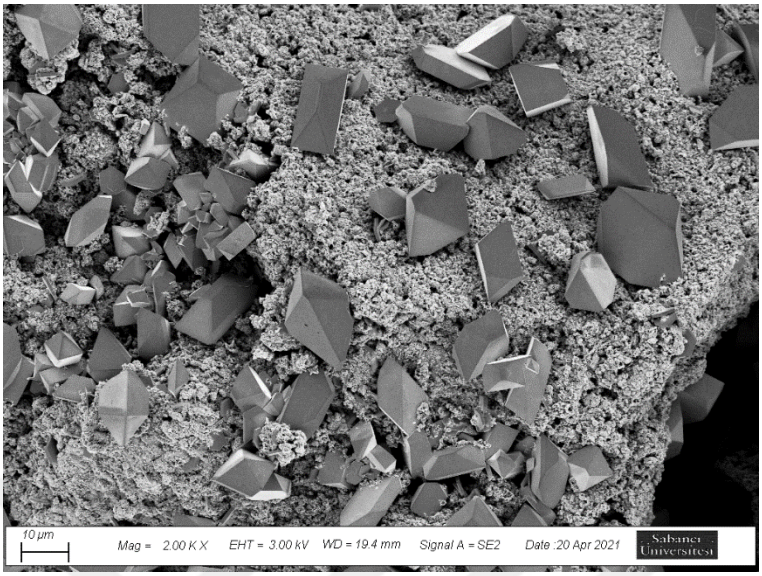

Figure 6.54. *$PbSO_4$ morphology encountered at the interior of P1.*

6.3.2.2. P2 vs P6

Surface morphologies at the end of the formation for P2 and P6 compared. P2 (high acid) samples showcase more $PbSO_4$ content compared to the P6 (low acid) sample, which is expected. Low acid almost showed no $PbSO_4$ formation at its surface, while for P2 $PbSO_4$ prisms with damaged surfaces encountered, see **Figure 6.55**. Size of these $PbSO_4$ crystals appears to be smaller than 10 µm which may lead to conclusion that these particles are in the middle of the formation process.

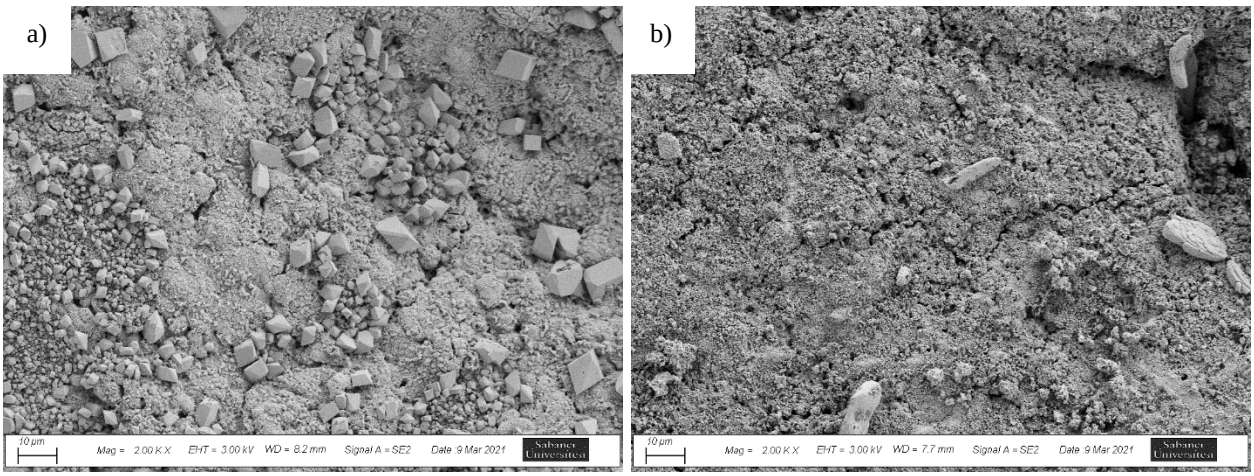

Figure 6.55. *Comparison between $PbSO_4$ particles encountered in a) P2 and b) P6 surfaces.*

Most interestingly the PbO_2 morphology at the surfaces of these samples shows completely opposite characteristics.

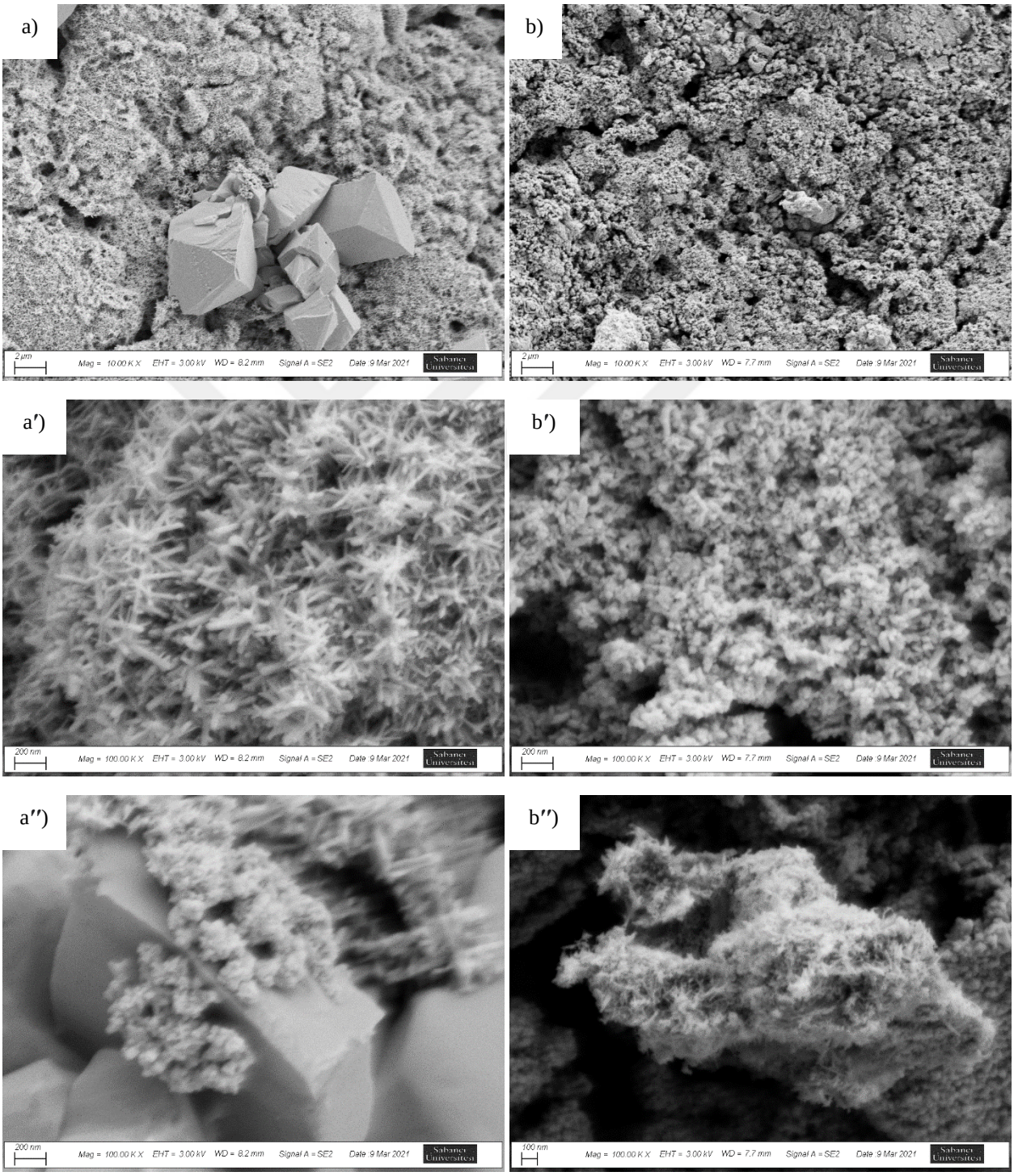

Figure 6.56. *PbO_2 morphologies encountered in a, a′, a′′) P2 and b, b′, b′′) P6 surface.*

Figure 6.56a and **Figure 6.56b** shows the low magnification view of the PAM structure in P2 and P6, respectively. **Figure 6.56a′** and **Figure 6.56b′** are the dominant PbO_2 morphology encountered in the P2 and P6, respectively. Finally, **Figure 6.56a″** and **Figure 6.56b″** showcase the minority morphologies in the P2 and P6, respectively. Results shows for the high acid sample, P2, majority of the PbO_2 are in needle like form and in some isolated cases spherical morphology encountered, for the case of P6 its vice versa.

Interior of these samples shows similar trend as well in terms of PbO_2 morphology. Needle like PbO_2 particles again dominates the P2 high acid sample, while spherical PbO_2 particles formed for the P6 sample, Metasomatic transformation of the $PbSO_4$ to PbO_2 evident, see **Figure 6.57b**. For both sample there are $PbSO_4$ particles encountered in some isolated regions.

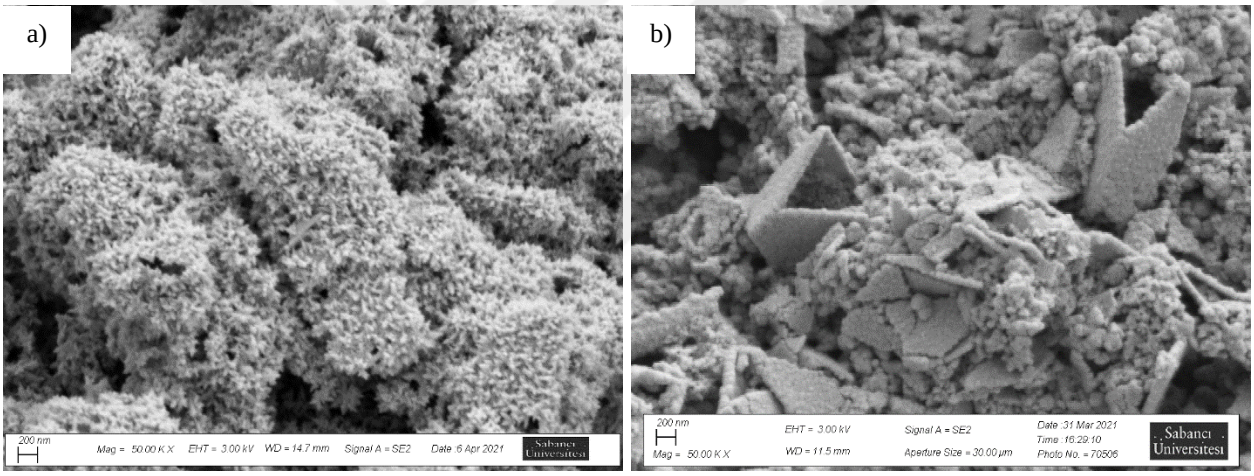

Figure 6.57. *PbO_2 morphologies encountered in a) P2 and b) P6 interior.*

Suggested explanation for this phenomenon as follows; Assuming schematic at the **Figure 6.6** is accurate, for the low acid samples, initial oxidation mechanism occurring close to current collector is metasomatic. Pb^{2+} cations produced from the $PbSO_4$ region find an electronic contact at the metasomatically produced spherical PbO_2 particles and retain the spherical morphology. For the high acid samples, however, even though the both solubility of $PbSO_4$ and Pb^{2+} diffusion coefficient is low, larger $PbSO_4$ region increases the chance to find an electronic contact via dissolution-precipitation mechanism, since larger $PbSO_4$ region shortens the distance for the Pb^{2+} to travel to become Pb^{4+}. This mechanism results in the needle like morphology. Results also shows that the rate of the dissolution-precipitation mechanism occurring in the high acid samples

is higher than the metasomatic one since in the high acid 1 Ah samples contain less $PbSO_4$, see **Figure 6.4**.

It is obvious that the polymorphic nature of the PbO_2 cannot be explained via XRD and SEM investigations alone. Up to this point PbO_2 used as general term and no distinction between α-PbO_2 and β-PbO_2 morphologies presented. In order to clearly identifying the characteristic morphologies of the PbO_2 modification transmission electron microscope (TEM) analysis conducted. Following section presents the results.

6.4. TEM Analysis

Several samples investigated under TEM with intent of finding both of the PbO_2 modifications. Interesting results emerged from the TEM analysis. Theoretical interplanar distance values are calculated by using the **Table 3.1**.

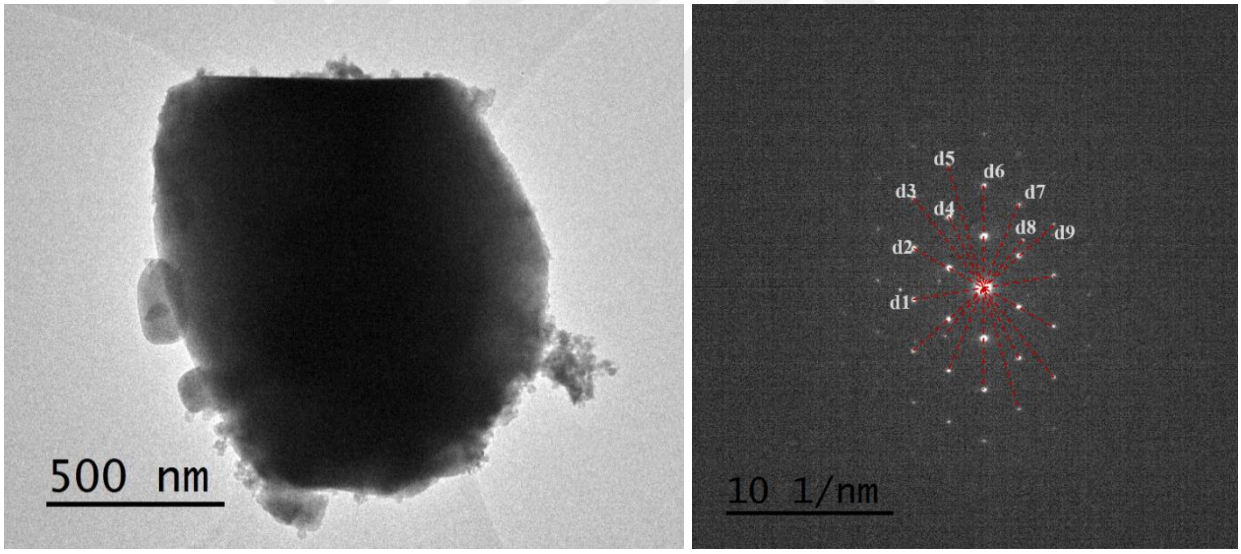

Interplanar Spacing (Å)	d1	d2	d3	d4	d5	d6	d7	d8	d9
Measured	2.33	4.17	1.47	2.11	1.32	3.28	1.85	2.72	3.56
Calculated	2.36	4.24	1.48	2.13	1.35	3.33	1.88	2.77	3.62
(hkl)	(131)	(020)	(133)	(202)	(323)	(021)	(132)	(211)	(120)

Figure 6.58. *$PbSO_4$ particle image and diffraction pattern.*

Initially we are able to identify a $PbSO_4$ crystal with well-developed faces and edges. **Figure 6.58** shows the $PbSO_4$ crystal found in the samples. Well-developed faces are similar to found in the SEM investigations. $PbSO_4$ crystal at the **Figure 6.58** is about 1.5 μm in size and some smaller PbO_2 crystals are visible around it. This leads to conclusion that this particular $PbSO_4$ is in the later stages of its formation process.

Two types of morphology encountered in the samples for the PbO_2. Needle like and spherical. Unfortunately, sieving out a single crystal PbO_2 was not possible. Hence, ring analysis done to identify the PbO_2 and its polymorphs. **Figure 6.59** shows the needle like morphology encountered in the samples. Electron diffraction analysis shows that these particles are in β-PbO_2 phase. Nomenclature d1, d2, … starts from the smallest ring from the ring patterns.

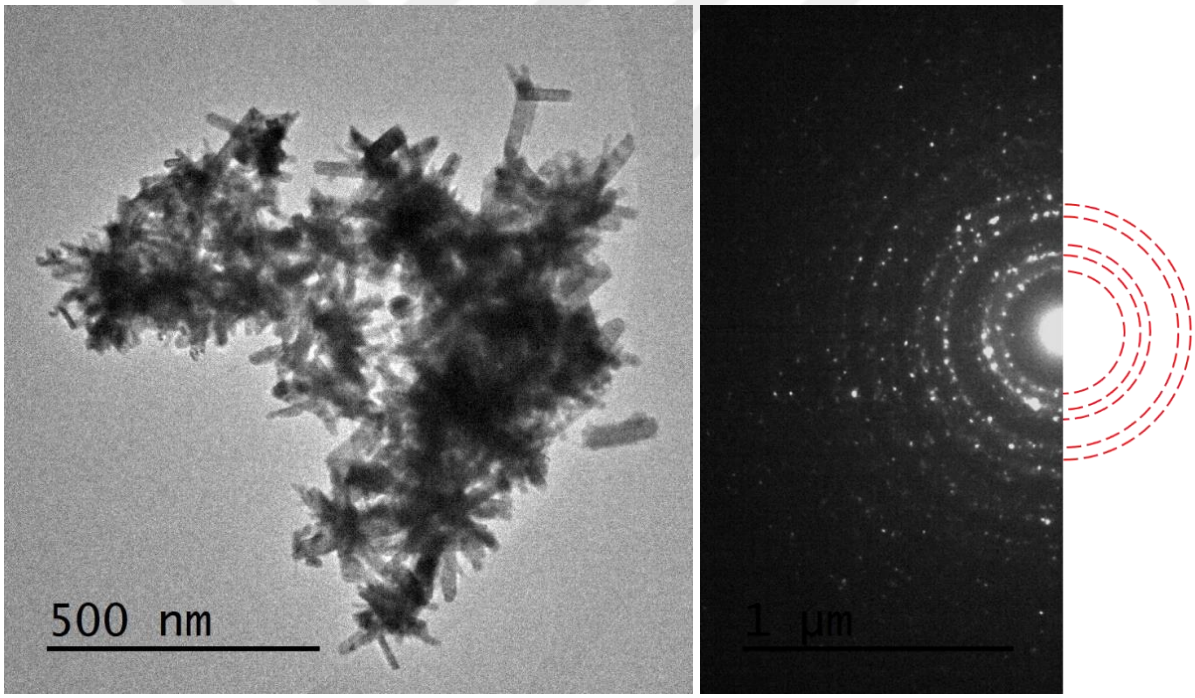

Interplanar Spacing (Å)	d1	d2	d3	d4	d5
Measured	3.45	2.74	2.43	1.83	1.66
Calculated	3.50	2.80	2.48	1.85	1.70
(hkl)	(110)	(101)	(200)	(121)	(002)

Figure 6.59. *Needle-like β-PbO_2 particles.*

After this finding initial assumption was the if β-PbO_2 is needle like and since the needle like morphology dominates the high acid samples then the β-PbO_2 most likely needle like morphology since it is known that β-PbO_2 prefers acidic mediums. By this assumption it can be expected α-PbO_2 have the spherical morphology. Unfortunately, when it comes to the lead acid batteries nothing that simple. Spherical morphology also was able to analyze with electron diffraction. **Figure 6.60** shows the β-PbO_2 particles that exhibit spherical morphology. Another clump of PbO_2 particles with spherical morphology is identified as β-PbO_2 polymorph with electron diffraction.

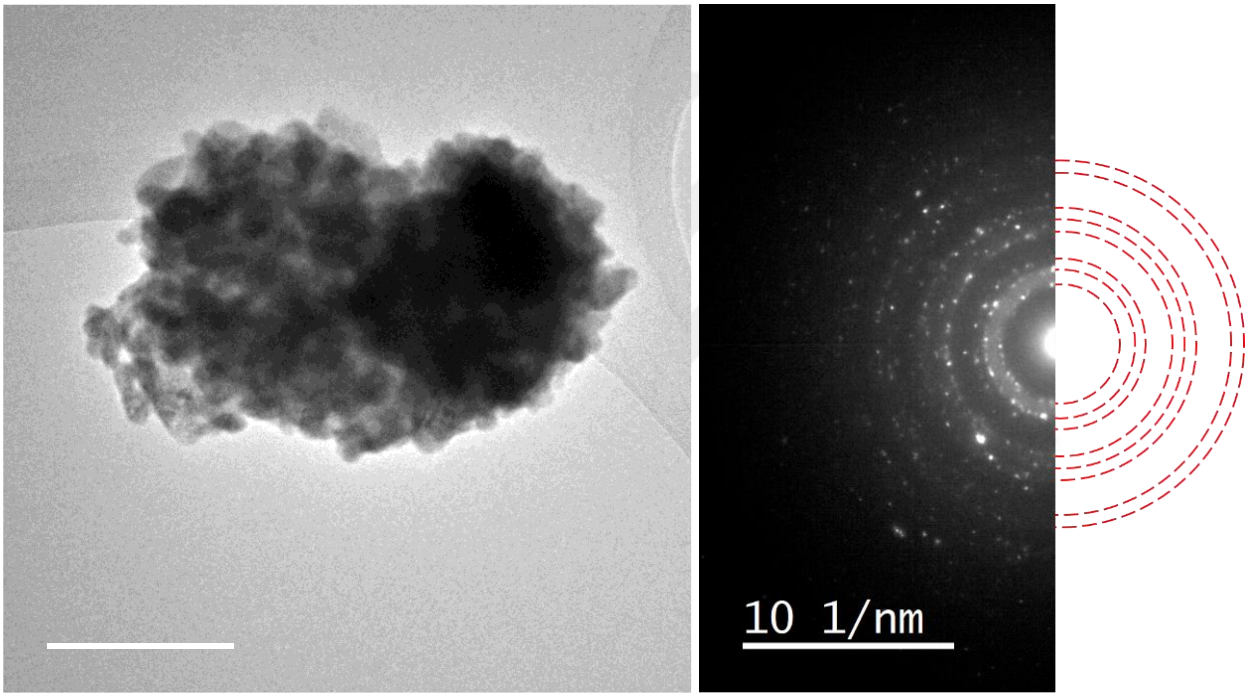

Interplanar Spacing (Å)	d1	d2	d3	d4	d5	d6	d7	d8
Measured	3.57	2.83	2.49	1.88	1.70	1.56	1.24	1.15
Calculated	3.50	2.80	2.44	1.85	1.65	1.53	1.22	1.13
(hkl)	(110)	(101)	(111)	(121)	(300)	(112)	(222)	(003)

Figure 6.60. *Spherical β-PbO_2 particles.*

Figure 6.61 shows another β-PbO_2 particles with spherical morphology. At this point the it is evident that the β-PbO_2 can be in both needle like and spherical morphology. Pavlov *et. al*. also observed needle like β-PbO_2 particles in the active mass of the positive electrodes but authors also

assigned the morphology similar to **Figure 6.60** to α-PbO_2[101]. With the hope of getting some single crystal electron diffraction pattern protrusions of the agglomerate at **Figure 6.61** investigated. At these protrusions, see **Figure 6.61**, α-PbO_2 diffraction patterns encountered instead of β-PbO_2. Similar results were published by Pavlov et. al. , i.e. PbO_2 crystals in the positive lead acid battery plates consist of crystalline region with different phase composition[30].

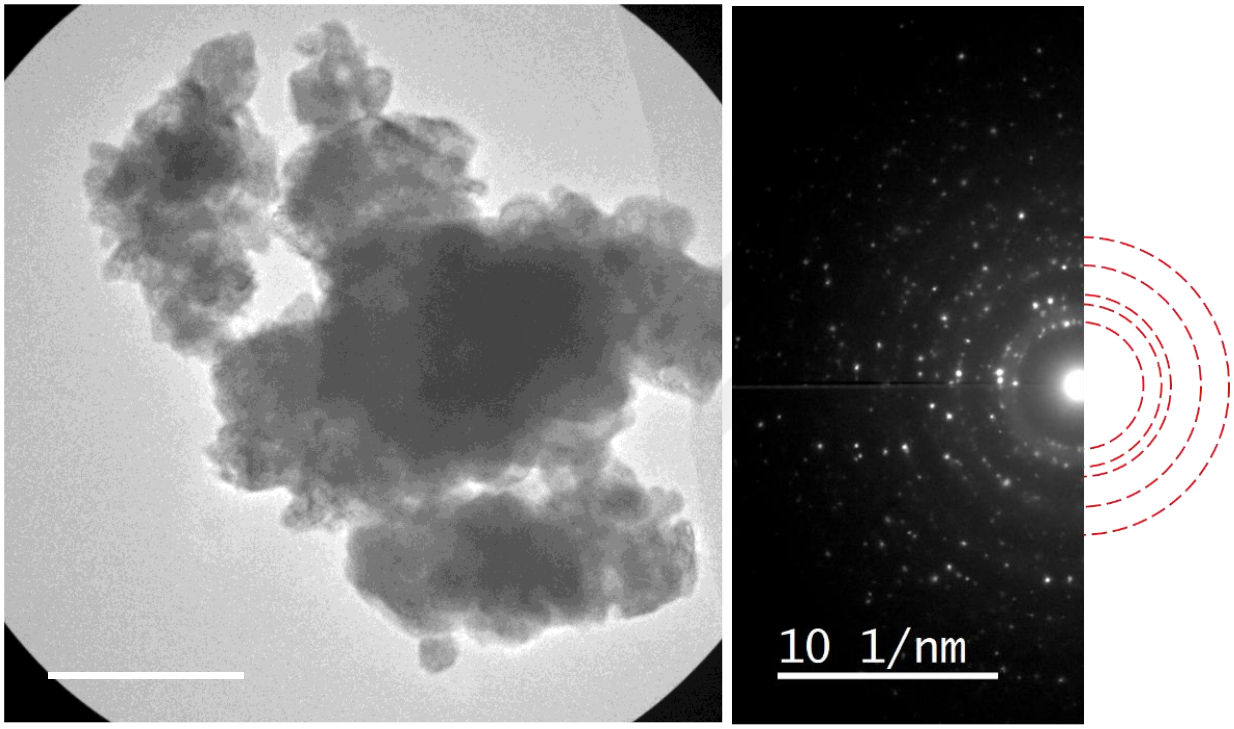

Interplanar Spacing (Å)	d1	d2	d3	d4	d5
Measured	3.47	2.72	2.43	1.83	1.49
Calculated	3.50	2.80	2.48	1.85	1.53
(hkl)	(110)	(101)	(200)	(121)	(112)

Figure 6.61. *Another spherical β-PbO_2 particle.*

Figure 6.62 shows the two edges of the agglomerate presented in the **Figure 6.61**. It is evident characteristic (110) peak of the β-PbO_2 disappeared. Both protrusions showcase α-PbO_2 characteristics. However, it should be noted that it appears to be these protrusions originated from the bulk of the agglomerate, this might mean that they precipitated later.

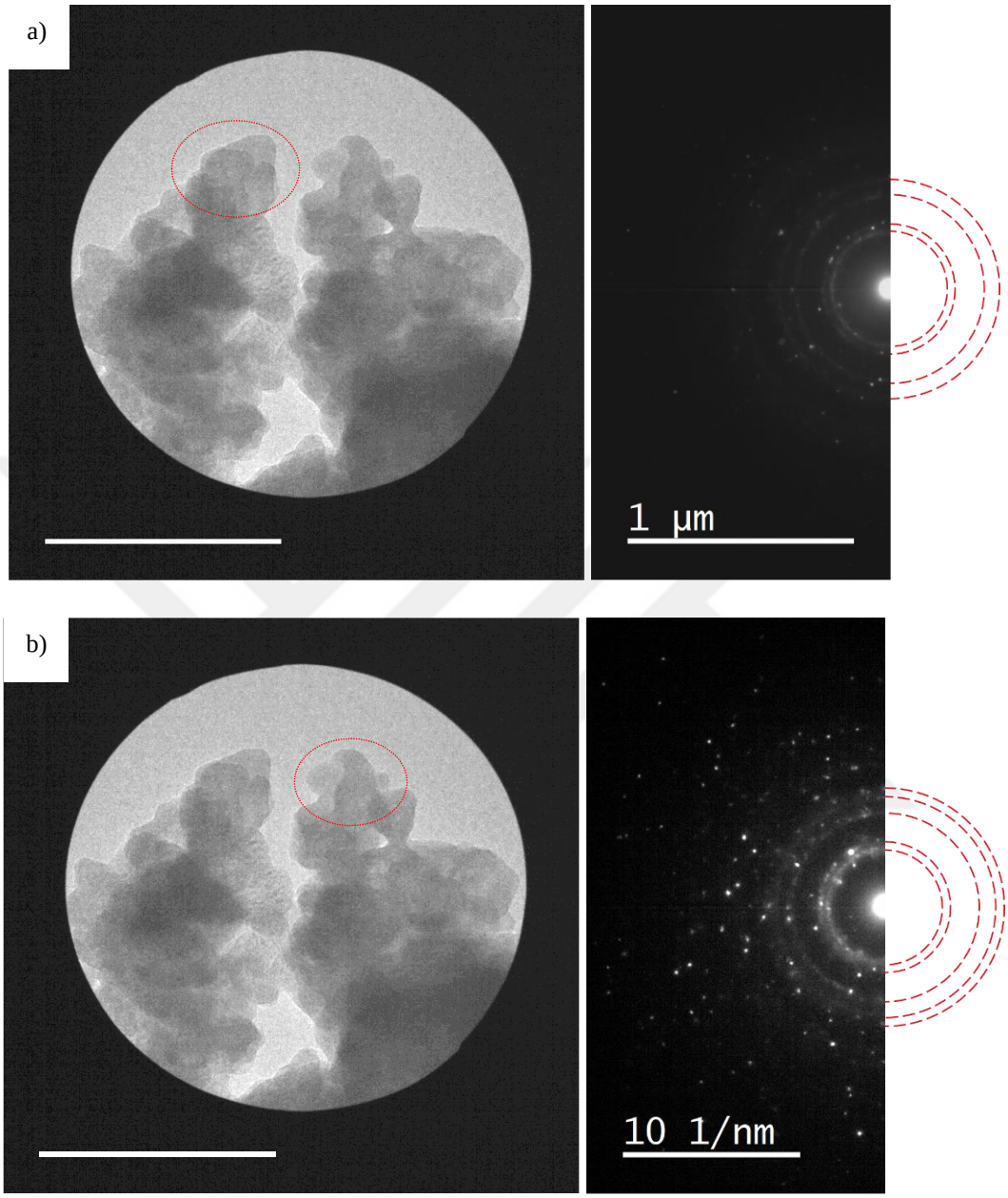

Interplanar Spacing (Å)		d1	d2	d3	d4	d5
Measured	a	3,08	2,72	1,88	1,62	—
	b	3,09	2,72	1,88	1,60	1,49
Calculated		3.12	2.73	1.91	1.64	1.53
(hkl)		(111)	(002)	(220)	(113)	(132)

Figure 6.62. *Spherical α-PbO_2 particles.*

Here, it is believed that if α-PbO_2 will form in the lead acid battery it will form first. Then one can expect the β-PbO_2 protrusions on the large α-PbO_2 agglomerate, not the other way around.

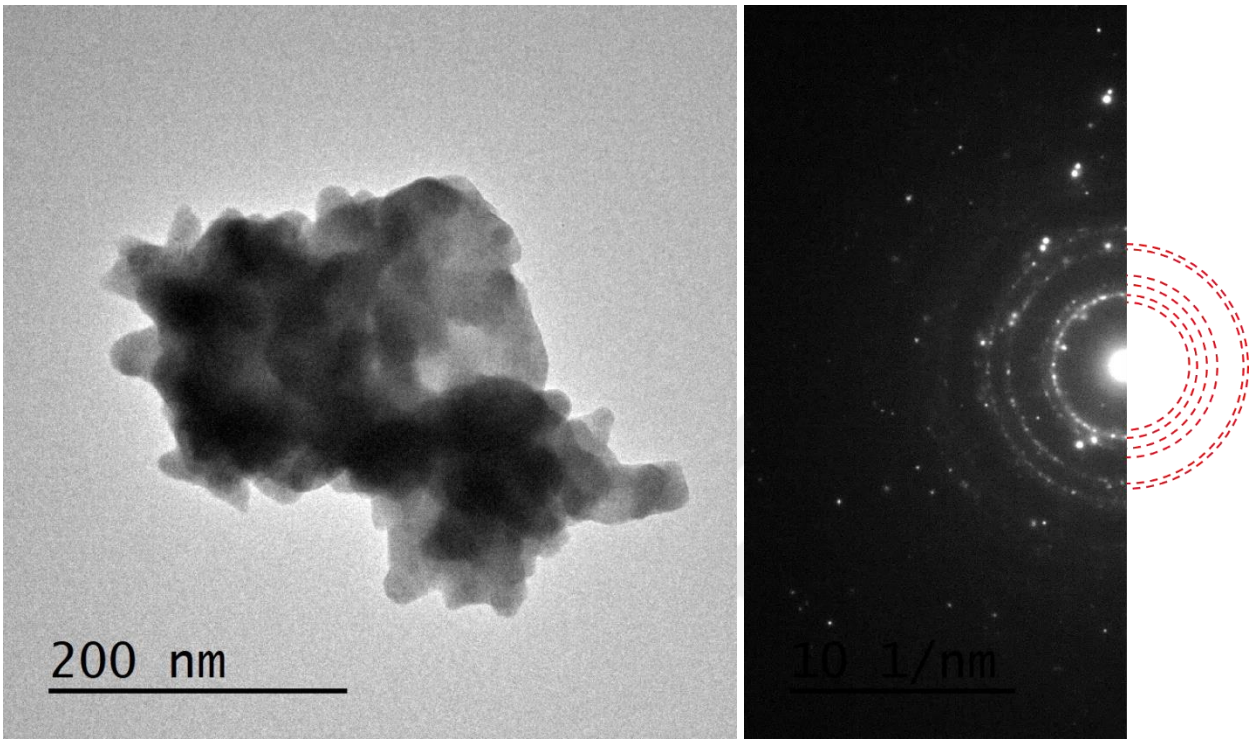

Interplanar Spacing (Å)	d1	d2	d3	d4	d5	d6
Measured	3.52	3.15	2.76	2.47	1.92	1.84
Calculated	3.50	3.12	2.73	2.44	1.91	1.82
(hkl)	(110)	(111)	(002)	(111)	(220)	(003)
Phase	β-PbO_2	α-PbO_2	α-PbO_2	β-PbO_2	α-PbO_2	α-PbO_2

Figure 6.63. *Another structure consists of both PbO_2 polymorphs.*

Figure 6.63 shows another structure that consists both α-PbO_2 and β-PbO_2. Most interesting results however came up somewhat haphazardly. As the crystals examined to get a good diffraction pattern, clear changes in the particle morphologies observed. Surprisingly this morphology changes also brought phase change. **Figure 6.64** shows the particle before the electron beam exposure.

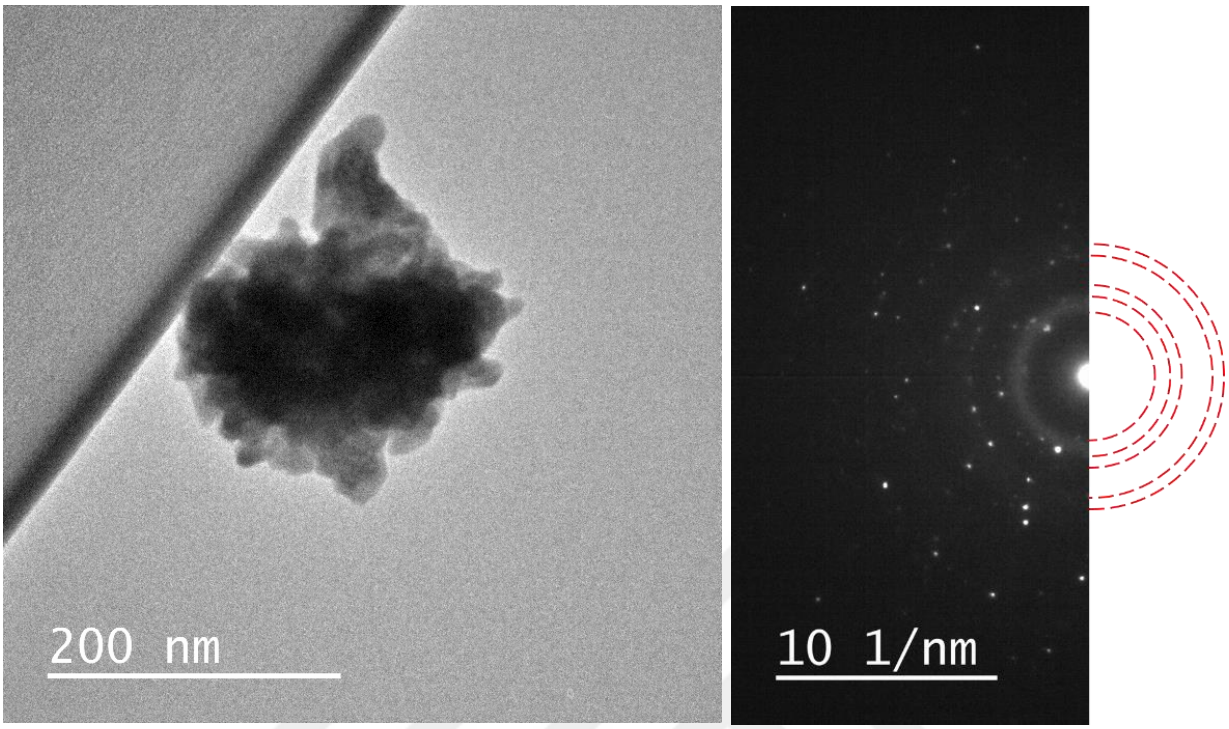

Interplanar Spacing (Å)	d1	d2	d3	d4	d5
Measured	3.44	2.77	2.42	1.82	1.67
Calculated	3.50	2.80	2.48	1.85	1.70
(hkl)	(110)	(101)	(200)	(121)	(112)

Figure 6.64. *Spherical β-PbO_2 particles. Before exposure to electron beam.*

When electron beam kept on the sample, morphology and the phase of the particles changed. Resulting morphology and the electron diffraction pattern presented at **Figure 6.65**.

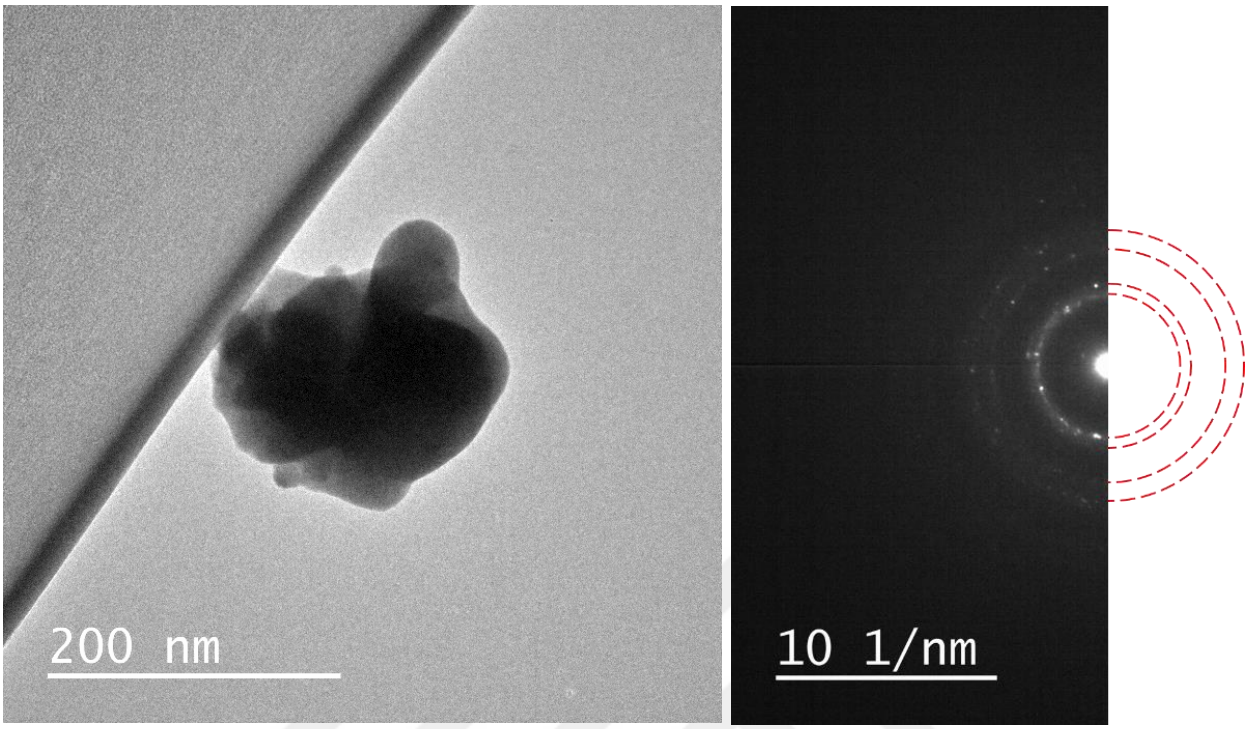

Interplanar Spacing (Å)	d1	d2	d3	d4
Measured	3.08	2.68	1.92	1.64
Calculated	3.12	2.73	1.91	1.67
(hkl)	(111)	(002)	(220)	(300)

Figure 6.65. *α-PbO_2 particles. After exposure to electron beam.*

Comparing **Figure 6.64** to **Figure 6.65**, it is clear that the particles after exposure become rounder. Protrusions around the **Figure 6.64** flatten and disappeared. TEM that these samples investigated has a dynamic camera, i.e. contrast dynamically adjusted during the morphology change. Hence one can say that, particle in the **Figure 6.65** seems to be more uniform and some regions become denser.

For to our knowledge there no mention of such phase transformation of β-PbO_2 to α-PbO_2 in the literature under electron beam exposure. As mentioned, the oxygen content of the α-PbO_2 is lower. It is also said that the β-PbO_2 is more prone to oxygen loss in the room temperature but it is stated that this oxygen loss does not change phase composition[33]. This property of β-PbO_2

might be enhanced under the vacuum condition of the TEM column. Also, it is generally found that the density of the α-PbO_2 is higher than the β-PbO_2 modification[6], which maybe correlated with the densification of some regions going through metamorphosis under the electron beam. Under the light of these statement, it is believed that the β-PbO_2 particles can transforms in to α-PbO_2 under the electron beam.

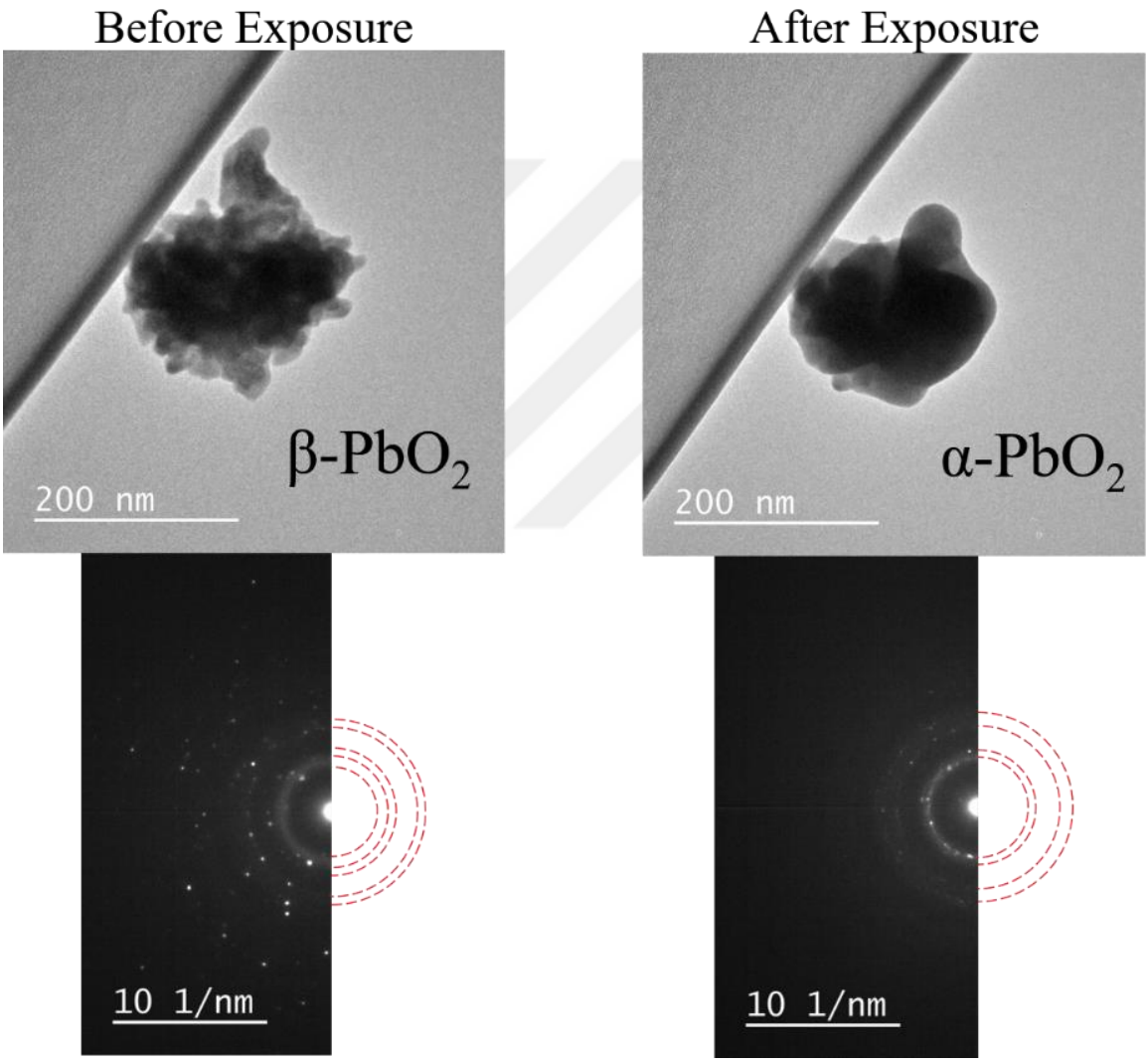

Figure 6.66. *Phase change of the β-PbO_2 particles after exposure to electron beam.*

Finally, **Figure 6.66** shows how the morphology and the electron diffraction patterns change after the particles are subjected to a high energy electron beam. This result become the most interesting finding of the research, since the characteristic α-PbO_2 morphology, if there is any, not clearly demonstrated.

7. CONCLUSION AND SUMMARY

For this M.Sc. thesis, characteristics of the PAM present in the lead acid battery positive electrodes are investigated. It is believed that among many independent parameters, macro and micro morphology of the PbO_2 structure as well as the PbO_2 polymorphism effect the performance of the battery. In that note, research focused on determining the characteristic morphologies of the PbO_2 polymorphs and the formation mechanisms of α-PbO_2 and β-PbO_2 modifications in the lead acid battery. Novel and dynamic E-pH diagrams are developed to simultaneously and clearly see the effects of the sulfate concentration, temperature and pH on the equilibrium potentials of the electrochemical and chemical reactions takes place in the cell. XRD, SEM and TEM investigations are conducted to understand the phase composition and morphology of the PAM produced with different formation procedures and new formation mechanism is proposed. Microscopic investigations showcased a possible phase change during morphological characterization.

Results obtained from the study are summarized below;

1. E-pH diagram of the $Pb/H_2SO_4/H_2O$ system changes considerably with both temperature and acid concentration. It appears to be temperature effects the chemical reactions more compared to the electrochemical reactions. Acid concentration especially shifts the stability regions of the $PbSO_4$ and PbO to the more acidic regions.
2. Low acid concentration leads to more metasomatic $PbSO_4$ to PbO_2 transformation.
3. Spherical PbO_2 morphology is dominant in the low acid samples, as the acid concentration is increased, dominant morphology of the PbO_2 appears to be needle like.
4. High acid density and low paste density results in the similar PAM morphology, this is due to the increase in the $PbSO_4$ region thickness.
5. SEM images showcases metasomatic transformation of the $PbSO_4$ leads to formation of spherical PbO_2 particles. If the proper formation time is given these spherical particles later agglomerates.
6. $PbSO_4$ crystals encountered in the high acid samples seems to be more stable, this corralled to the decrease in solubility of the $PbSO_4$ in H_2SO_4 solutions.
7. In the light of the XRD results it can be said that the rate of the metasomatic transformation is lower than dissolution-precipitation mechanism, however, if the

initial part of the oxidation is dominated by the metasomatic transformation then the extent of oxidation is larger, i.e. more PbO_2 is produced in low acid samples compared to the high acid samples.

8. No metasomatic transformation is observed for the high acid samples, reason explained in terms of the extent of sulfation. For high acid samples sulfated region of the porous cured paste increases, see **Figure 6.6**, as the sulfation takes place acid concentration decreases in the more interior of the now sulfated paste. This facilitates better $PbSO_4$ solubility and diffusion for Pb^{2+} ions, see **Figure 6.52**. Since the distance for the Pb^{2+} diffusion to find electronic contact is smaller, relatively sluggish metasomatic transformation cannot occur.
9. It is believed that if the first oxidation is metasomatic (and spherical), low acid samples, remaining dissolution-precipitation results in the spherical morphology as well.
10. Even though $PbSO_4$ to PbO_2 transformation metasomatic, resulting PbO_2 cannot retain the shape of the precursor crystals, like in the 4BS, because of the large difference in the molar volumes (or densities). When $PbSO_4$ transform in to PbO_2 structure shrinks and developed stresses causes to crystal to break. However, when 4BS surface sulfated to $PbSO_4$ interior of the 4BS particles are not affected, now, when the $PbSO_4$ layer on the 4BS oxidize to PbO_2 there are possible sites for the PbO_2 cling. This mechanism is not very efficient for the 3BS pastes and almost all of the 3BS crystals transforms in to $PbSO_4$, probably due to their size[87].

8. REFERENCES

[1] D. E. Handorf, “The Baghdad battery - Myth or reality?,” *Plat. Surf. Finish.*, vol. 89, pp. 84–87, 2002.

[2] X. Lu and F. Anariba, “Fostering innovation through an active learning activity inspired by the baghdad battery,” *J. Chem. Educ.*, vol. 91, no. 11, pp. 1929–1933, 2014, doi: 10.1021/ed400869c.

[3] B. Franklin and C. Darwin, *Experiments and Observations on Electricity, Made at Philadelphia In America*, vol. XXX. 1749.

[4] D. D. Sarma and A. K. Shukla, “Building better batteries: A travel back in time,” *ACS Energy Lett.*, vol. 3, no. 11, pp. 2841–2845, 2018, doi: 10.1021/acsenergylett.8b01966.

[5] G. Plante´, “Recherches sur la polarization voltaique,” *Comptes Rendus French Acad. Sci.*, vol. 6, no. XLIX, p. 402, 1859.

[6] D. Pavlov, *Lead-Acid Batteries: Science and Technology A Handbook of Lead-Acid Battery Technology and Its Influence on the Product Second Edition*. Elsevier B.V., 2017.

[7] D. Pavlov, “Ernst Voss: The Gaston Planté medallist 1989,” *J. Power Sources*, vol. 30, no. 1–4, pp. 3–5, 1990, doi: 10.1016/0378-7753(93)80057-V.

[8] I. Buchmann *et al.*, *Lead-Acid Battery Technologies Fundamentals, Materials, and Applications*. CRC Press Taylor & Francis Group, 2015.

[9] J. Garche, E. Karden, P. T. Moseley, and D. A. J. Rand, *Lead-Acid Batteries for Future Automobiles*. Elsevier B.V., 2017.

[10] H. J. Bergveld, D. Danilov, P. H. L. Notten, V. Pop, and P. P. L. Regtien, *Encyclopedia of Electrochemical Power Sources*. 2009.

[11] H. Budde-Meiwes *et al.*, “A review of current automotive battery technology and future prospects,” *Proc. Inst. Mech. Eng. Part D J. Automob. Eng.*, vol. 227, no. 5, pp. 761–776, 2013, doi: 10.1177/0954407013485567.

[12] J. Perkins, “Materials and Mechanisms Determining the Performance of Lead-Acid Storage Batteries An Invited Review,” *Mater. Sci. Eng.*, vol. 28, pp. 167–199, 1977.

[13] P. Ruetschi, “Review on The Lead-Acid Battery Science and Technology,” *J. Power Sources*, vol. 2, pp. 3–24, 1977.

[14] A. B. Garrett, S. Vellenga, and C. M. Fontana, “The Solubility of Red, Yellow, and Black Lead Oxides (2) and Hydrated Lead Oxide in Alkaline Solutions. The Character of the Lead-Bearing Ion,” *J. Am. Chem. Soc.*, vol. 61, no. 2, pp. 367–373, 1939, doi: 10.1021/ja01871a041.

[15] I. M. Steele, J. J. Pluth, and J. W. Richardson, “Crystal Structure of Tribasic Lead Sulfate (3PbO·PbSO4·H2O) by X-Rays and Neutrons: An Intermediate Phase in the Production of Lead Acid Batteries,” *J. Solid State Chem.*, vol. 132, no. 1, pp. 173–181, 1997, doi: 10.1006/jssc.1997.7440.

[16] I. M. Steele and J. J. Pluth, “Crystal Structure of Tetrabasic Lead Sulfate (4PbO · PbSO4) : An Intermediate Phase in the Production of Lead-Acid Batteries,” *J. Electrochem. Soc.*, vol. 145, no. 2, pp. 528–533, 1998, doi: 10.1149/1.1838298.

[17] D. Pavlov and E. Bashtavelova, “A study of the oxidation of 4PbO·PbSO4 crystals in cured paste to PbO2 agglomerates during formation of positive plates for lead/acid batteries,” *J. Power Sources*, vol. 31, no. 1–4, pp. 243–254, 1990, doi: 10.1016/0378-7753(90)80076-P.

[18] J. K. Vilhunen and J. Tummavuori, “Processes during preparation of lead/acid battery positive plates from tetrabasic lead sulfate (4BS) pastes,” *J. Power Sources*, vol. 46, no. 2–3, pp. 269–283, 1993, doi: 10.1016/0378-7753(93)90025-V.

[19] H. Ozgun, L. T. Lam, D. A. J. Rand, and S. K. Bhargava, “Effect of plate preparation on active-material utilization and cycleability of positive plates in automotive lead/acid batteries,” *J. Power Sources*, vol. 52, no. 2, pp. 159–171, 1994, doi: 10.1016/0378-7753(94)01945-2.

[20] V. Danel and V. Plichon, “Study of Pb(II) in various H2O-H2SO4 mixtures by differential pulse polarography: solubility of lead sulphate, diffusion coefficient of Pb(II) and half-wave potential of Pb(Hg)/Pb(II),” *Electrochim. Acta*, vol. 27, no. 6, pp. 771–774, 1982, doi: 10.1016/0013-4686(82)85073-1.

[21] P. Delahay, M. Pourbaix, and P. Van Rysselberghe, “Potential-pH Diagram of Lead and its

Applications to the Study of Lead Corrosion and to the Lead Storage Battery," *J. Electrochem. Soc.*, vol. 98, no. 2, p. 57, 1951, doi: 10.1149/1.2778106.

[22] D. Pavlov and N. Kapkov, "Lead/Acid Batterry Possitive Plates Manufactured From 4PbO.PbSO4 Pastes Prepared From Leady Oxide and Red Lead," *J. Power Sources*, vol. 31, pp. 189–201, 1990.

[23] D. Pavlov and N. Kapkov, "Lead-Acid Battery Pastes Containing 4PbO · PbSO4 and Pb3O4," *J. Electrochem. Soc.*, vol. 137, no. 1, pp. 16–21, 1990, doi: 10.1149/1.2086354.

[24] S. R. Ellis, N. A. Hampson, M. C. Ball, and F. Wilkinson, "The lead dioxide electrode," *J. Appl. Electrochem.*, vol. 16, no. 2, pp. 159–167, 1986, doi: 10.1007/BF01093347.

[25] V. H. Dodson, "Some Important Factors That Influence the Composition of the Positive Plate Material in the Lead-Acid Battery," *J. Electrochem. Soc.*, vol. 108, no. 5, p. 401, 1961, doi: 10.1149/1.2428100.

[26] N. E. Bagshaw, R. L. Clarke, and B. Halliwell, "The preparation of lead dioxide for X-ray diffraction studies," *J. Appl. Chem.*, vol. 16, no. 6, pp. 180–184, 2007, doi: 10.1002/jctb.5010160604.

[27] P. Rüetschi, "Influence of Crystal Structure and Interparticle Contact on the Capacity of PbO2 Electrodes," *J. Electrochem. Soc.*, vol. 139, no. 5, pp. 1347–1351, 1992, doi: 10.1149/1.2069410.

[28] I. Petersson and E. Ahlberg, "On the question of electrochemical activity of differently formed lead dioxides," *J. Power Sources*, vol. 91, no. 2, pp. 137–142, 2000, doi: 10.1016/S0378-7753(00)00460-2.

[29] D. Devilliers, M. T. Dinh Thi, E. Mahé, V. Dauriac, and N. Lequeux, "Electroanalytical investigations on electrodeposited lead dioxide," *J. Electroanal. Chem.*, vol. 573, no. 2, pp. 227–239, 2004, doi: 10.1016/j.jelechem.2004.07.008.

[30] D. Pavlov, I. Balkanov, T. Halachev, and P. Rachev, "Hydration and Amorphization of Active Mass PbO2 Particles and Their Influence on the Electrical Properties of the Lead-Acid Battery Positive Plate," *J. Electrochem. Soc.*, vol. 136, no. 11, pp. 3189–3197, 1989, doi: 10.1149/1.2096424.

[31] D. Pavlov, “The Lead-Acid Battery Lead Dioxide Active Mass: A Gel-Crystal System with Proton and Electron Conductivity,” *J. Electrochem. Soc.*, vol. 139, no. 11, pp. 3075–3080, 1992, doi: 10.1149/1.2069034.

[32] D. Pavlov, “Suppression of premature capacity loss by methods based on the gel-crystal concept of the PbO2 electrode,” *J. Power Sources*, vol. 46, no. 2–3, pp. 171–190, 1993, doi: 10.1016/0378-7753(93)90016-T.

[33] W. Mindt, “Electrical Properties of Electrodeposited PbO2 Films,” *J. Electrochem. Soc.*, vol. 116, no. 8, p. 1076, 1969, doi: 10.1149/1.2412217.

[34] S. Ikari, S. Yoshizawz, and S. Okada, “Discharge Behaviours of Electrodeposited a- and β-PbO2 Electrode,” *J. Electrochem. Soc. Japan*, vol. 27, no. 2, p. E-223 E-227, 1959, doi: 10.20551/jscswabun.7.2_204_2.

[35] H. N. Cong and P. Chartier, “Electrodeposited α-PbO2 and β-PbO2 in sulfuric acid: Recharge, cycling and morphology,” *J. Power Sources*, vol. 13, no. 3, pp. 223–233, 1984, doi: 10.1016/0378-7753(84)80005-1.

[36] M. E. Herron, K. J. Roberts, S. E. Doyle, J. Robinson, and F. C. Walsh, “In-situ X-Ray diffraction studies of lead dioxide in sulphuric acid during potential cycling,” *Phase Transitions*, vol. 39, no. 1–4, pp. 135–144, 1992, doi: 10.1080/01411599208203477.

[37] M. E. Herron, D. Pletcher, and F. C. Walsh, “A combined electrochemical and in-situ X-ray diffraction study of the cycling of well-defined lead dioxide layers on platinum,” *J. Electroanal. Chem.*, vol. 332, no. 1–2, pp. 183–197, 1992, doi: 10.1016/0022-0728(92)80350-D.

[38] S. C. Barnes and R. T. Mathieson, *The Potential-pH Diagram Of Lead In The Presence Of Sulphate Ions And Some Of Its Implications In Lead–Acid Battery Studies*. Pergamon Press Ltd, 1965.

[39] D. Pavlov, “Formation of Lead-Acid Batteries and Structure of Positive and Negative Active Masses,” in *Valve-Regulated Lead-Acid Batteries*, 2004, pp. 37–108.

[40] M. G. Mayer and D. A. J. Rand, “Leady oxide for lead/acid battery positive plates: Scope for improvement?,” *J. Power Sources*, vol. 59, no. 1–2, pp. 17–24, 1996, doi: 10.1016/0378-

7753(96)02296-3.

[41] D. Pavlov and G. Papazıov, “Dependence of the properties of the lead-acid battery positive plate paste on the processes occurring during its production,” *J. Appl. Electrochem.*, vol. 6, pp. 339–345, 1976.

[42] V. Iliev and D. Pavlov, “The influence of PbO modification on the kinetics of the 4PbO·PbSO4 lead-acid battery paste formation,” *J. Appl. Electrochem.*, vol. 9, no. 5, pp. 555–562, 1979, doi: 10.1007/BF00610941.

[43] B. Culpin, “The Role of Tetrabasic Lead Sulphate in the Lead/Acid Positive Plate,” *J. Power Sources*, vol. 25, pp. 305–311, 1989.

[44] V. H. Dodson, “The Composition and Performance of Positive Plate Material in the Lead-Acid Battery,” *J. Electrochem. Soc.*, vol. 108, no. 5, p. 406, 1961, doi: 10.1149/1.2428101.

[45] D. Pavlov, M. Dimitrov, T. Rogachev, and L. Bogdanova, “Influence of paste composition and curing program used for the production of positive plates with PbSnCa grids on the performance of lead acid batteries,” *J. Power Sources*, vol. 114, no. 1, pp. 137–159, 2003, doi: 10.1016/S0378-7753(02)00593-1.

[46] D. Pavlov, G. Papazov, and V. Iliev, “Mechanism of the Processes of Formation of Lead-Acid Battery Positive and Negative Plates,” *J. Electrochem. Soc.*, vol. 119, no. 1, pp. 135–149, 1972.

[47] D. A. Jones, *Principles and Prevention of Corrosion*. Prentice Hall, 1996, 1996.

[48] M. Pourbaix, *Atlas of Electrochemical Equilibria in Aqueous Solutions*. National Association of Corrosion Engineers, 1974.

[49] P. Ruetschi and R. T. Angstadt, “Anodic Oxidation of Lead at Constant Potential,” *J. Electrochem. Soc.*, vol. 111, no. 12, p. 1323, 1964, doi: 10.1149/1.2425996.

[50] K. R. Bullock, “The Effect of Anion Activity on Electrochemical Equilibria: Three-Dimensional Potential-pH Diagram for Pb/H2SO4/H2O System,” *J. Electrochem. Soc.*, vol. 127, no. 3, pp. 662–664, 1980, doi: 10.1149/1.2129728.

[51] D. Pavlov, A. Kirchev, M. Stoycheva, and B. Monahov, “Influence of H2SO4 concentration

on the mechanism of the processes and on the electrochemical activity of the Pb/PbO 2/PbSO4 electrode," *J. Power Sources*, vol. 137, no. 2, pp. 288–308, 2004, doi: 10.1016/j.jpowsour.2004.06.006.

[52] W. Haidinger, "Zweite Klasse: Geogenide. II. Ordnung. Baryte VII. Bleibaryt. Plattnerit.," in *Handbuch der Bestimmenden Mineralogie*, Vienna: Braumüller & Seidel, 1845, p. 500.

[53] K. Harris, R. J. Hill, and D. A. J. Rand, "Crystalline Phase Composition of Positive Plates in Lead/Acid Traction Batteries Under Simulated Electric Vehicle Service," *J. Power Sources*, vol. 8, pp. 175–196, 1982.

[54] H. Bode and E. Voss, "Uber die Bleidioxydmodifikationen beim Akkumulator," *Z. Elektrochem*, vol. 60, no. 9, pp. 1053–1056, 1956.

[55] J. Taggart, E. Foord, A. Rosenzweig, and T. Hanson, "Scrutinyite, Natural Occurrences Of α-PbO2 from Bingham , New Mexico, U.S.A., And Mapimi, Mexico," vol. 26, pp. 905–910, 1988.

[56] U. B. Thomas, "The Electrical Conductivity of Lead Dioxide," *J. Electrochem. Soc.*, vol. 94, no. 1, pp. 42–49, 1948, doi: 10.1016/0019-1035(72)90060-7.

[57] K. Micka, M. Svatá, and V. Koudelka, "Study of Structural Factors of Lead-Acid Battery Electrodes," *J. Power Sources*, vol. 4, no. 1, pp. 43–51, 1979, doi: 10.1016/0378-7753(79)80036-1.

[58] R. J. Hill, "Calculated X-Ray Powder Diffraction Data for Phases Encountered in Lead/Acid Battery Plates," *J. Power Sources*, vol. 9, pp. 55–71, 1983.

[59] F. Vallat-Joliveau, A. Delahaye-Vidal, M. Figlarz, and A. de Guibert, "New Preparation Methods and Accurate X-Ray Powder Diffraction Data for Tribasic Lead Sulfate Hydrate, Precursor of The Active Material in Lead/Acid Batteries," *J. Power Sources*, vol. 55, no. 1, pp. 97–100, 1995, doi: 10.1016/0378-7753(94)02163-W.

[60] D. Pavlov and T. Rogachev, "Dependence of The Phase Composition of The Anodic Layer on Oxygen Evolution and Anodic Corrosion of Lead Electrode in Lead Dioxide Potential Region," *Electrochim. Acta*, vol. 23, no. 11, pp. 1237–1242, 1978, doi: 10.1016/0013-4686(78)85079-8.

[61] W. B. White, F. Dachille, and R. Roy, “of the Oxides of Lead,” vol. 49, no. 1942, 1956.

[62] P. T. Moseley, J. L. Hutchison, and M. A. M. Bourke, “The Defect Structure of Lead Dioxide,” *J. Electrochem. Soc.*, vol. 129, no. 4, pp. 876–880, 1982, doi: 10.1149/1.2123991.

[63] S. M. Caulder and A. C. Simon, “Thermal Decomposition Mechanism of Formed and Cycled Lead Dioxide Electrodes and Its Relationship to Capacity Loss and Battery Failure,” *J. Electrochem. Soc.*, vol. 121, no. 12, p. 1546, 1974, doi: 10.1149/1.2401730.

[64] B. Monahov and D. Pavlov, “Hydrated structures in the anodic layer formed on lead electrodes in H2SO4 solution,” *J. Appl. Electrochem.*, vol. 23, no. 12, pp. 1244–1250, 1993, doi: 10.1007/BF00234807.

[65] J. Burbank, “Anodization of Lead in Sulfuric Acid,” *J. Electrochem. Soc.*, vol. 103, no. 2, p. 87, 1956, doi: 10.1149/1.2430250.

[66] H. B. Mark, “Technical Notes The Discharge Properties of a-PbO2 in Dilute H2S04 Electrolyte,” *J. Electrochem. Soc.*, vol. 109, no. 7, pp. 634–638, 1962.

[67] D. Pavlov, “Mechanism of the Anodic Oxidation of Lead in Sulphuric Acid Solutions,” *Berichte der Bunsengesellschaft*, pp. 398–404, 1966, doi: 10.1149/1.2132697.

[68] D. Pavlov, “Processes of formation of divalent lead oxide compounds on anodic oxidation of lead in sulphuric acid,” *Electrochim. Acta*, vol. 13, no. 10, pp. 2051–2061, 1968, doi: 10.1016/0013-4686(68)80115-X.

[69] D. Pavlov, C. N. Poulieff, E. Klaja, and N. Iordanov, “Dependence of the Composition of the Anodic Layer on the Oxidation Potential of Lead in Sulfuric Acid,” *J. Electrochem. Soc.*, vol. 116, no. 3, p. 316, 1969, doi: 10.1149/1.2411836.

[70] D. Pavlov, “Processes in solid state at anodic oxidation of a lead electrode in H2SO4 solution and their dependence on the oxide structure and properties,” *Electrochim. Acta*, vol. 31, no. 9, pp. 845–854, 1978, doi: 10.1016/0013-4686(78)87005-4.

[71] B. A. Thompson and R. L. Strong, “Oxygen in Lead Oxide,” *J. Phys. Chem.*, vol. 67, no. 6, pp. 594–597, 1963.

[72] D. Pavlov, “Semiconductor mechanism of the processes during electrochemical oxidation

of PbO to PbO2," *J. Electroanal. Chem.*, vol. 118, no. C, pp. 167–185, 1981, doi: 10.1016/S0022-0728(81)80539-6.

[73] F. Lappe, "Some physical properties of sputtered PbO2 films," *J. Phys. Chem. Solids*, vol. 23, no. 11, pp. 1563–1566, 1962, doi: 10.1016/0022-3697(62)90237-8.

[74] Z. Takehara and K. Kanamura, "The SEM Observation of the Potentiostatic Oxidation of Lead Sulfate on a Gold Plate in Sulfuric Acid Solution," *J. Electrochem. Soc.*, vol. 134, no. 1, pp. 13–18, 1987, doi: 10.1149/1.2100394.

[75] Z. Takehara and K. Kanamura, "The Oxidation of PbSO4 to PbO2 in Sulfuric Acid Solution," *J. Electrochem. Soc.*, vol. 134, no. 7, pp. 1604–1610, 1987, doi: 10.1246/bcsj.60.1567.

[76] N. Munichandraiah and S. Sathyanarayana, "Insoluble anode of α-lead dioxide coated on titanium for electrosynthesis of sodium perchlorate," *J. Appl. Electrochem.*, vol. 18, no. 2, pp. 314–316, 1988, doi: 10.1007/BF01009281.

[77] B. Monahov, D. Pavlov, A. Kirchev, and S. Vasilev, "Influence of pH of the H2SO4 solution on the phase composition of the PbO2 active mass and of the PbO2 anodic layer formed during cycling of lead electrodes," *J. Power Sources*, vol. 113, no. 2, pp. 281–292, 2003, doi: 10.1016/S0378-7753(02)00583-9.

[78] B. ming Chen, Z. cheng Guo, X. wan Yang, and Y. dong Cao, "Morphology of alpha-lead dioxide electrodeposited on aluminum substrate electrode," *Trans. Nonferrous Met. Soc. China (English Ed.*, vol. 20, no. 1, pp. 97–103, 2010, doi: 10.1016/S1003-6326(09)60103-5.

[79] J. Burbank, "The Role of Antimony in Positive Plate Behavior in the Lead-Acid Cell," *J. Electrochem. Soc.*, vol. 111, no. 10, p. 1112, 1964, doi: 10.1149/1.2425931.

[80] A. C. Simon, C. P. Wales, and S. M. Caulder, "Morphological Changes in the Lead Dioxide Electrode During Its Reduction and Reoxidation," *J. Electrochem. Soc.*, vol. 117, no. 8, p. 987, 1970, doi: 10.1149/1.2407744.

[81] A. C. Simon, S. M. Caulder, and J. T. Stemmle, "Structural Transformations of the PbO2 Active Material during Cycling," *J. Electrochem. Soc.*, vol. 122, no. 4, pp. 461–466, 1975,

doi: 10.1149/1.2134240.

[82] C. A. C. Simon, S. M. Caulder, and J. T. Stemmle, “Closure to “ Discussion of ‘ Structural Transformations of the PbO2 Active,” *J. Electrochem. Soc.*, vol. 122, no. 4, pp. 461–466, 1975.

[83] T. G. Chang, “Structural Changes of Positive Active Material in Lead-Acid Batteries in Deep-Discharge Cycling,” *J. Electrochem. Soc.*, vol. 131, no. 8, pp. 1755–1762, 1984, doi: 10.1149/1.2115955.

[84] R. J. Hill and I. C. Madsen, “Structural Parameters of β - PbO2 and Their Relationship to the Hydrogen-Loss Concept of Lead-Acid Battery Failure,” *J. Electrochem. Soc.*, vol. 131, no. 7, pp. 1486–1491, 1984, doi: 10.1149/1.2115878.

[85] Z. Takehara, K. Kanamura, and M. Kawanami, “The Oxidation Reaction of Lead Sulfate Formed at the Interface Between the Grid and the Active Material,” *J. Electrochem. Soc.*, vol. 136, no. 3, pp. 620–625, 1989, doi: 10.1149/1.2096698.

[86] L. Zerroual, F. Tedjar, J. Guitton, and A. Mousser, “Mechanism of PbO2 formation in lead/acid battery positive plates,” *J. Power Sources*, vol. 41, no. 3, pp. 231–238, 1993, doi: 10.1016/0378-7753(93)80041-M.

[87] S. Grugeon-Dewaele, S. Laruelle, L. Torcheux, J.-M. Tarascon, and A. Delahaye-Vida, “Optimization of the Positive Active Material Capacity in Lead-Acid Cells Through Control of the Basic Lead Sulfate Precursor,” *J. Electrochem. Soc.*, vol. 145, pp. 3358–3365, 1998.

[88] M. Dimitrov and D. Pavlov, “Influence of grid alloy and fast charge on battery cycle life and structure of the positive active mass of lead acid batteries,” *J. Power Sources*, vol. 93, no. 1–2, pp. 234–257, 2001, doi: 10.1016/S0378-7753(00)00598-X.

[89] L. T. Lam, A. M. Vecchio-Sadus, H. Ozgun, and D. A. J. Rand, “Conversion of tetrabasic lead sulfate to lead dioxide in lead/acid battery plates,” *J. Power Sources*, vol. 38, no. 1–2, pp. 87–102, 1992, doi: 10.1016/0378-7753(92)80098-V.

[90] L. T. Lam, H. Ozgun, L. M. D. Cranswick, and D. A. J. Rand, “Pulsed-current formation of tetrabasic lead sulfate in cured lead/acid battery plates,” *J. Power Sources*, vol. 42, no. 1–2, pp. 55–70, 1993, doi: 10.1016/0378-7753(93)80137-E.

[91] S. Grugeon-Dewaele *et al.*, "Soaking and formation of tetrabasic lead sulfate," *J. Power Sources*, vol. 64, no. 1–2, pp. 71–80, 1997, doi: 10.1016/S0378-7753(96)02505-0.

[92] D. Pavlov and E. Bashtavelova, "A Model of the Structure of the Positive Lead-Acid Battery Active Mass," *J. Electrochem. Soc.*, vol. 131, no. 7, pp. 1468–1476, 1984, doi: 10.1149/1.2115876.

[93] D. Pavlov and E. Bashtavelova, "Structural Properties of the PbO2 Active Mass Determining Its Capacity and the 'Breathing' of the Positive Plate during Cycling," *J. Electrochem. Soc.*, vol. 133, no. 2, pp. 241–248, 1986, doi: 10.1149/1.2108555.

[94] A. Winsel and E. Bashtavelova, "Nanostructure and agglomerate-of-spheres model," *J. Power Sources*, vol. 73, no. 2, pp. 242–250, 1998, doi: 10.1016/S0378-7753(97)02814-0.

[95] D. Pavlov, E. Bashtavelova, D. Simonsson, and P. Ekdunge, "Processes at the Micro-Level in the Oxidation Of PbSO4 to PbO2 During Charging of Lead/Acid Battery Positive Plates," *J. Power Sources*, vol. 30, pp. 77–97, 1990.

[96] D. Pavlov, G. Petkova, M. Dimitrov, M. Shiomi, and M. Tsubota, "Influence of fast charge on the life cycle of positive lead-acid battery plates," *J. Power Sources*, vol. 87, no. 1, pp. 39–56, 2000, doi: 10.1016/S0378-7753(99)00358-4.

[97] D. Pavlov and I. Balkanov, "The PbO2 Particle: Exchange Reactions Between Ions of the Electrolyte and the PbO2 Particles of the Lead-Acid Battery Positive Active Mass," *J. Electrochem. Soc.*, vol. 139, no. 7, pp. 1830–1835, 1992, doi: 10.1149/1.2069506.

[98] R. Amadelli, A. Maldotti, A. Molinari, F. I. Danilov, and A. B. Velichenko, "Influence of the Electrode History and Effects of the Electrolyte Composition and Temperature on O2 Evolution At B-Pbo2 Anodes in Acid Media," *J. Electroanal. Chem.*, vol. 534, no. 1, pp. 1–12, 2002, doi: 10.1016/S0022-0728(02)01152-X.

[99] J. Cao, H. Zhao, F. Cao, and J. Zhang, "The Influence Of F- Doping on The Activity of Pbo2 Film Electrodes in Oxygen Evolution Reaction," *Electrochim. Acta*, vol. 52, no. 28, pp. 7870–7876, 2007, doi: 10.1016/j.electacta.2007.06.038.

[100] D. Pavlov and B. Monahov, "Mechanism of the Elementary Electrochemical Processes Taking Place during Oxygen Evolution on the Lead Dioxide Electrode," *J. Electrochem.*

Soc., vol. 143, no. 11, pp. 3616–3629, 1996, doi: 10.1149/1.1837261.

[101] D. Pavlov, I. Balkanov, and P. Rachev, "Orthorhombic PbO Formation during the Discharge of Lead Acid Batteries PbO2 Active Mass," *J. Electrochem. Soc.*, vol. 134, no. 10, pp. 2390–2398, 1987, doi: 10.1149/1.2100210.

[102] "LabTools Tables for Laboratory Use," in *LabTools Tables for Laboratory Use,* p. 64.